Theoretical Insights into Propane Dehydrogenation over Refractory Metal Oxide Catalysts

---

A Dissertation

Presented to
the faculty of the School of Engineering and Applied Science
University of Virginia

---

in partial fulfillment
of the requirements for the degree

Doctor of Philosophy

by

Xuhui Feng

August

2015

APPROVAL SHEET

The dissertation
is submitted in partial fulfillment of the requirements
for the degree of
Doctor of Philosophy

Feng

AUTHOR

Matthew Neurock

Advisor

Robert Davis

Ian Harrison

Joshua Choi

Geise Geoffrey

Accepted for the School of Engineering and Applied Science:

James H. Ay

Dean, School of Engineering and Applied Science

August
2015

Abstract

The catalytic production of propylene from propane is carried out commercially over supported Pt catalysts, but the limited yields of propylene, catalyst deactivation and the high costs of Pt have led to increasing efforts in the development of new catalysts that can carry out the non-oxidative conversion of propane to propylene. Low-cost refractory metal oxides such as α-Al_2O_3 and α-Cr_2O_3 which have shown some industrial promise were examined with first-principle theoretical calculations and compared herein. Mixed Cr-Al oxide complexes, namely, Cr/α-Al_2O_3 and amorphous Cr_2O_3/α-Al_2O_3 were also examined herein. Density functional theory calculations were used to examine the influence of catalyst structure, surface composition, and possible active sites on the overall reaction energetics and plausible reaction mechanisms to provide fundamental insights into catalytic dehydrogenation and aid in the development of new catalytic materials.

For α-Al_2O_3, the dominant surface structures are either clean Al_2O_3 surface or the fully hydroxylated surface depending on partial pressures of water and the actual reaction conditions. Both surfaces were examined in detail as well as the influence of oxygen vacancies on the reaction energetics for propane dehydrogenation. The theoretical results for the catalytic activation of propane on the clean α-Al_2O_3 surface indicate that the initial activation of propane proceeds via the heterolytic splitting of C-H bond over the Al-O site pair to form Al-propyl and O-H intermediates resulting in an activation barrier of 101.0 kJ/mol. The subsequent activation of C-H bond in propyl proceeds at an adjacent O site to form propylene and OH* with a barrier that was 93.6 kJ/mol. The strong binding of H to the O sites (-115.8 kJ/mol) makes it very difficult to remove H* via H_2

recombination as the intrinsic activation barrier is 260.5 kJ/mol, thus resulting in an overall barrier for the activation of propane to propylene of 328.0 kJ/mol. Therefore, while the Al_2O_3 surface is very reactive in the activation of C-H bonds, it cannot carry the persistent activity for catalysis.

The results on the Al_2O_3 surface indicate that the surface will be likely ready to form a fully hydroxylated surface. The activation of the C-H bond of propane over the hydroxylated Al_2O_3 surface does not proceed via a direct heterolytic activation over Al-O pairs but instead via the homolytic splitting on two OH*, resulting in a higher initial C-H activation barrier of 183.3 kJ/mol than that on clean surface. The 2nd C-H splitting proceeds at the OH group binding propyl in the 1st step with a barrier of 115.8 kJ/mol. The barrier for H_2 recombination was calculated though to be somewhat higher (337.7 kJ/mol) even though the O-H bond is weaker. This is due to a much less stable transition state. As such, the terminal OH species that result from hydroxylation do not improve catalytic activity of α-Al_2O_3. The presence of O* vacancies can influence propane dehydrogenation as well. Theoretical results, however show that the strong binding of propyl brought by O vacancy inhibits catalytic activity.

The activation of propane was explored over chromia and supported chromia complexes. Propane activation proceeds via the heterolytic C-H activation over Cr-O site pair. On α-Cr_2O_3, the metal Cr site binds both propyl and H more strongly, while O site binds them much more weakly which prevents the formation of a deep energy well that one cannot escape. In H_2 recombination, the barrier is calculated to be significantly lower at 29.0 kJ/mol, so then the highest point in energy profile is the transition state of 2nd C-H activation (248.4 kJ/mol), and the total barrier for turnover cycle is lower (260.5 kJ/mol) than those on α-Al_2O_3 facets. Therefore, the weaker H binding on O sites helps this surface to gain better activity.

On monomer grafted Cr/α-Al_2O_3 complex, binding properties of Cr sites are similar to α-Cr_2O_3; while the adjacent O site binds H less weakly (0.0 kJ/mol vs 86.8 kJ/mol) affected by the fully hydroxylated α-Al_2O_3 base. Through the same favored pathway on a single Cr-O pair, the moderate binding properties lead to moderate energies in the activation of C-H bonds, and also a moderate barrier in H_2 recombination. So there is no deep well or high peak in the energy profile, and the total barrier (221.9 kJ/mol) is lower than previous cases. The dimer and the trimer Cr/α-Al_2O_3 complexes have similar binding properties and catalytic activities to the monomer case.

On amorphous Cr_2O_3/α-Al_2O_3 complexes, bindings on Cr sites are not as strong as on α-Cr_2O_3 and Cr/α-Al_2O_3, and bindings on O sites are similarly moderate as on Cr/α-Al_2O_3, so both Cr and O sites have moderate binding properties. As a result, the activation of C-H bonds and the recombination of H_2 both have feasible barriers, so the overall barriers on amorphous Cr_2O_3/α-Al_2O_3 complexes (210 – 240 kJ/mol) are also moderate, similar to the grafted Cr/α-Al_2O_3 complexes.

By comparing all the examined cases, we see that the strong binding of the reaction species lead to either deep energy wells in C-H activation or high energy peaks in H_2 recombination as on α-Al_2O_3 surfaces, and thus raise the overall barrier; while weak bindings on α-Cr_2O_3 result in shallower energy well in the 1st C-H activation and lower activation energy for H_2 recombination, but it also leads to higher barrier for the 2nd C-H activation, so the resulted overall barrier are also quite high. On the mixed Al-Cr oxide complexes, the moderate binding strengths for reaction species lead to energy profiles without deep wells or high peaks, and thus the overall barriers for the turnover cycle are lower.

Bader charge analysis was used to understand the reactivity on the different surfaces examined. The results show that α-Al_2O_3 surfaces have very strong electron affinities that prevent the loss of adsorbates which retain negative charge in the surface. The α-Cr_2O_3 surface is a weak electron acceptor overall, but the electron acceptability of the O site and the Cr site are quite polarized which acts to increase the barrier of the 2nd C-H activation step. The mixed Al-Cr oxide complexes are weak electron acceptors as well, but the electron acceptability between O and Cr sites is more balanced. Therefore, the mixed Al-Cr oxide complexes hold the charges from reaction intermediates moderately in C-H activations, and also release them with low barriers in the desorption of products, so their electronic properties determine the moderate binding properties and thus higher activities for the turnover cycle of propane activation.

Acknowledgements

Firstly I would like to thank my advisor, Dr. Matthew Neurock, for his guidance and instruction in my Ph.D. research. This work would not have been done without his expertise and advice. I would like to thank my collaborator Dr. Lijun Xu, who was a post-doctoral researcher in our group, for his insightful advice and suggestions in many aspects. Thanks to Honeywell UOP for funding my research project. Thanks to ChemE faculty and staff for providing the fantastic education and the family-like environment. Thanks to our group members for the great time together. I would also like to thank Dr. Robert Davis, Dr. Ian Harrison, Dr. Joshua Choi and Dr. Geoffrey Geise for serving on my Ph.D. committee. I want to thank my family, especially my wife Yifei, for their unconditionally support and companionship throughout the past six years. Last, I want to dedicate the dissertation to my grandma in heaven. May her soul rest in peace forever.

Table of Contents

List of Figures

List of Tables

Chapter 1 Introduction

The demand for propylene has significantly increased over the past two decades as a result of the increased demand for polypropylene which is widely used in the production of a number of consumer products such as packing materials and outdoor clothing [1, 2], as well as in the synthesis of other chemical intermediates such as cumene. [2] Much of the propylene production is currently met by the steam cracking of higher saturated hydrocarbon feedstock and is often a co-product of ethylene. [3, 4] The broad molecular product distribution that results from hydrocarbon cracking, however, significantly limits the yields and the cost to selectively produce propylene. In addition, the energy costs associated with cracking are very high as cracking is typically carried out at temperatures as high as 1123 K. [4] In addition to the increased demand for propylene, there has be an increased demand for the selective production of propylene over ethylene that has occurred in the past few years. [3, 5] The cracking processes are currently optimized more for the use of ethane over propane due to the increased production of shale gas. As a result, ethylene has been the primary target rather than propylene thus increasing the demand for propylene. [5, 6] This has therefore led to new on-purpose paths for propylene production with higher throughputs, better selectivities, and lower energy costs.

1.1 Propylene Production via Propane Dehydrogenation (PDH)

Currently, there are three on-purpose paths to produce propylene: propane dehydrogenation (PDH), olefin metathesis, and the conversion of methanol to propylene.

[2, 5, 7] Propane dehydrogenation which involves the direct activation of propane, an abundant low-cost feedstock derived from natural gas, crude oil or refinery by-product streams to form propylene, is the most predominant path and holds the most hope for future growth. [7] The past decade has witnessed significant growth in the industrial production of propylene from propane, especially in areas with locally abundant propane sources such as the Middle-East and the United States. [1, 3, 7, 8]

PDH can proceed through either oxidative or non-oxidative pathways. The oxidative path typically results in high conversion and reactivity at relatively mild reaction conditions, due to the exothermicity of the reaction that is driven by formation of water. [8-10] The selectivity to desired propylene product, however, is quite low and decreases with increases in conversion [11]. The reason is that, under an oxidative reaction environment, further activation of propylene is prone to occur at the temperature needed for propane activation as the C-H bonds in propylene are weaker than those in propane [8, 11, 12]. Most of the research efforts in this area have therefore been predominantly from academia as this route has yet to be used in the industrial production of propylene. [10, 11]

In contrast, the non-oxidative path can result in higher selectivities as it involves a more direct route to dehydrogenate propane to propylene and hydrogen. Moreover, the co-product (H_2) in this path is also a valuable product used in chemical/petrochemical processes such as hydrocracking [4, 8]. The non-oxidative route has therefore been increasingly used in the industrial production of propylene. [1, 3, 8]

The non-oxidative path however is fairly endothermic and requires high reaction temperature (823 – 923 K) to carry out C-H bond activation. [1, 8] There are significant issues, however, in the physical and chemical stability of the catalysts used at such high temperatures. Moreover, the high operating temperatures also facilitate thermal cracking and coke deposition on catalysts which lead to catalyst deactivation [13-15]. As such, it would be desirable to establish new catalytic materials that can operate at lower temperatures that can suppress these side reactions and catalyst deactivation.

1.2 Commercial PDH Catalysts and Current Challenges

The predominant catalysts used in commercial PDH processes are made up of either platinum (Pt) or chromium (Cr). [8, 16] The Pt-based catalysts are typically comprised of bimetallic Pt alloys (mainly Pt-Sn) supported on oxides like alumina, whereas the Cr-based materials involve chromia complexes supported on alumina. Pt-based catalysts were developed by Universal Oil Products (UOP) and used commercially in the Oleflex process whereas the Cr-based catalysts were commercialized in the CATOFIN process by Lummus. [8, 17]

These two series of catalysts both report selectivities for propylene that are higher than 85%; the selectivity in the Oleflex process is 89-91% while that in the CATOFIN process is greater than 86%. The catalytic activity in these processes is not high, the per-pass conversion in Oleflex is around 35%, and that in CATOFIN is 48-53%. [5, 18]

The catalysts in both the Oleflex and CATOFIN processes have issues with catalyst deactivation mainly caused by thermal cracking and coke deposition. [13-15] In both processes, the catalysts need to be regenerated by burning off coking deposits in a separate parallel reactor in CATOFIN and continuous catalyst regenerator (CCR) in Oleflex, resulting in higher cost in both capital and operating expenses. Moreover, the regeneration of catalysts needs to be carried out quite frequently as coke formation is rapid. [2] In the CATOFIN process, the reactors are switched over every 5-20 minutes to regenerate the catalyst. In Oleflex process, catalyst is continuously regenerated in CCR. [8] Therefore, the length of catalyst life time is restricted by the high frequency and high temperature of regeneration, with 1.5-3 years in CATOFIN, and 1-2 years in Oleflex. [18, 19]

Both processes are also limited by operational costs. The Pt-based Oleflex catalysts require the use of noble metal (Pt) which is very expensive. Less expensive, more durable catalysts that demonstrate high activities and selectivities are needed to further develop both of these PDH processes.

1.3 New Progress and Opportunities in Catalyst Development for PDH

UOP recently examined series of refractory metal oxides (ZrO_2, α-Cr_2O_3, α-Al_2O_3, etc.) for possible commercial use. [20] These oxides demonstrate very good resistance to high temperature degradation and deactivation, and their costs are much lower compared to noble metals. [19] Moreover, some of these materials have been found to readily activate the initial C-H bond of propane which is critical for PDH. ZrO_2, for example, was found to readily activate the C-H bonds of the methyl group of 2-propanol-d_8 [21]

and methane in isotope exchange experiment [22]. In the industrial chromia/alumina (CrO_x/Al_2O_3) catalyst, the α-Cr_2O_3 is thought to be active for PDH [23]. α-Al_2O_3, which has a very similar structure to α-Cr_2O_3, may also be active. This is consistent with the reactivity of other alumina catalysts, including γ-Al_2O_3 [24]) and aluminum hydroxide clusters ($(HO)_3Al(OH_2)_x$ (x=0, 1)) [25] which activate the C-H bonds of methane and propane, respectively. Therefore, α-Al_2O_3 may be active in carrying out C-H scission for small alkanes.

Therefore, given their high-temperature resistance, low cost, and potential activity in PDH, a series of refractory oxides including α-Al_2O_3, ZrO_2 and CrO_x supported on α-Al_2O_3 were synthesized and tested by our industrial collaborators at UOP. Their results indicate that while α-Al_2O_3 is not active, both CrO_x/α-Al_2O_3 and ZrO_2 appear to be active as well as selective [20]. Most notably, ZrO_2 demonstrated selectivities that are close to those found commercially and activities that are ~ 40% of the current commercial Pt-based catalyst as reported in UOP's patents. [19, 26, 27]

In order to understand the reactivity of these oxides, we systematically examined the elementary surface reactions steps involved in the dehydrogenation of propane to propylene over a range of different refractory oxides including ZrO_2, α-Al_2O_3 and CrO_x/α-Al_2O_3 and the influence of the oxide structure and composition. A better understanding of how the structure and composition of the catalyst influences the activity and selectivity will provide important mechanistic information that can aid in the design of new catalytic materials.

Previous experimental and kinetic modeling studies provide some insights into the reaction mechanism for isobutane dehydrogenation on CrO_x and suggest that the reaction preferentially occurs over a single Cr-O pair. [28] Gascón et al. found that the dehydrogenation of propane over $Cr_2O_3/\gamma\text{-}Al_2O_3$ followed Langmuir-Hinshelwood kinetics in which the adsorption of propylene demonstrated the best fit to the data. [29] *Ab initio* theoretical calculations can be used to probe such mechanistic interpretations and examine in more detail the elementary steps involved in the reaction, intrinsic reaction energies, activation energies, the nature of the active sites, and the features that control activity as well as selectivity.

1.4 Comparative DFT Study in Our Work

First principle density functional theory (DFT) calculations were carried out in the work herein to examine elementary steps involved in PDH over $\alpha\text{-}Al_2O_3$, $\alpha\text{-}Cr_2O_3$, grafted $Cr/\alpha\text{-}Al_2O_3$ complexes and amorphous $Cr_2O_3/\alpha\text{-}Al_2O_3$ complexes. The results are compared with theoretical studies on ZrO_2 by Dr. Lijun Xu [30] in our group and experimental results from UOP [19, 26, 27] We calculated the lowest energy surface structures, the nature of the active sites, activation and overall reaction energies for elementary steps over these different oxide surfaces in order to understand the mechanisms that control the conversion of propane to propylene and how the structure and properties of the different refractory oxides control the catalytic activity and selectivity.

We examined in detail the nature of the active and inactive sites on the pure oxides α-Al_2O_3 and α-Cr_2O_3 vs ZrO_2. By understanding the differences between these oxides, we subsequently examined a series of different mixed Cr-Al oxide surfaces in order to try to tune the catalytic features. The goal of this work is to understand the critical factors that influence the activation of propane and its selective conversion to propylene and establish initial structure-activity relationships for a series of well-defined refractory metal oxide surfaces in PDH. In addition to the development of structure-reactivity relationships, we examined the changes in the electronic structure as a function of the reaction coordinate and of the materials used, in order to further our understanding of the reaction mechanism from the aspect of charge transfer, and to develop a general model for the correlation of the charge acceptance of a refractory metal oxide and their catalyst activity.

1.5 Document Overview

This dissertation is comprised of 8 chapters. Chapter 1 provides an overview on the dehydrogenation of propane and the basis for our collaboration with UOP and the theoretical studies on the non-oxidative propane dehydrogenation over refractory oxides. Chapter 2 discusses the methods that are used in carrying out the proposed study.

Chapter 3 examines the structure and reactivity of different α-Al_2O_3 surface facets that may be present in the catalytic activity for propane dehydrogenation and other refractory oxides. All of the surfaces examined were found to be active for the initial and subsequent C-H bond scissions reactions of propane but are limited by the desorption of propylene and the recombination and desorption of H_2.

In Chapter 4, we extend the analysis to crystalline α-Cr_2O_3 which has similar structure to α-Al_2O_3. In comparison with α-Al_2O_3, the results show that the recombination of hydrogen and desorption of H_2 occurs quite readily but the barriers to activate the C-H bonds of propane and the bound propyl intermediate are much higher due to weaker binding properties of O sites on α-Cr_2O_3. The overall activity, however, appears to be somewhat higher than that on the α-Al_2O_3.

Chapter 5 summarizes and compares the pure refractory oxides that we have examined, including α-Al_2O_3, α-Cr_2O_3 and ZrO_2 (which was studied by Dr. Lijun Xu). The results indicate that the moderate binding properties and moderately weak electron acceptability of oxides are important in balancing the C-H activation and product removal to maintain higher rates and selectivies for direct propane dehydrogenation. The most active and selective materials appear to be ZrO_2 and the mixed metal oxide systems (such as CrO_x/α-Al_2O_3 examined in Chapter 6 and 7) which can readily activate C-H bonds to form the propene and allow for facile recombination and desorption of H_2.

Chapter 6 examines well-defined chromia clusters grafted onto the well-defined Al_2O_3 support to begin to explore the use of mixed metal oxides that demonstrate weaker interactions between H and C-intermediates and the surface O along moderate C-H activation properties of the Cr/α-Al_2O_3. While H_2 recombination is a little more difficult on the Cr/α-Al_2O_3 system, it does not contribute to the total barrier, so that the overall catalytic activity is higher on the mixed Cr/α-Al_2O_3 surface than on α-Cr_2O_3.

We extend the efforts on the mixed Cr/α-Al_2O_3 surfaces to begin to probe simple models that mimic some of the properties of the amorphous Cr_2O_3/α-Al_2O_3 system in Chapter 7. The amorphous system models show that the binding of hydrogen and hydrocarbon intermediates is moderate compared to the other systems examined due to the more moderate coordination states of O and Cr sites. The activity on the amorphous Cr_2O_3/α-Al_2O_3 is close to that found for grafted Cr/α-Al_2O_3.

Chapter 8 summarizes the work and concludes that the critical catalytic features that tend to maximize catalytic activity are moderate electron densities on the O sites that carry out C-H activation. The M-O site pairs must have strong enough interactions to activate the C-H bonds but weak enough to allow for the rapid recombinative desorption of H_2.

Chapter 2 Computational Methods

2.1 Density Functional Theory (DFT) and Calculation Details

The density functional theory (DFT) is a quantum mechanical theory that has been proved to successfully describe the electronic structures of many-body systems like atoms, molecules and condensed-phase matters. [31, 32] The theoretical basis of DFT method is Hohenberg-Kohn theorem that the ground-state properties of a many-electron system are uniquely determined by the electron density that depends on only 3 spatial coordinates. [33] Therefore, by applying functionals of the electron density, the many-body problem of interacting electrons can be reduced to a single-body problem of non-interacting electrons moving in an effective potential. The effective potential is composed of the external potential and the effects of exchange-correlation interactions between electrons. The external potential is generated by the nucleus which is assumed to be static by the Born-Oppenheimer Approximation due to the huge difference in mass of nuclei and electrons.

In our study, the DFT calculations were carried out using the Vienna ab initio simulation package (VASP). The adsorption energies of reaction intermediates on surface sites, the reaction energies and the activation barriers in all the elementary steps were examined in detail for propane dehydrogenation reaction on different surfaces.

Gradient corrections to the exchange and correlation energies were modeled using the Perdew-Wang 91 [34] form of the generalized gradient approximation (GGA) [35]. The core electrons were described using the projector augmented wave (PAW)-based pseudo-potentials. [36] The valence electrons were modeled using plane wave basis sets with cut-off energy to be 38594.0 kJ/mol. The electronic convergence criterion is $96.5*10^{-6}$ kJ/mol. All of the structural optimizations were carried out until the maximum force on each atom in the system is lower than 4.8 kJ/mol/Å. A 3×3×1 k-point sampling of the Brillouin zone was found to provide sufficient accuracy for all the modeled structures. [37]

The activation energies were calculated within the framework of transition state theory and the use of the harmonic oscillator approximation [38]. The optimized reactant and product structures were used to construct an initial minimum energy pathway (MEP) by the nudged elastic band (NEB) approach [39-41] . In the NEB simulations, eight images between the initial and final states were optimized on the potential energy surface until the maximum force on each atom was lower than 24.1 kJ/mol/Å, and a spring force is applied to maintain the equal distance between images along the MEP. Then, the two consecutive images with the highest energies along the minimum energy path were used to provide an initial transition state structure that was subsequently refined by using the Dimer approach [42-44] to walk uphill along the potential energy path and isolate the transition state. The structures were converged when the forces on all of the atoms in the calculated transition state were found to be less than 4.8 kJ/mol/Å.

2.2 Computational Details for Metal Oxide Models

The computational details for all the oxide substrates applied in our calculations are summarized in Table 2.1. The α-Al_2O_3 (0 0 0 1) surface was modeled using a 3x3 supercell using lattice constants of *a* = 4.78 Å, *b* = 4.78 Å, *c* = 18.86 Å. The Al terminated surface was modeled using 4 layers of Al (36 Al atoms) and 2 layers of O (54 O atoms), and a vacuum layer of 15.71 Å above the surface. The bottom 4 layers in the slab were fixed to the lattice positions whereas the top two layers were free to relax. The fully hydroxylated α-Al_2O_3 surface and the α-Al_2O_3 surface with O vacancies both used the same supercell as α-Al_2O_3, and were constructed based on α-Al_2O_3 (0 0 0 1) slab.

Table 2.1 Summary of computational details for metal oxide models

	Cell Size *a*b*c* (Å)	Vacuum Thickness (Å)	Atomic Layers	Freezed Layers
3*3 α-Al_2O_3 (0 0 0 1)	4.78*4.78*18.86	15.71	6	Bottom 4
2*2 α-Cr_2O_3 (0 0 0 1)	4.96*4.96*26.65	22.71	6	Bottom 4
1*1 m-ZrO_2 (-1 1 1)	5.20*5.26*5.37	12.00	4	Bottom 2
1*2 t-ZrO_2 (1 0 1)	3.66*3.66*5.30	12.00	3	Bottom 1

The α-Cr_2O_3 (0 0 0 1) surface was modeled using a 2×2 supercell with the lattice constants are *a* = 4.96 Å, *b* = 4.96 Å, *c* = 26.65 Å and the vacuum layer is 22.71 Å. The supercell is comprised of 6 layers in total, made up of 4 layers of Cr and 2 layers of O, with 16 Cr and 24 O atoms respectively. Similar to the simulations for Al_2O_3, the bottom 4 layers of the slab were frozen, and the top two layers were free to relax in optimizations.

The grafted Cr/α-Al_2O_3 complexes and amorphous Cr_2O_3/α-Al_2O_3 complexes are both constructed based on the slab of the fully hydroxylated α-Al_2O_3 surface, namely the α-Al_2O_3 (0 0 0 1) slab the shown in Table 2.1.

The calculations on ZrO_2 oxide were carried out by Dr. Xu in our group over the monoclinic (-1 1 1) and the tetragonal (1 0 1) faces of ZrO_2, termed as m-ZrO_2 (-1 1 1) and t-ZrO_2 (1 0 1) for short, respectively (see Table 2.1). [30]

2.3 Reaction Energies Calculations

The adsorption energies of reaction species were calculated via subtracting the energy of the adsorbate bound to the oxide surface by the sum of energies of the isolated oxide surface and the gas phase adsorbate. Taking propane molecule as example, the adsorption energy is calculated via Eq. 2-1,

$$E_{\text{ads}} = E_{\text{propane-surface}} - [E_{\text{surface}} + E_{\text{propane(g)}}]. \qquad \text{(Eq. 2-1)}$$

where E_{ads} is the adsorption energy, $E_{\text{propane-surface}}$ is the energy of propane bound to surface, E_{surface} is the energy of oxide substrate and $E_{\text{propane(g)}}$ is the energy of propane molecule in gas phase. When testing the adsorption energy of H, the 1/2 of H_2(g) energy was used.

The reaction energy for either an elementary step or the turnover cycle is calculated via subtracting the sum of products' energies by the sum of reactants' energies. Taking a reaction starting from propane molecule in gas phase as example, such as the 1st C-H bond activation of propane or the overall reaction of propane dehydrogenation, the reaction energy is calculated via Eq. 2-2,

$$E_{\text{rxn}} = E_{\text{product}} - [E_{\text{surface}} + E_{\text{propane(g)}}]. \qquad \text{(Eq. 2-2)}$$

where is E_{rxn} the reaction energy, E_{product} is the product energy or the sum of products' energies, E_{surface} is the energy of the oxide surface and $E_{\mathrm{propane(g)}}$ is the energy of propane molecule in gas phase.

The activation energy of an elementary step was defined as the difference between the transition state energy and the sum of reactants' energies. Taking the 1st C-H bond activation of propane as example,

$$E_{\mathrm{act}} = E_{\mathrm{ts}} - [E_{\mathrm{surface}} + E_{\mathrm{propane(g)}}]. \qquad \text{(Eq. 2-3)}$$

where is E_{act} the activation energy, E_{ts} is the transition state energy, E_{surface} is the energy of the oxide surface and $E_{\mathrm{propane(g)}}$ is the energy of propane molecule in gas phase.

In all the three equations above, the zero-energy reference state is the sum of the isolated oxide substrate and the gas phase propane molecule, which is also the zero-energy reference state for the overall reaction energy profile.

The overall activation barrier of propane dehydrogenation, however, is defined as the energy difference between the highest-energy state and the lowest-energy state along the reaction coordinate of the turnover cycle. The highest-energy state is usually the transition state of an elementary step like the 2nd C-H bond activation of H_2 recombination; the lowest energy state is most likely not the zero-energy reference state for reaction energy profile, but might be propane bound to the surface or product in the 1st or the 2nd C-H bond activation. This barrier would be used as the main indicator for the catalytic activity of an oxide substrate in our study, since it includes the energies of the most stable state and the most difficult state to reach along the reaction path, and is calculated from the reaction/activation energies of the most important elementary steps.

2.4 Bader Charge Analysis

In order to understand how the electronic features of the catalyst control catalytic reactivity, we carried out detailed analyses to follow the electronic structure evolution and charge transfer along the reaction coordinate for a range of different reactions. More specifically, we used the Bader atoms-in-molecules charge analysis approach with a grid-based algorithm including core charges [45]. The Bader Charge on atom is defined as the charge difference between isolated atom and atom in a molecule [46]: positive values means losses of electronic density compared to neutral atom, and negative values means gains of electronic density compared to neutral atom.

The Bader charge analysis results aid in determining the reaction mechanism of elementary reaction steps through monitoring the charge evolution on reaction intermediates like H/propyl and reaction sites like O/Al. The charge analysis results also reflect the electron affinity/acceptability of oxide substrates through the amounts of charge transfer between propane and the substrates during the reaction, thus help to build the relation between electronic properties and catalytic activities.

Chapter 3 PDH on α-Al_2O_3 (0 0 0 1) Surfaces

3.1 Introduction and Surface Morphologies of α-Al_2O_3 (0 0 0 1)

The Al-terminated Al_2O_3 (0 0 0 1) surface is considered to be the lowest-energy surface of α-Al_2O_3. [47-49] The Al sites in the top layer of this surface are coordinated to only three O atoms and as such, are unsaturated in terms of valence electrons and bonding as compared to bulk Al atoms which are bound to six O atoms. The unsaturated Al sites on the surface are therefore strong Lewis acidic and readily accept electrons. They can readily react with water resulting in the hydroxylation of the surface at high enough partial pressures of water.

Previously published reports [50-54] indicate that water dissociatively adsorbs to form H-O_s and HO-Al_s bonds where O_s and Al_s denote initial substrate O and Al sites. Liu used X-ray photoemission spectroscopy to show that hydroxylation of the clean α-Al_2O_3 surface begins at partial pressures of water 0.0017 atm at room temperature. [50] Shen spectroscopically observed that the so-called "fully hydroxylated" surface could be formed under direct exposure to air, where the top layer Al cations are etched away by hydroxyl groups as $Al(OH)_3$. The hydrogens that result add to 2nd layer O sites to form terminal OH sites. This surface was found to be the stable form at 873 K in their sum-frequency vibration spectroscopy. [54]

Theoretical studies by Schneider [49] reported the phase diagram for α-Al_2O_3 (see Figure 3.1), and demonstrated that the surface is fully hydroxylated when the chemical potential of water (relative to isolate water chemical potential at 0 K) is greater than -

144.7 kJ/mol, while the dry/clean surface is dominant when it is chemical potential is lower than -144.7 kJ/mol.

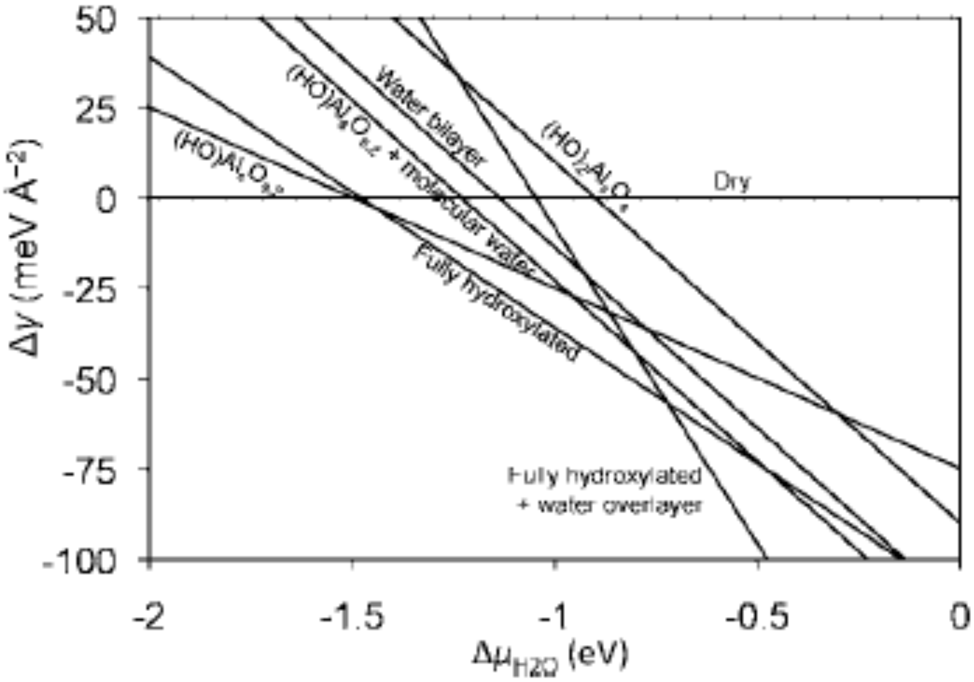

Figure 3.1 α-Al_2O_3 surface energy change vs H_2O chemical potential in different morphologies

The change in the chemical potential of water at temperature T relative to the chemical potential of water at 0 K can be calculated as [49]

$$\Delta\mu_{H_2O}(T,P) = \mu_{H_2O}(T,P) - E_{H_2O}^{DFT} \qquad \text{(Eq. 3-1)}$$

where $\mu_{H_2O}(T,P)$ equals to,

$$\mu(T,P) = \mu(T,P^0) + k_B T \ln(P/P^0) \qquad \text{(Eq. 3-2)}$$

The value of $\mu(T,P^0)$ can be approximately calculated by a linear increase in the temperature multiplied by the temperature coefficient α.

$$\mu(T,P^0) \approx \mu(298K,P^0) + \alpha(T - 298K). \quad \text{(Eq. 3-3)}$$

Previous studies by Damidot [55] and Job [56] reported the values that:

$$\mu(298K,P^0) = -228.6 \text{ kJ/mol} \quad \text{(Eq. 3-4)}$$

$$\alpha = -0.1887 \text{ kJ/mol/K} \quad \text{(Eq. 3-5)}$$

$E_{H_2O}^{DFT}$ is the internal formation energy of water at 0 K, and can be calculated as:

$$E_{H_2O}^{DFT} = E_{H_2O} - (E_{H_2} + \frac{1}{2}E_{O_2}) = -2.52 \text{ eV}. \quad \text{(Eq. 3-6)}$$

The relative chemical potential for water was calculated to be 184.3, 162.1, and 141.8 eV under in the presence of 10, 200 and 3000 ppm of water, respectively. The different partial pressures of water were chosen in order to compare with the results for reactions run at 1 atm and 893.15 K set in the UOP patents for propane dehydrogenation over zirconia [19].

The fully hydroxylated Al_2O_3 surfaces as well as the dry Al_2O_3 surfaces can both exist. The predominant surface under working conditions is set by the reaction temperatures and partial pressures of water in UOP's experiment. We examined both the dry as well as hydroxylated surfaces herein in detail. Furthermore, we examined the dry surface along with the O vacancies created by removing an O anion in the 2nd layer, in order to investigate the effects of these vacancies.

3.2 Dry/Clean α-Al_2O_3 (0 0 0 1) Surface

3.2.1 Adsorption of Reactants, Intermediates and Products onto α-Al_2O_3 Surface

The Al-terminated α-Al_2O_3 (0 0 0 1) is shown in Figure 3.2 where the Al atoms in the top layer (shown in yellow) are coordinated to 3 oxygen atoms (shown in red) in the 2nd layer; while the bulk Al atom shown in purple are coordinated to 6 O anions.

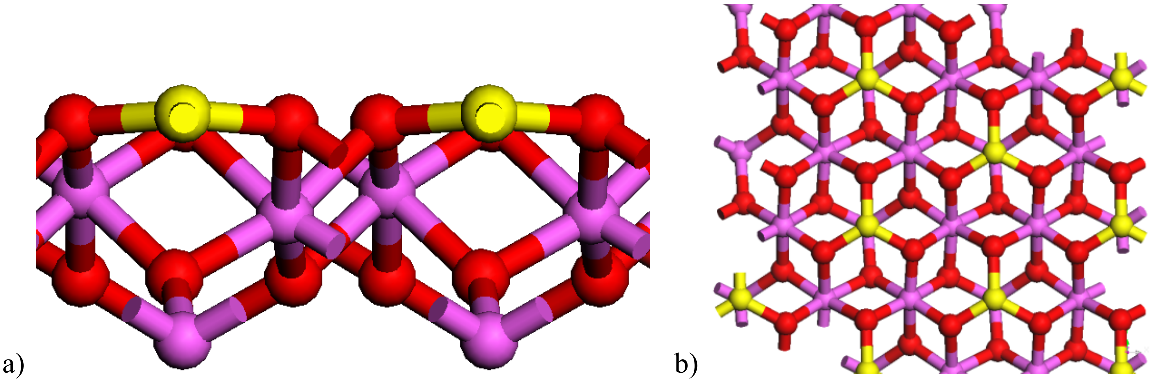

Figure 3.2 The clean α-Al_2O_3 (0 0 0 1) surface: a) Side view; b) Top view.

Note: Al (Yellow: 1st layer; Purple: 3rd, 4th, and 6th layers); O (Red: 2nd and 5th layers)

Table 3.1 Adsorption energies of reaction species on different sites of α-Al_2O_3 surface

Species-Sites	**H-O**	**H-Al**	**Propyl-O**	**Propyl-Al**
E_{ads} (kJ/mol)	-114.8	180.4	-156.3	-32.0

The adsorption energies were calculated for all of the reactants, intermediates and products by examining the binding of these species onto the surface Al sites in top-layer Al or the O sites in the 2nd-layer (see Table 3.1). The H and propyl intermediates that form as a result of C-H activation were calculated to bind strongly to the O sites on the surface, and more weakly to the Al site, respectively.

The PDH reaction is thought to proceed via the following elementary steps: the activation of the first C-H bond to generate propyl and atomic H intermediates on the surface, the activation of the C-H bond of the adsorbed propyl intermediate to form propylene and a surface bound H, the recombinative desorption of H_2 and the desorption of propylene from the surface. [28, 57, 58] The activation of the first C-H bond of propane can proceed either by heterolytic splitting to form a negatively charge propyl ($CH_3CHCH_3^{(\delta-)}$) and a positively charged hydrogen H $^{(\delta+)}$ atom that bind to the Lewis acid Al site and the more basic surface O site respectively, or by homolytic splitting to form propyl and hydrogen radicals that both bind to exposed O sites on the surface (H-O and propyl-O). The subsequent activation of the C-H bond of the propyl intermediate proceeds via homolytic C-H splitting to form propylene which desorbs and a second OH that binds to a neighboring O* site.

3.2.2 Activation of the 1st C-H Bond of Propane on α-Al_2O_3 Surface

The activation of the 1st C-H bond of propane was calculated to preferentially proceed heterolytically over an Al-O site pair (1-2 pathway) rather than homolytically over an O-O site pair (1-3 pathway). In the 1-2 pathway, the C-H bond is activated to form a propyl$^{\delta-}$ and H$^{\delta+}$ species that bind to vicinal Al$^{\delta+}$ and O$^{\delta-}$ sites, respectively to form Al$^{(\delta+)}$-propyl$^{(\delta-)}$ and O$^{(\delta-)}$-H$^{(\delta+)}$ surface intermediates (see Figure 3.3.1). The activation barrier and reaction energy for this heterolytic C-H splitting were calculated to be 101.3 kJ/mol and 2.9 kJ/mol, respectively.

In the 1-3 path, the C-H bond of propane is homolytically activated to form into propyl (δ·) and H (δ·) radicals that bind to the surface oxygen atoms and form O-propyl and O-H surface intermediates (see Figure 3.3.2). While the overall reaction energy (-26.05 kJ/mol) is slightly more favored than that for the heterolytic C-H activation (+2.9 kJ/mol), the activation barrier of 158.2 kJ/mol is 56.9 kJ/mol higher than the barrier for the heterolytic C-H activation. The lower reaction energy is due to the stronger propyl-O bond than the propyl-Al bond. The higher activation barrier associated with the homolytic activation is due to the very weak coordination between the propyl radical that forms in the transition state and the surface 1-O site as can be seen in structures in Figure 3.3.2. The calculated results are shown in Table 3.2.

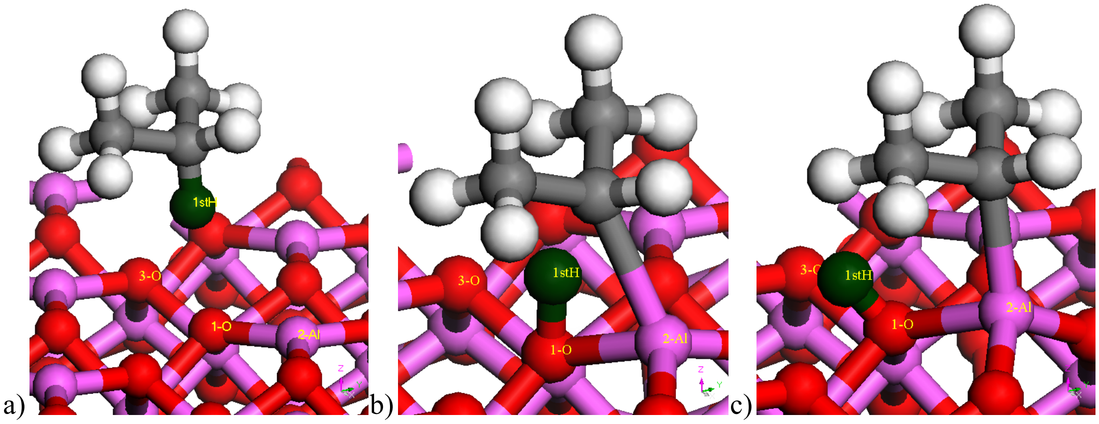

Figure 3.3.1 1-2 pathway of 1^{st} C-H activation on adjacent Al-O pair: a) Reactant, b) transition and c) product states.

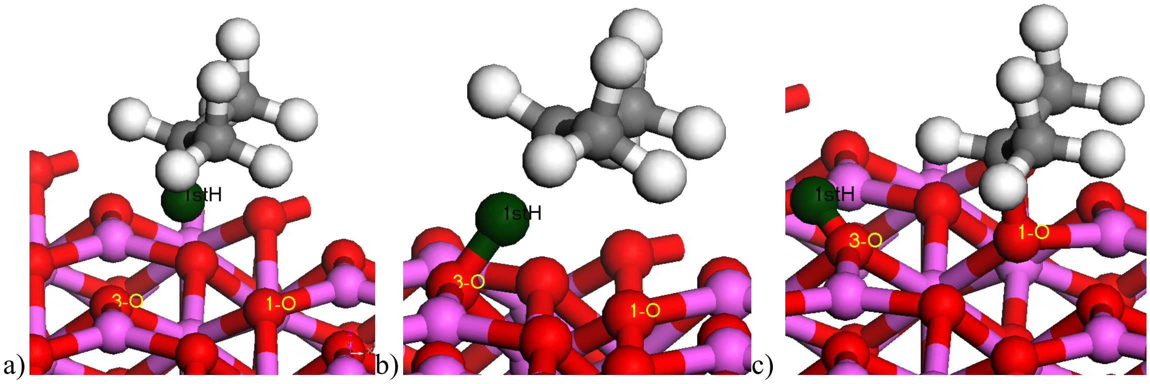

Figure 3.3.2 1-3 pathway of 1st C-H activation on two O sites: a) Reactant, b) transition and c) product states.

Notes: The C and hydrogen atoms of the alkane are shown in grey and white respectively, whereas the color of the H atom that results from C-H activation is shown in dark green. The number before the element in reaction sites is a label given in the order of closest distance to the active1-O site (e.g. 2-Al and 3-O).

Table 3.2 Energetics and transition state structures for the heterolytic (1-2) and homolytic (1-3) paths for the initial C-H activation

Path	**E_{rxn} (kJ/mol)**	**E_{act} (kJ/mol)**	**H-O (Å)**	**C-Al/O (Å)**
1-2 Path	2. 9	101.3	1.2	2.2
1-3 Path	-26.0	158.2	1.2	2.9

The H-O distance in the transition state for the heterolytic (1-2) path was calculated to be 1.2 Å which is close to H-O bond distance in the fully dissociated product state (1.0 Å), whereas the distance between the central C atom of the propyl intermediate and the Al surface site is 2.2 Å which is also quite close to propyl-Al bond length of 2.0 Å in the product state. This implies that both the 1st H and propyl are greatly stabilized by their interaction with the $Al^{(\delta+)}$ and $O^{(\delta-)}$ sites in the transition state. The homolytic C-H activation proceeds predominantly via a hydrogen abstraction from the single 3-O site. The 1-O site in the O-O pair is too far away to efficiently stabilize the $(CH_3)_2CH(\cdot)$ radical that forms in the transition state, resulting in C-O distance of 2.9 Å in the transition state as opposed to the C-O bond length of 1.5 Å for the propyl-bound product state.

A Bader charge analysis was carried out for both pathways to analyze how charges on each of the atoms change along the reaction coordinate. The results presented in Figure 3.4.1 clearly show that in the 1-2 path, propane is split into propyl anion and H cation in the transition state which is consistent with the formation of the $Al^{(\delta+)}$-$H^{(\delta-)}$ and $O^{(\delta-)}$-$H^{(\delta+)}$ product state. This can be seen by the increase in negative charge on the propyl from +0.12 e in the reactant state to -0.43 e on the transition state and the increase in the positive charge on the H from -0.19 e in the reactant state to +0.25 e in the transition state. Charge transfer occurs through the surface Al-O site pair as the positive charge on the Al is decreased from +2.26 e in the reactant state to +1.97 e in the transition state and the negative charge on the O is decreased from -1.47 e in the reactant state to -1.20 e in the transition state.

In comparison, the homolytic activation of the C-H bond proceeds over the O-O site pair via a hydrogen abstraction step, resulting in the formation of propyl and hydrogen radical like species (see Figure 3.4.2). The hydrogen atom rapidly undergoes electron transfer into the oxide upon C-H activation to form a proton that is stabilized by its interaction with the negatively charged oxygen in the transition state. The charge on the hydrogen increases from -0.14 e in the reactant state to +0.21 e in the transition state whereas the charge on the propyl intermediate only increases from 0.05 e to 0.07 e in the transition state reflecting the free radical character of the propyl group. The propyl group subsequently rebinds to the surface to form the resulting propoxide product.

In the heterolytic 1-2 path, the charge stabilization of the propyl$^{(\delta-)}$ and H$^{(\delta+)}$ intermediates formed in the transition state are significantly stabilized by the Al$^{(\delta+)}$-O$^{(\delta-)}$ site pair which result in no overall charge transfer to the Al_2O_3 substrate in the heterolytic C-H activation shown in Fig. 3.4.1 and the relatively low activation barrier of 101.3 kJ/mol. The barriers reported herein agree with previous studies by Mota [59] who indicated low barriers for the activation of light alkanes on adjacent Al-O atoms over aluminum-zeolite complex structures as well as with those from Sautet and Copéret for methane activation on γ-Al_2O_3 [24].

In the 1-3 path, the C-H activation appears to proceed homolytically resulting in the formation of a propyl species in the transition state, which has significant free radical character and is weakly held to the surface thus resulting in a negative overall charge flow of -0.77 into the oxide substrate. This leads to an activation barrier 56.9 kJ/mol higher than that for the heterolytic activation.

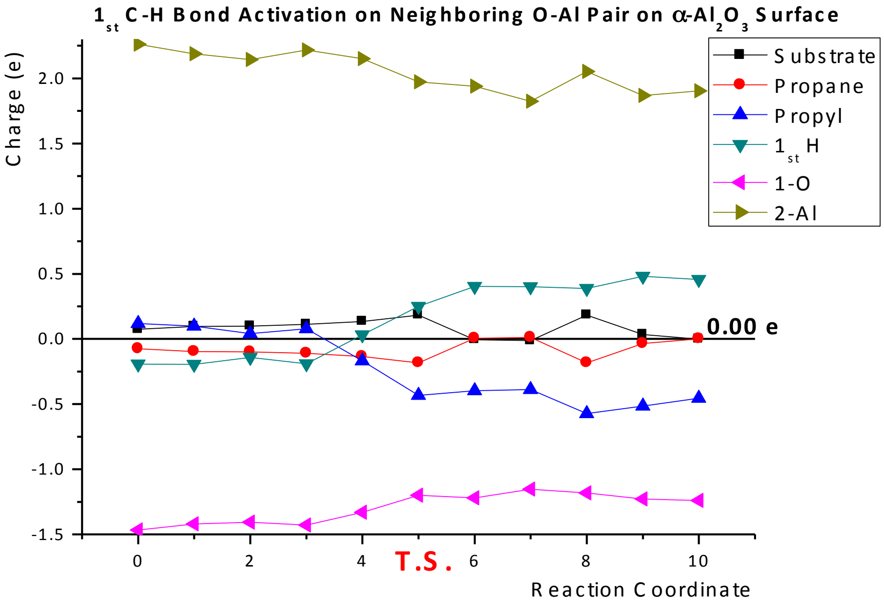

Figure 3.4.1 Bader charge analysis of 1-2 reaction path for 1st C-H activation

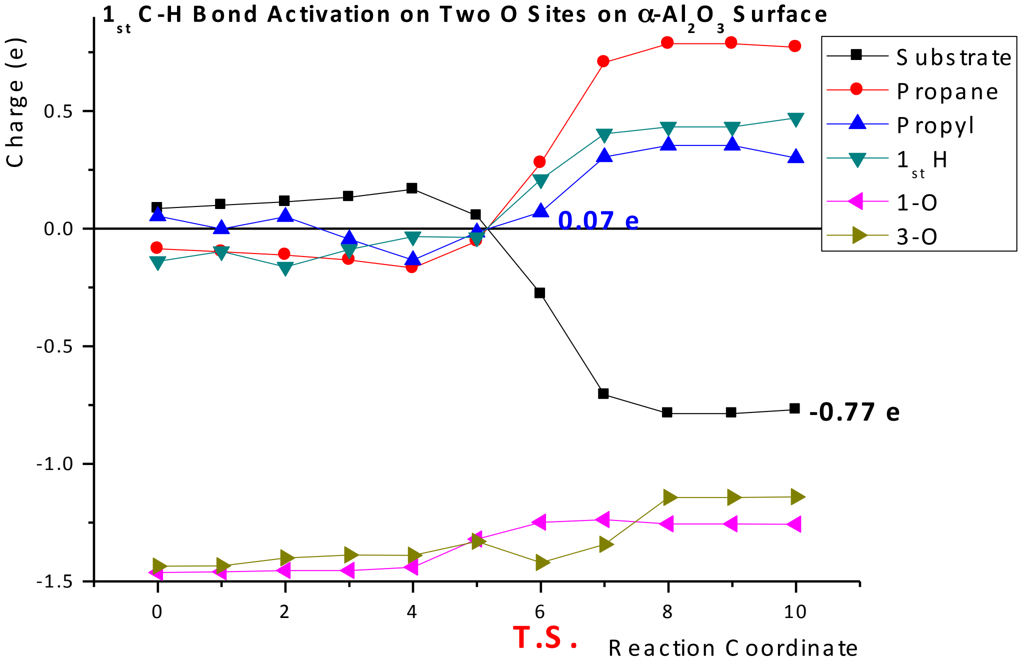

Figure 3.4.2 Bader charge analysis of 1-3 path for 1st C-H activation

3.2.3 2^{nd} C-H Bond Activation of Propane on Adjacent O Site

The Al-bound propyl intermediate that forms from the initial 1-2 heterolytic C-H activation of propane was used to examine the subsequent C-H activation to form propylene. The C-H activation in this second step was calculated to occur most favorably at an adjacent O site (see Figure 3.5). The activation barrier and the reaction energy for this second C-H activation step were also found to be moderate at 93.6 kJ/mol and -90.4 kJ/mol, respectively. The reaction results in the formation of propylene which desorbs and a surface H which is stabilized in the TS with close distances to both O site (1.4 Å) and terminal C (1.3 Å) as compared to the H-O bond length of 1.0 Å in product state and the C-H bond length of 1.1 Å in reactant state (see Table 3.3).

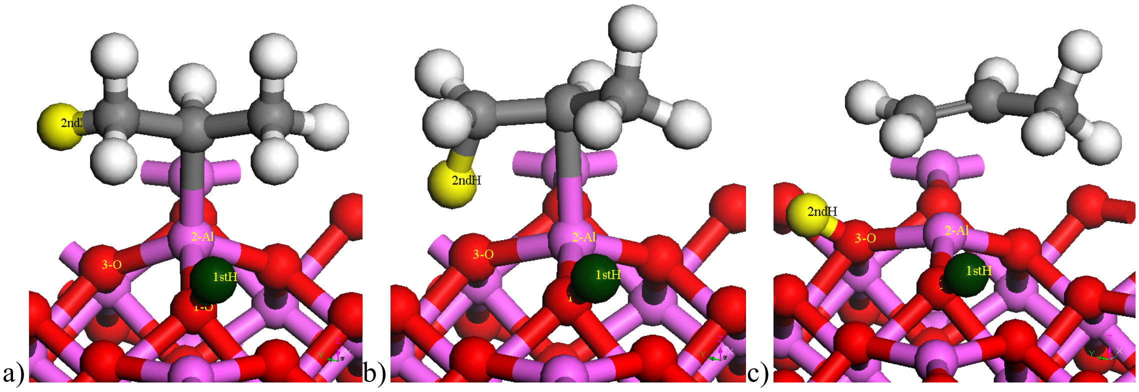

Figure 3.5 The 2^{nd} C-H bond activation on the vicinal O site: a) Reactant, b) TS and c) product states.

Table 3.3 Evolution of bond distances during the 2nd C-H activation on the vicinal O site

	Reactant	**TS**	**Product**
2nd H-O (Å)	3.1	1.4	1.0
C-Al (Å)	2.0	2.2	2.5

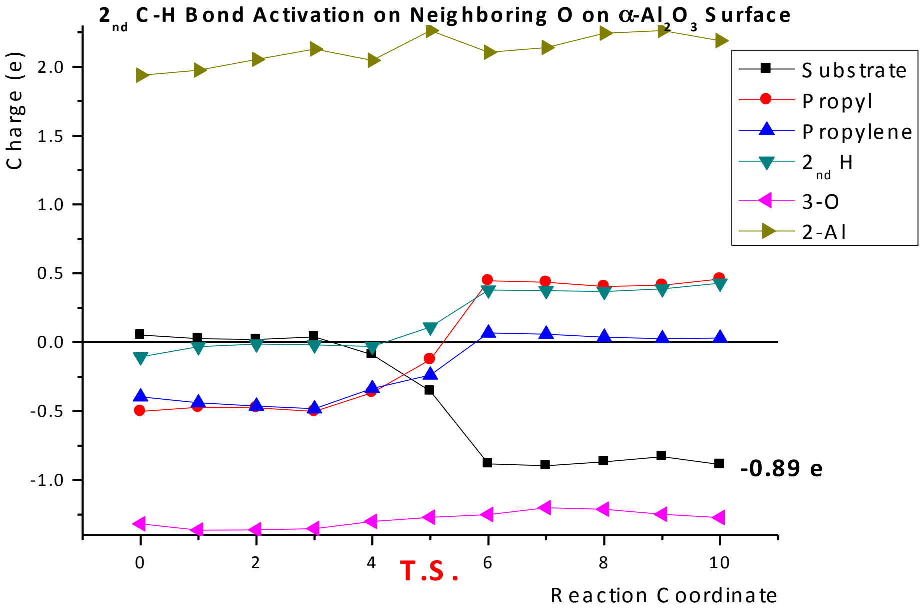

Figure 3.6 Bader charge analysis of the intermediates and Al and O atoms in the surface for the activation of C-H bond of the bound propyl intermediate over a neighboring O site

A detailed Bader charge analysis shown in Figure 3.6 indicates that this reaction proceeds homolytically as both the propylene and H species lose electron density as the reaction proceeds to ultimately form the uncharged propylene and H $^{(\delta+)}$ product, and as such there is a net charge flow (-0.89 e) into the Al_2O_3 substrate.

3.2.4 Desorption of H_2 from the Adjacent O-Al-O Triplet

In order to regenerate the active sites, both the propylene and the two H atoms bound to O sites must desorb from the surface to continue the reaction cycle. H_2 desorption requires a recombination of the two H atoms bound to the O sites. This does not occur directly, but instead requires the migration of hydrogen from the Al site to the O of the oxide substrate which has an activation barrier of 256.3 kJ/mol. The high barrier here suggests that the surface hydrogen that forms prefers to stay bound to the O sites on the surface and will not desorb as H_2. This path requires a charge transfer as the H+ migrates from the $O^{\delta-}$ to an $Al^{\delta+}$ site resulting in the formation of $H^{\delta-}$ which can then react with $H^{\delta+}$ on the neighboring $O^{\delta-}$ site.

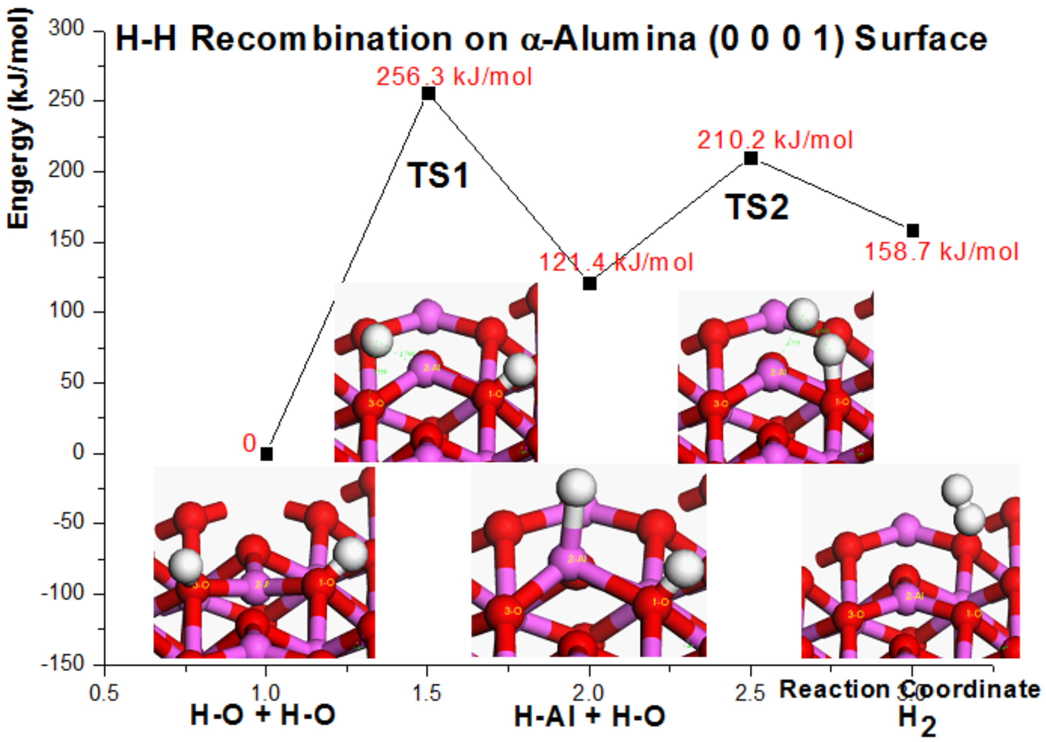

Figure 3.7 The reaction energy profile for the recombinative desorption of atomic hydrogen from the vicinal sites on the α-Al_2O_3 (0 0 0 1) surface

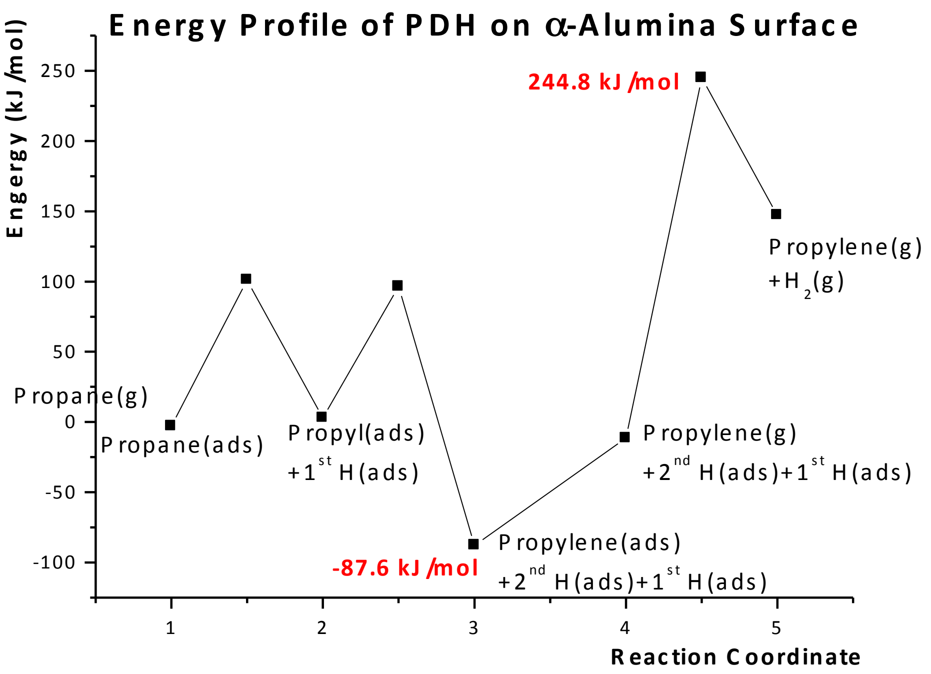

Figure 3.8 The reaction energy profile for the partial dehydrogenation of propane to propylene and hydrogen on α-Al_2O_3 (0 0 0 1) surface

The energetics for the overall 1-2 heterolytic C-H reaction path are shown in Figure 3.8. The relatively low activation barriers of 101.3 and 93.6 kJ/mol to activate the C-H bonds of propane and the resulting propyl intermediates are the result of the strong stabilization of the resulting $H^{\delta+}$ by its strong interactions with the $O^{\delta-}$ sites of the α-Al_2O_3 surface. These strong $O^{\delta-}$-$H^{\delta+}$ bonds, however, lead to the formation of very stable products (-87.6 kJ/mol), thus makes it very difficult to desorb the hydrogen atoms as H_2 from the surface. The overall apparent activation energy with respect to the gas phase propane is calculated to be 244.8 kJ/mol, and an intrinsic barrier with respect to the lowest energy point is 332.4 kJ/mol which indicates that α-Al_2O_3 (0 0 0 1) is catalytically inactive. Therefore, although both C-H bond activation steps involved in the dehydrogenation of propane to propylene have moderate barriers, the removal of H from the surface and the regeneration of reaction sites are very difficult.

The detailed charge analysis indicates that the α-Al_2O_3 (0 0 0 1) substrate is a very good electron acceptor and as such there is significant electron transfer from the reactant to the substrate during the reaction. The strong electron affinity of the Al_2O_3 surface makes it difficult for electrons to release back to the hydrogen, thus results in very high activation barriers for the desorption of H_2 which ultimately limit the propane dehydrogenation.

3.3 α-Al_2O_3 (0 0 0 1) Surface with O Vacancies

In previous studies carried out on ZrO_2, we found that oxygen vacancies which are known to be present promoted the activation of propane. [30] We examined the influence of oxygen vacancy here by removing an oxygen atom from the 2nd-layer of the α-Al_2O_3 (0 0 0 1) surface (see Figure 3.9). The removal of oxygen from the lattice resulted in a reconstruction of the surface where the 2-Al site moves closer to the 3-Ob site to help stabilize the O-vacancy.

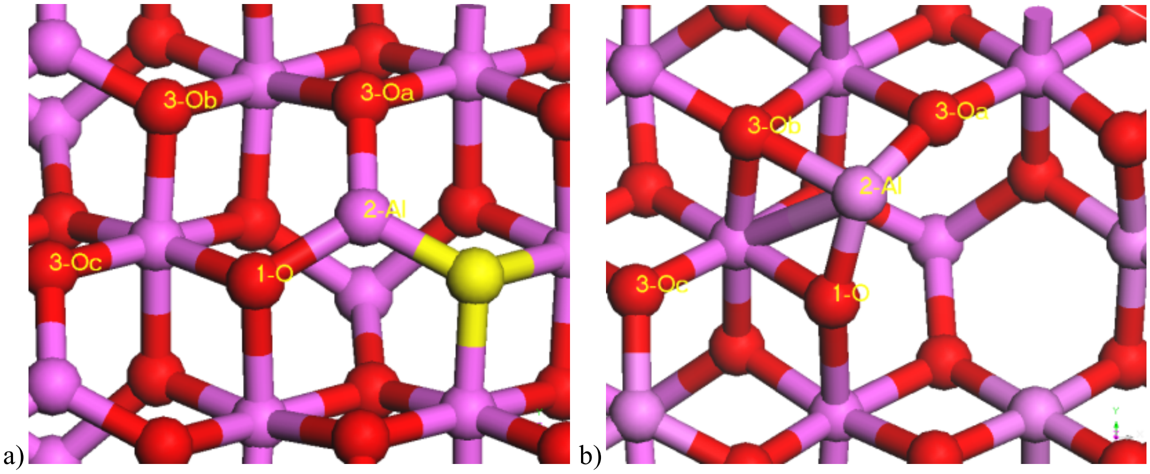

Figure 3.9 α-Al_2O_3 (0 0 0 1): a) the pristine Al_2O_3 surface; b) the Al_2O_3 surface with an O vacancy after relaxation.

Note: The yellow atom in the pristine surface is the one that is removed to generate the O-vacancy. 1-O and 2-Al sites are marked for consistency with clean surface; 3-Oa, 3-Ob, and 3-Oc are marked as potential reaction sites.

3.3.1 Adsorption of Reactants, Intermediates and Products onto α-Al_2O_3 Surface with an O-Vacancy

The adsorption of the reactant, intermediate and product species were examined on Al and O sites on the defect Al_2O_3 surface that correspond with those examined on the defect-free surface, and the results are listed in Table 3.4. The adsorption of H on 1-O site was calculated to be weaker than that on the clean surface (-56.9 kJ/mol vs -115.1 kJ/mol), and that on the other two adjacent O sites of Al is further weakened (-8.7 kJ/mol for 3-Oa and -18.3 kJ/mol for 3-Ob); while the adsorptions of H and propyl group on 2-Al site becomes much stronger (-62.2 kJ/mol vs 180.5 kJ/mol for H; -210.3 kJ/mol vs -

29.9 kJ/mol for propyl). These results are all consistent with the fact that the 2-Al site is more unsaturated on this surface and as such forms stronger bonds to an electron donator to compensate for the loss of the Al-O bond in the lattice. The adjacent O sites lose charge to 2-Al site to partially compensate and as a result they bind H more weakly. For O-3c site which is not adjacent to Al, the H binding is stronger (-59.8 kJ/mol).

Table 3.4 Adsorption energies of reaction intermediates on different sites of O-defective α-Al_2O_3 surface

Species-Sites	**H-(1-O)**	**H-(3-Oa)**	**H-(3-Ob)**	**H-(3-Oc)**	**H-(2-Al)**	**Propyl-(2-Al)**
E_{ads} **(kJ/mol)**	-56.9	-8.7	-18.3	-59.8	-62.2	-210.3

The adsorption of H was also tested on the two unsaturated inner-layer Al sites (marked as Un-Ala and Un-Alb in Figure 3.10), which were found to be very weak (positive at 58.9 kJ/mol). It would be very difficult for H to form bridge bonds with these two Al sites, and, in addition, this path resulted in a high activation energy of 165.0 kJ/mol for the 1st C-H bond activation in subsequent calculations.

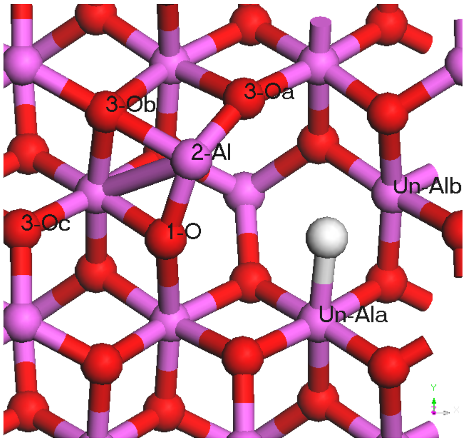

Figure 3.10 H bridge-bonding with two unsaturated inner-layer Al sites on α-Al_2O_3 with O vacancy

3.3.2 Propane Dehydrogenation on α-Al_2O_3 Surface with O Vacancy

Similar to results for the ideal α-Al_2O_3 surface, the 1st C-H bond activation step occurs via the heterolytic splitting over the Al-O site pair to form a metal-alkyl and O-H intermediates as is shown in Figure 3.11 and Table 3.6. The stronger binding of propyl on 2-Al site near the O-vacancy increases the exothermicity of this reaction (from 2.9 kJ/mol from the results on the clean surface to -153.2 kJ/mol on the surface with O-vacancies) and lowers the activation barrier (from 101.3 to 21.2 kJ/mol) (see Table 3.5). The second C-H bond breaking step is still favored on a nearby 3-Oc site (Figure 3.12), but the activation energy increases from 93.6 kJ/mol on the ideal α-Al_2O_3 surface to 208.4 kJ/mol near the O* vacancy, and the reaction energy also increases from -90.4 kJ/mol to 143.6 kJ/mol. This is the result of the weaker H binding to 3-Oc site near the O* vacancy.

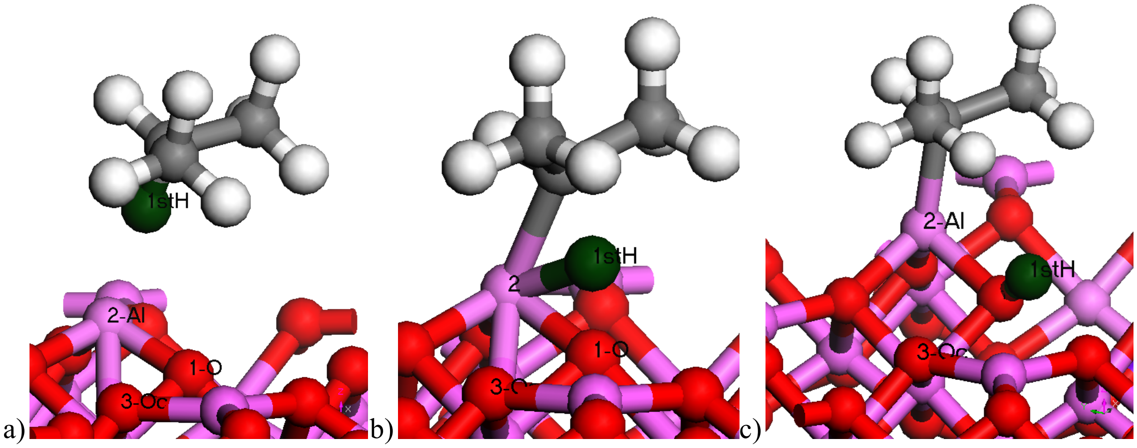

Figure 3.11 The 1st C-H bond activation on α-Al_2O_3 surface with O vacancy: a) reactant, b) transition and c) product states.

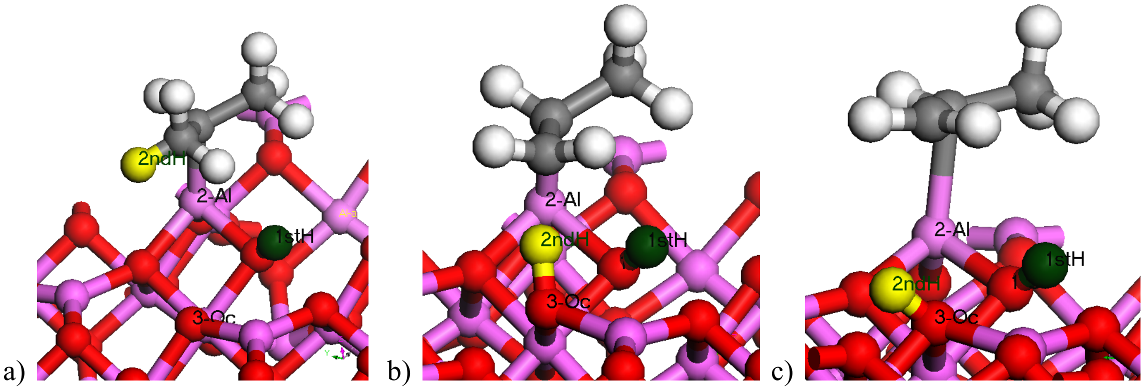

Figure 3.12 The activation of the terminal C-H bond of the propyl intermediate on a vicinal O on the defect Al_2O_3 surface: a) reactant, b) transition and c) product state.

Table 3.5 Reaction and activation energies of C-H activation on O-Al pair on O-defective α-Al_2O_3 surface

	E_{rxn} (kJ/mol)	E_{act} (kJ/mol)
1st C-H Activation	-153.2	21.2
2nd C-H Activation	143.6	208.3

Table 3.6 Evolution of bond distances during the 1st C-H activation on Al-O pair site on O-defective α-Al_2O_3 surface

	Reactant	**TS**	**Product**
1st H-O (Å)	2.7	1.3	1.0
C-Al (Å)	3.1	2.1	2.0

Table 3.7 Evolution of bond distances during the 2nd C-H activation on a vicinal O site on O-defective α-Al_2O_3 surface

	Reactant	**TS**	**Product**
2nd H-O (Å)	3.7	1.1	1.0
C-Al (Å)	2.0	2.0	2.1

Detailed Bader charge analyses on both C-H activation steps reported in Fig. 3.13.1 and 3.13.2 confirmed that the reaction proceeds via the heterolytic and homolytic C-H bond activation steps to ultimately form propylene and hydrogen. The first C-H activation step proceeds by the heterolytic C-H activation of propane as the propyl species becomes negatively charged changing from +0.28 e in the reactant state to -0.27 e in the transition state and -0.50 e in the product state whereas the H becomes positively charged changing from -0.33 e in reactant state to -0.010 e in the transition state and +0.32 e in the product state (see Fig. 3.13.1). In the second C-H activation step (Fig. 3.13.2), the anionic propyl intermediate transfers charge back to the substrate as is changes in charge from -0.62 e in the reactant state to -0.22 e in the transition state to +0.27 e in the product state. The resulting hydrogen that binds to the surface becomes protonic thus changing from -0.07 e in the reactant state to +0.26 e in the transition state and +0.51 e in the product state. As a result, there is a net injection electron density into the surface as the charge changes from +0.19 e to -0.61 e in the product state. As was the case for the ideal α-Al_2O_3 surface, there is a significant transfer of negative charge from propane to substrate after 2nd C-H activation (-0.61 e). While the vacancies in the α-Al_2O_3 surface change the resulting energetics, they do not change the mechanisms as the surface is still a strong electron acceptor which limits its overall rate.

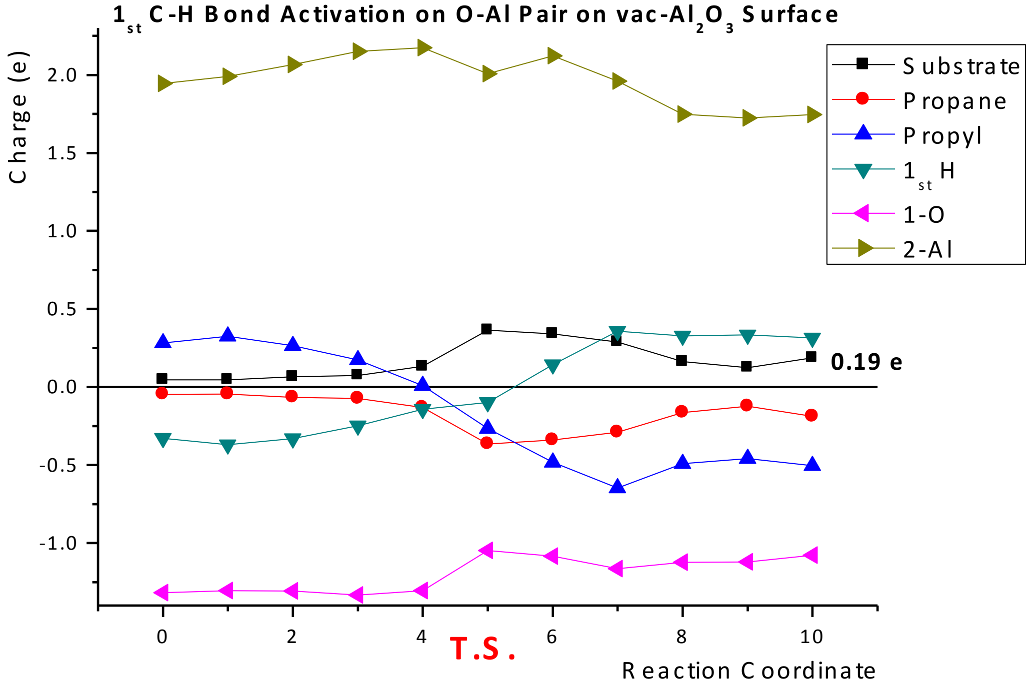

Figure 3.13.1 Bader charge analysis for the 1st C-H bond breaking on the defect surface

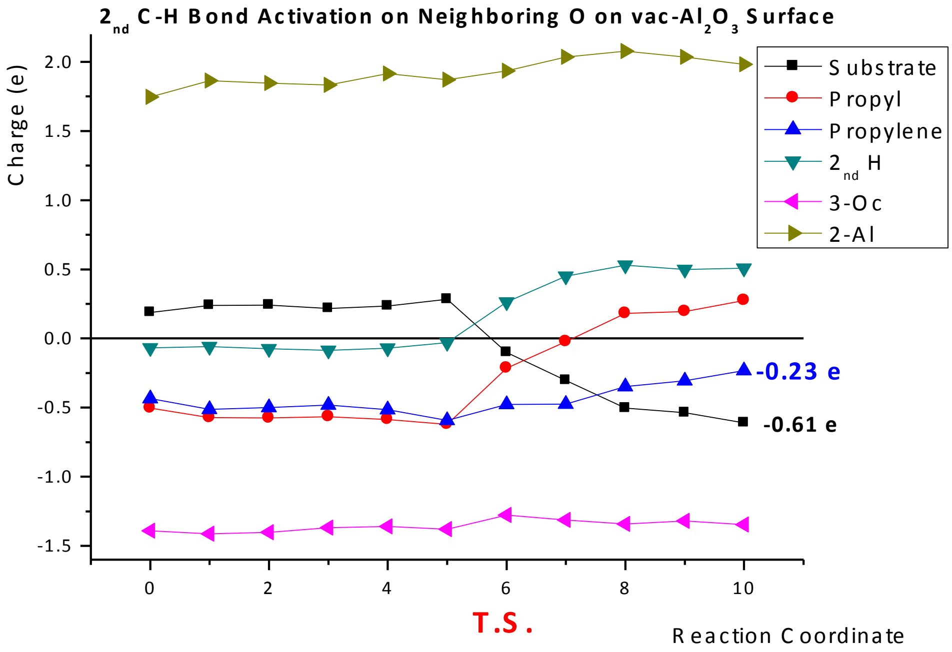

Figure 3.13.2 Bader charge analysis for the 2nd C-H bond breaking on the defect surface

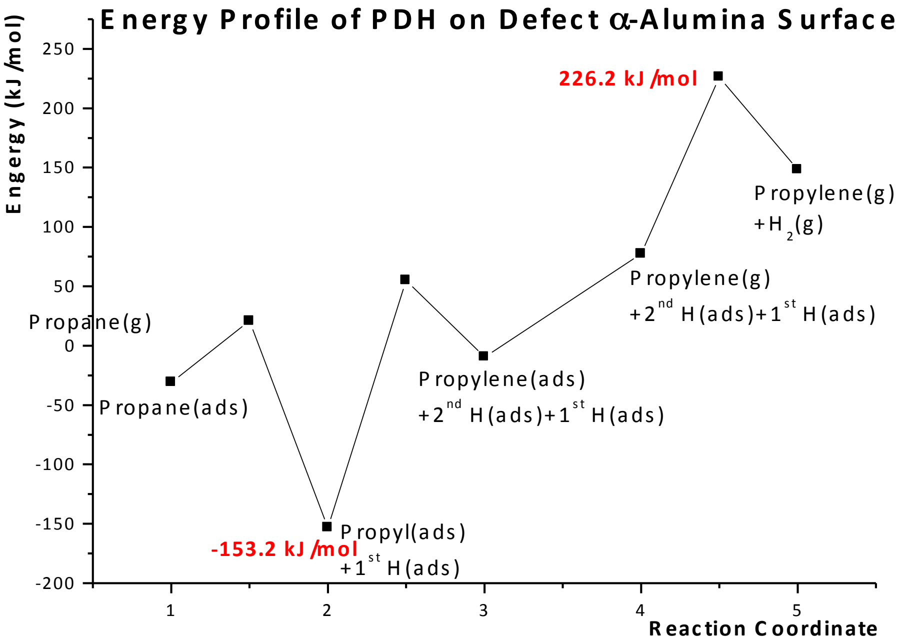

Figure 3.14 Energy profile of PDH reaction cycle on defect α-Al_2O_3 surface

After the activation of both C-H bonds and the desorption of propylene, there are two H left on 1-O site and 3-Oc site. Similarly to the results found for the perfect Al_2O_3 surface, the two H atoms cannot recombine directly. One of the hydrogens must first diffuse to Al site where there is electron transfer from the Al to the H to form $H^{\delta-}$. This is followed by the associative recombination of the $H^{\delta+}$ and $H^{\delta-}$ and the removal of H_2. The highest energy is still the transition state for H transfer to Al site which has an overall barrier of 226.2 kJ/mol. The barrier measured with respect to the lowest energy adsorbed state (-153.2 kJ/mol of propyl* + H*), however, is still very high at 379.4 kJ/mol (see Figure 3.14), indicating very little activity under reaction condition.

Therefore, while the O vacancies in α-Al_2O_3 surface weaken the binding of H to the O sites, this is offset by the increase the Al-propyl bond strength. Although the intrinsic barrier for the desorption of H_2 on the defect surface alone is not very high, the barrier from the adsorbed state is very high due to the low energy well in 1st C-H activation.

In summary, these two cases both suggest that the binding energies for the reaction intermediates (H and propyl) on the pristine Al_2O_3 surface and Al_2O_3 surface with oxygen vacancies are too strong and as such they inhibit catalytic turnover required from PDH reaction.

3.4 The Fully Hydroxylated α-Al_2O_3 (0 0 0 1) Surface

In the first two systems examined, we assumed that the ideal Al-terminated α-Al_2O_3 is the most favorable under reaction conditions. The presence of water, however, can significantly alter the composition of the Al_2O_3 surface. The dissociative adsorption of water was first examined on the clean Al_2O_3 surface. Water strongly interacts with the Al_2O_3 surface and dissociates over the Al-O site pair with an activation barrier of only 10.6 kJ/mol, which is consistent with previous reports that indicate that the α-Al_2O_3 is readily hydroxylated [50, 51].

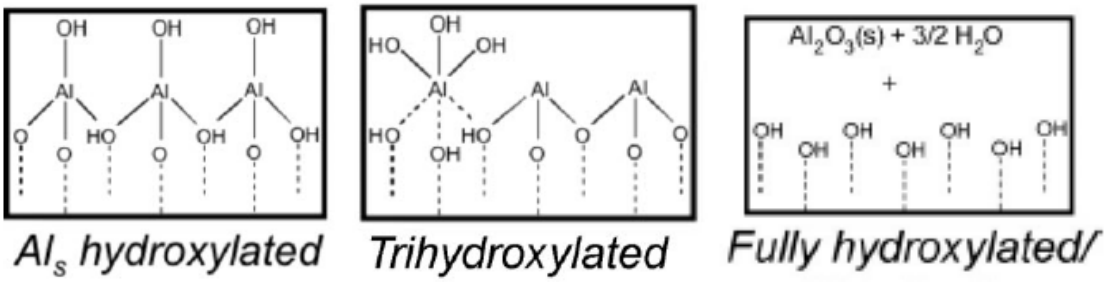

Figure 3.15 The formation process of OH-terminated fully hydroxylated surface [49]

The subsequent dissociation of water can proceed and go on to form a fully hydroxylated surface. The path responsible as suggested by Schneider [49] is shown in Figure 3.15. The initial dissociative adsorption of water onto an Al-O site pair weakens the neighboring Al-O sites thus allowing 2^{nd} and 3^{rd} water molecules to dissociately adsorb at vicinal Al-O sites. This further weakens their Al-O bonds and promotes the etching of the top-layer Al atoms resulting in $Al_2O_3(s) + 3/2H_2O$ and leaving a hydrogenated 2^{nd} layer O sites exposed as new OH terminal sites.

From this model, we were able to construct a fully hydroxylated surface (see Figure 3.16): first, all of the Al atoms in the top layer of the pristine Al_2O_3 (0 0 0 1) surface were removed to mimic the etching of Al sites; the resulting terminal oxygens were then capped with H atoms to generate the fully OH terminated surface. The terminal

OH sites have two different configurations as is reported in the literature [49]: 2/3 of them are roughly perpendicular to the surface, and the left 1/3 of them are tilted from the surface normal and roughly parallel to the surface.)

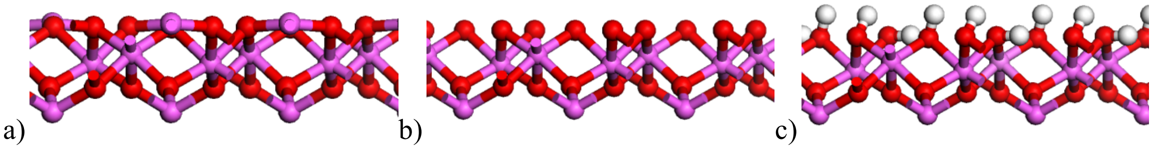

Figure 3.16 Construction of OH-terminated fully hydroxylated α-Al_2O_3 surface: a) Clean Al-terminated surface, b) Top-layer Al atoms removed and c) Fully hydroxylated OH-terminated surface.

3.4.1 Adsorption of Reactants, Intermediates and Products onto the Fully Hydroxylated α-Al_2O_3 Surface

There are no exposed Al or O sites on the fully hydroxylated surface so the only possible sites on the surface that can carry out the reaction are the surface hydroxyl groups. As shown in Figure 3.16, there are two configurations for OH groups: perpendicular and parallel. In order for a resulting propyl intermediate to bind to the perpendicular OH sites, it would need to take on a nearly parallel configuration. This would result in strong steric repulsion between propyl and terminal OH groups. In contrast, it would be much easier for propyl to bind to the parallel OH group thus relieving steric repulsion effects. Therefore, the parallel OH sites were chosen to be the binding site for the resulting propyl that forms upon the activation of the C-H bond of propane. The binding energy of the propyl at this site is quite strong at -118.9 kJ/mol vs -32.0 kJ/mol on Al site on the pristine dry Al_2O_3 surface (see Table 3.8). For H, both parallel and perpendicular OH groups were examined as the H is significantly smaller than the propyl group and as such can bind to both sites. The hydrogen binding energies at these two sites are both about -70.4 kJ/mol, which is weaker than hydrogen binding to an O site on the dry surface (-115.1 kJ/mol).

Table 3.8 Adsorption energies of reaction intermediates on OH sites of fully-hydroxylated α-Al_2O_3 surface

Species-Sites	**H-OH**	**Propyl-OH**
E_{ads} (kJ/mol)	-70.4	-118.9

3.4.2 Propane Dehydrogenation on Fully Hydroxylated α-Al_2O_3 Surface

The closest OH pair that can activate the secondary C-H bond of propane are shown as shown in Figure 3.17.

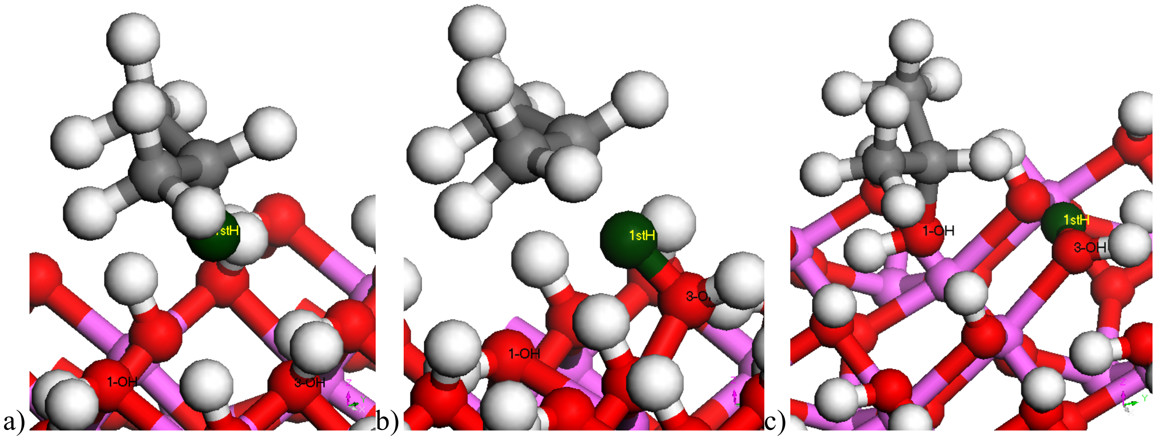

Figure 3.17 1^{st} C-H activation on a fully hydroxylated Al_2O_3(0 0 0 1) surface: a) the reactant state, b) the transition state and c) the product state.

Table 3.9 Evolution of bond distances during the 1st C-H activation on two OH sites of fully-hydroxylated α-Al_2O_3 surface

	Reactant	**TS**	**Product**
1st H-OH (Å)	2.6	1.2	1.0
C-OH (Å)	3.6	3.1	1.5

Although the binding energies of H and propyl are quite strong on OH sites, there is a significant barrier (181.4 kJ/mol) required to activate the C-H bond (see Table 3.10). This is due to the formation of an unstable propyl species in the TS where the closest distance between the central carbon and the OH group in the transition state is 3.1 Å versus the 1.5 Å C-OH bond length in the product state (see Table 3.9). A Bader charge analysis confirmed that this reaction proceeds via the homolytic C-H activation at the two O sites. The results in Fig. 3.18 show that that the propyl species in the transition state is essentially a free radical (0.08 e). The resulting propyl and hydrogen products that bind to the surface oxygens are cationic in nature both with charges of ~ +0.4 e, leading to an electron charge transfer from propane molecule into the oxide surface (-0.86 e). (Figure 3.18)

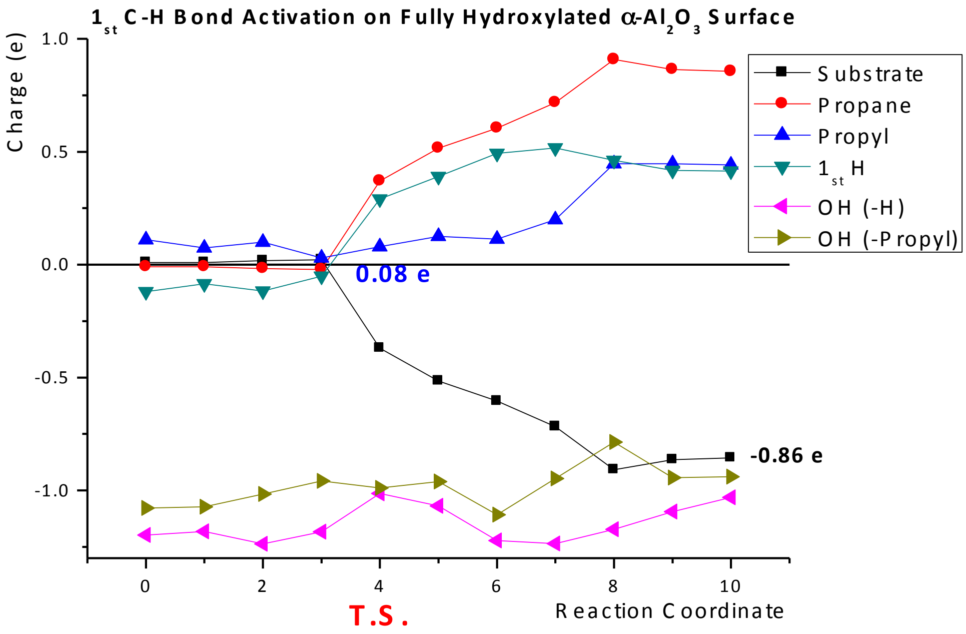

Figure 3.18 Bader charge analysis of 1st C-H activation on the fully hydroxylated α-Al_2O_3 surface

Table 3.10 Reaction and activation energies of C-H activation on fully-hydroxylated α-Al_2O_3 surface

	E_{rxn} (kJ/mol)	E_{act} (kJ/mol)
1st C-H Activation	37.6	181.4
2nd C-H Activation	-52.1	115.8

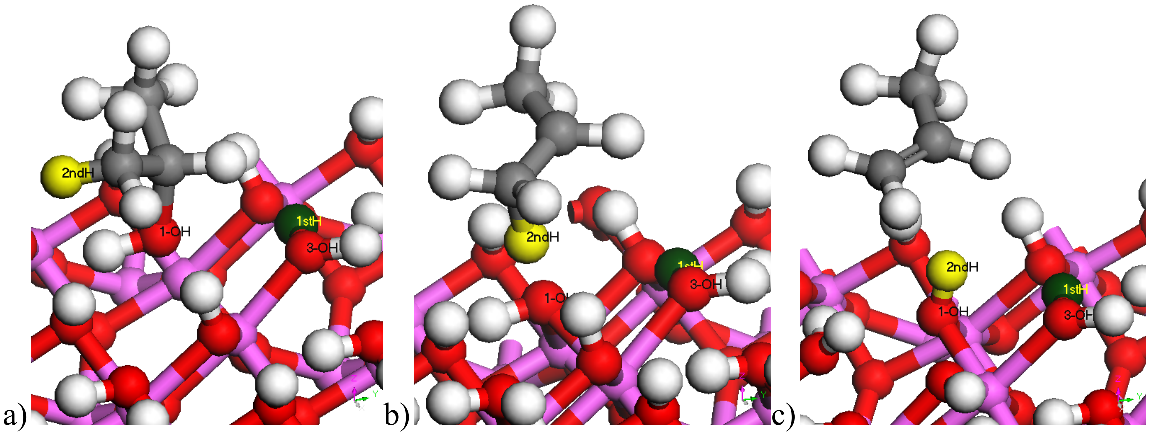

Figure 3.19 The activation of a terminal C-H bond of bound propyl surface intermediate on the fully hydroxylated Al_2O_3 (0 0 0 1) surface: a) the reactant state, b) the transition state and c) the product state.

Table 3.11 Evolution of bond distances during the 2nd C-H activation on the OH site on fully-hydroxylated α-Al_2O_3 surface

	Reactant	**TS**	**Product**
2nd H-OH (Å)	2.7	1.6	1.0
C-OH (Å)	1.5	3.1	3.9

The preferred site to activate the C-H of the bound propyl intermediates was calculated to be the same OH species that binds the propyl group from the 1st step (see Figure 3.19). The activation of the terminal C-H bond of the bound propyl surface intermediate weakens the interaction of the propyl to the surface hydroxyl group, thus results in the formation of propylene which desorbs and a hydrogen atom that binds to the initial OH site. The reaction energy for this step is rather low at -52.1 kJ/mol, and the activation energy is moderate at 115.8 kJ/mol (see Table 3.10). The moderate barrier is due to the well stabilized 2^{nd} H in the transition state, since it is still bound to propyl with a distance of 1.2 Å, plus it is also not far from the target OH (1.6 Å) (see Table 3.11).

A Bader charge analysis indicates that there is proton transfer as the propylene fragment of the propyl group is initially positively charged in the reactant state but becomes charge-neutral in the product state as hydrogen is transferred as a proton from the propyl to an OH site on the Al_2O_3 surface. In the product, the propylene molecule is neutral and 2^{nd} H binding to the surface hydroxyl group is cationic in nature, resulting in a significant amount of charge transfer into the oxide surface (-0.98 e). (Figure 3.20)

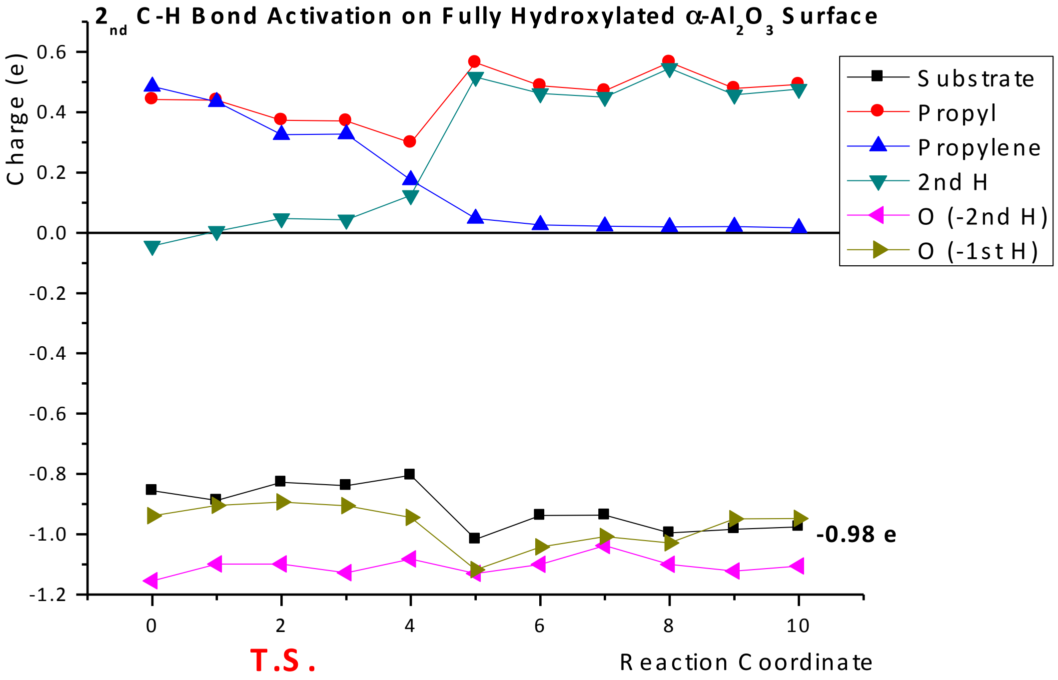

Figure 3.20 Bader charge analysis of the C-H activation of the bound propyl intermediate to form propylene and hydrogen on the fully hydroxylated α-Al_2O_3 surface

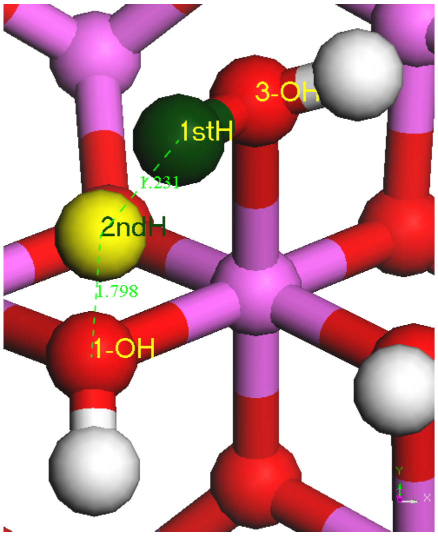

Figure 3.21 TS of H_2 recombination on the fully hydroxylated α-Al_2O_3 surface

The hydrogens that result from the C-H bond activations are strongly held to OH sites on the surface. The recombination of the two hydrogens is difficult as there is only a weak stabilization of the transition state shown in Figure 3.21. While the 1^{st} H strongly interacts with its initial 3-O center (0.97 A), the distance between the 2^{nd} H and its 1-O center is rather long at 1.8 Å. As a result, the barrier for this reaction is extremely high at 338.2 kJ/mol. It is even higher than that on the dry surface. In the end, the total barrier for reaction cycle is the same as that for this step (338.2 kJ/mol) (see Figure 3.22), suggesting that the fully hydroxylated surface is inactive.

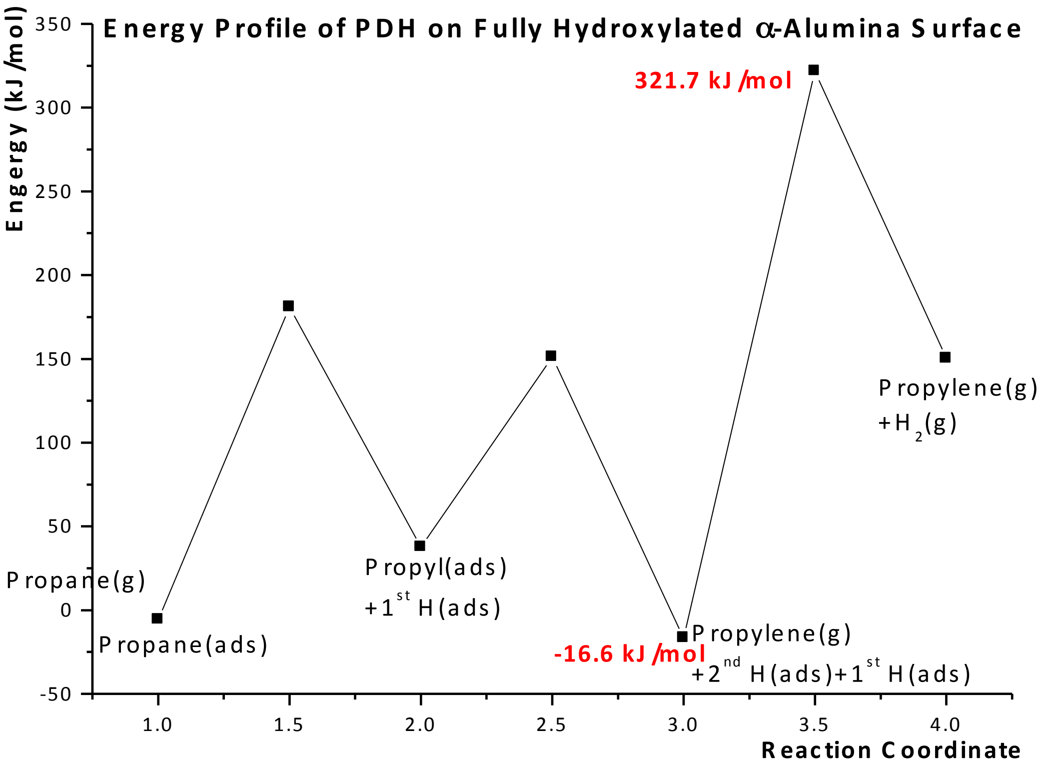

Figure 3.22 The reaction energy profile for the PDH reaction cycle on fully hydroxylated α-Al_2O_3 surface

A charge transfer analysis suggests that there is significant charge transfer into the Al_2O_3 substrate with an injection of -0.98 e after two C-H bond activation steps. This charge is transferred back as two protons are combined to form H_2 similar to the results found on the non-hydroxylated surfaces. The results indicate that all of the α-Al_2O_3 surfaces examined are good electron acceptors. While this tends to help in the initial activation of the C-H bonds, it results in an overbinding of the products which ultimately inhibit or block propane dehydrogenation.

3.5 Conclusions for α-Al_2O_3 Surfaces

The DFT results reported herein are consistent with the experimental results from UOP which showed that the likely α-Al_2O_3 surfaces present under reaction conditions are not active for the PDH reaction. The dry, fully hydroxylated and surfaces with oxygen vacancies all indicate that while C-H activation can proceed, these reactions are ultimately blocked by surface intermediates formed under reaction conditions.

The results on the anhydrous α-Al_2O_3 surface indicate that the formed hydrogen atoms bind too strongly to the O sites resulting in a very stable low energy state, thus prevents the recombination of H and the desorption of H_2. On the anhydrous α-Al_2O_3 surface with O* vacancies, the O-H bonds are weaker, but this is compensated by the strong Al-propyl bonds thus increases the overall barrier for the desorption of the propylene. The results from the fully hydroxylated surface indicate that neither H nor propyl binds too strongly to the surface and as such there is no deep energy well formed. The H_2 recombination, however, must proceed through 1-3 reaction leading to the formation of unstable H in the TS, thus the activation barrier for this step is extremely high. The high barriers that result from activating strong O-H bonds to form H-H as well as the unstable transition states hinder the overall catalytic activity for PDH reaction cycle.

From the aspect of charge evolution during reaction, all these substrates appear to be good electron acceptors, and thus there is a strong flow of charge into the Al_2O_3 surface during the C-H bond activation reactions on all the substrates studied. The results suggest that the significant charge transfer to the surface hinders catalytic turnover in the PDH reaction.

Chapter 4 PDH on α-Cr_2O_3 (0 0 0 1) Surface

The crystalline α-Cr_2O_3 (0 0 0 1) structure is very similar to the structure of α-Al_2O_3 (0 0 0 1) and is thought to be one of the active surfaces in the commercial CrO_x/Al_2O_3 catalyst. [23, 60-62] We therefore examined and compared the reactivity of the α-Cr_2O_3 with that of α-Al_2O_3 in order to understand the factors that control the catalytic activity of these materials.

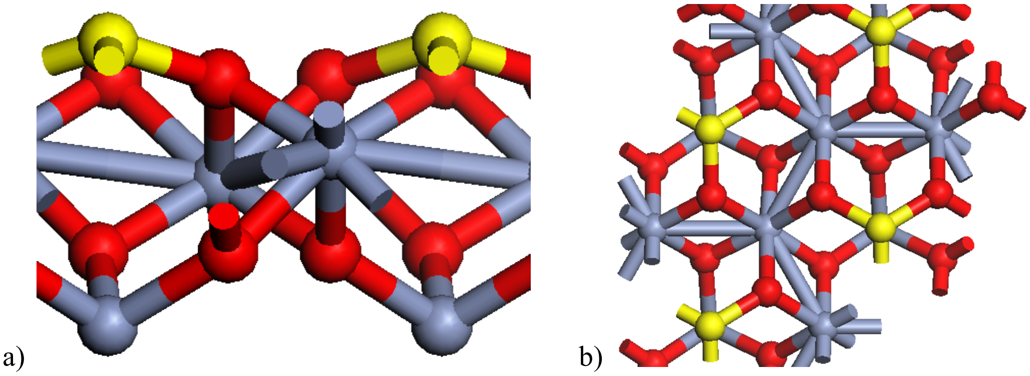

Figure 4.1 Structure of α-Cr_2O_3 (0 0 0 1) after relaxation: a) Side view; b) Top view.

Note: Cr (Yellow: 1st layer; Grey: 3rd, 4th, and 6th layers), O (Red: 2nd and 5th layers)

4.1 Adsorption of Reactants, Intermediates and Products onto α-Cr_2O_3 Surface

We compared the binding energies for different reaction intermediates in the activation of propane on the anhydrous α-Al_2O_3 and the α-Cr_2O_3 surfaces. The results indicate that hydrogen does not bind to the O site on the α-Cr_2O_3 as the adsorption energy is 82.0 kJ/mol. It binds instead to the Cr cation site with binding energy of -78.2 kJ/mol. This is characteristically different than on α-Al_2O_3 where H binds very strongly to the O (-114.8 kJ/mol) but does not interact favorably with the cationic Al center (180.4 kJ/mol). The binding energies for propyl on α-Al_2O_3 and α-Cr_2O_3 surfaces are also quite different. The propyl binds strongly to the cationic Cr center (-246.0 kJ/mol); while propyl bound to the O site was found to be unfavorable ultimately leading to a significant surface reconstruction which prevented calculating an actual value ("N/A" in Table 4.1). The propyl binds much weaker to the cationic Al site (-31.8 kJ/mol) and stronger to the O site (-156.3 kJ/mol) on α-Al_2O_3 than on the Cr and O-sites of the α-Cr_2O_3 surface.

Table 4.1 Comparison of the DFT-calculated binding energies for important intermediates in the activation of propane over the α-Cr_2O_3 (0 0 0 1) and α-Al_2O_3 (0 0 0 1) surfaces

E_{ads} (kJ/mol)	**H-O**	**H-Cation**	**Propyl-Cation**	**Propyl-O**
α-Cr_2O_3	82.0	-78.2	-246.0	N/A
α-Al_2O_3	-114.8	180.4	-31.8	-156.3

4.2 C-H Activation of Propane on α-Cr_2O_3 Surface

The initial activation of the secondary C-H bond of propane can proceed via either the 1-2 path on an adjacent Cr-O pair or via the 1-5 path over the two nearest Cr sites and as such both sites were examined. The 1-2 path was calculated to be the preferred path as the initial activation barrier (119.6 kJ/mol) is lower than that on the 1-5 path (156.3 kJ/mol) (see Table 4.3). The differences are due to the fact that both the propyl and H species that form are much more stably bound to the Cr and O centers as $Cr^{\delta+}$-$C^{\delta-}$ and $O^{\delta-}$-$H^{\delta+}$ site pairs in the transition state for the 1-2 path; the 1-5 path results in unstabilized propyl in the transition state (see Figure 4.2.1-4.2.2 and Table 4.2). The results are similar to those found on α-Al_2O_3 as the reaction predominantly proceeds via the heterolytic splitting of the C-H bond over adjacent metal-O pair. The results from a Bader charge analysis confirmed that the reaction proceeds via a heterolytic mechanism involving the formation of a propyl anion and H cation in TS.

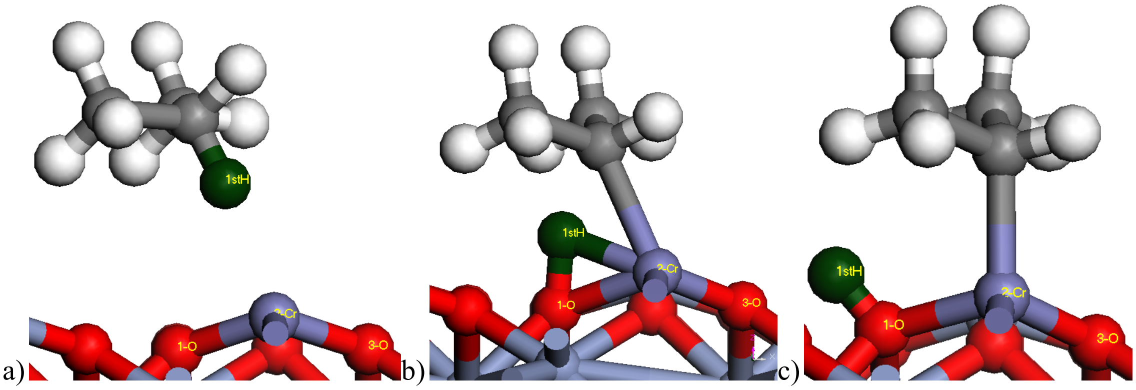

Figure 4.2.1 The activation of the first C-H bond of propone via the heterolytic 1-2 pathway on neighboring Cr-O pair: a) the reactant, b) the transition state and c) the product state.

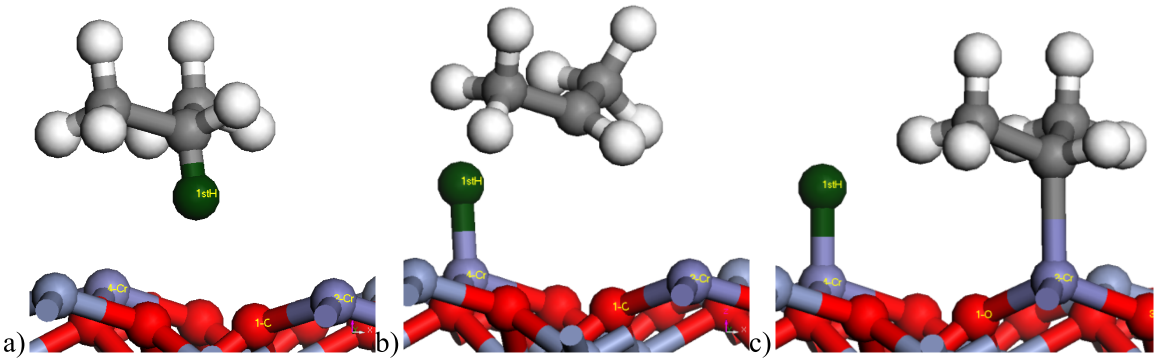

Figure 4.2.2 The activation of the secondary C-H bond of propane via the homolytic 1-5 pathway on two nearest Cr sites: a) the reactant, b) the transition state and c) the product state.

Table 4.2 Energetics comparison between the heterolytic (1-2) and homolytic (1-5) paths for the initial C-H activation on α-Cr_2O_3 surface

Path	E_{rxn} **(kJ/mol)**	E_{act} **(kJ/mol)**
1-2 Path	45.7	119.6
1-5 Path	-118.0	156.3

Table 4.3 Evolution of bond distances during the 1st C-H activation through different paths on α-Cr_2O_3 surface

Path	**Bond Distance**	**Reactant**	**TS**	**Product**
1-2 Path	**1st H-O (Å)**	2.7	1.2	1.0
	C-Cr (Å)	3.3	2.2	2.0
1-5 Path	**1st H-Cr (Å)**	2.5	1.6	1.6
	C-Cr (Å)	4.3	3.8	2.0

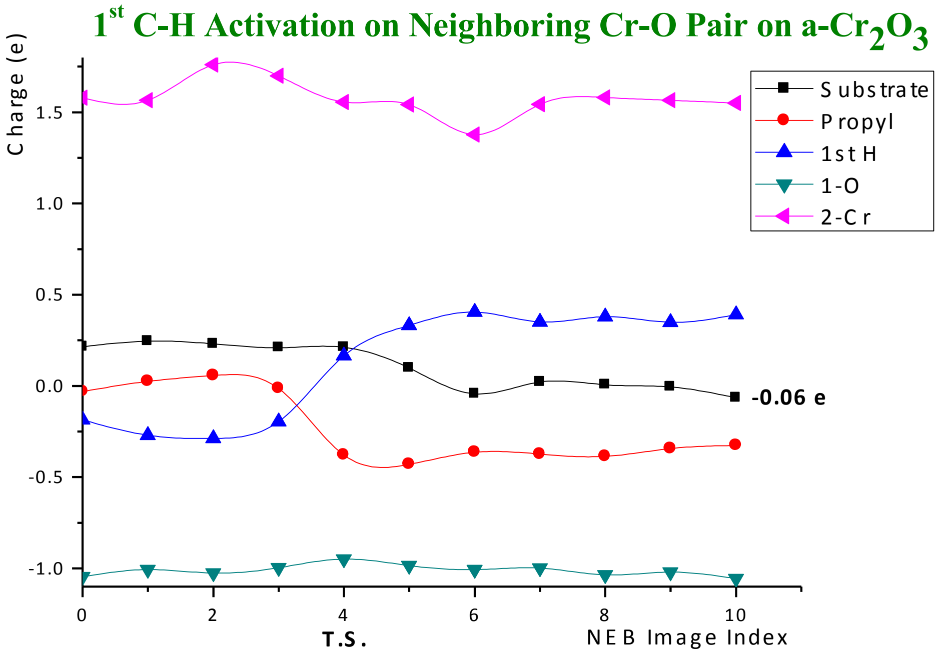

Figure 4.3 Bader charge analysis of the activation of the 1st C-H bond of propane over the Cr-O pair on α-Cr_2O_3 surface

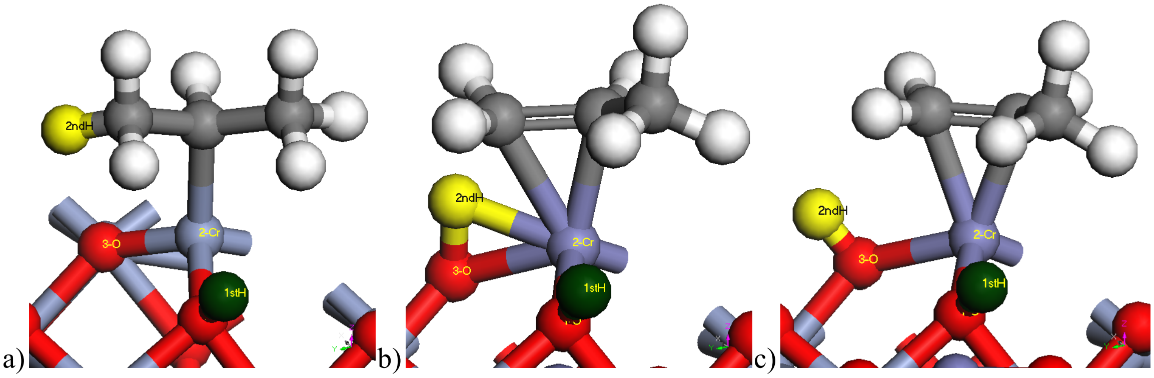

Figure 4.4.1 The activation of the C-H bond of the bound propyl intermediate at an adjacent O site: a) the reactant, b) the transition state and c) the product state to form a bound propylene product.

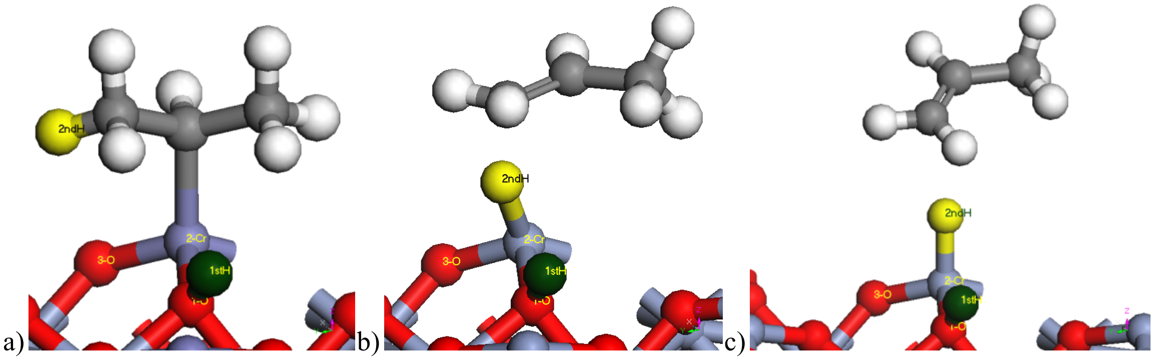

Figure 4.4.2 The activation of the C-H bond of the bound propyl intermediate direct at the Cr center via C-H insertion: a) the reactant, b) the transition state and c) the product state.

Table 4.4 Energetics comparison between the 2nd C-H activation of propane on different sites on α-Cr_2O_3 surface

Path	E_{rxn} **(kJ/mol)**	E_{act} **(kJ/mol)**
2nd H-O Path	113.1	164.0
2nd H-Cr Path	119.8	202.6

Table 4.5 Evolution of bond distances during the 2nd C-H activation of propane through different paths on α-Cr_2O_3 surface

Path	**Bond Distance**	**Reactant**	**TS**	**Product**
2nd H-O Path	**2nd H-O (Å)**	3.0	1.2	1.0
	C-Cr (Å)	2.0	2.0	2.1
2nd H-Cr Path	**2nd H-Cr (Å)**	3.1	1.6	1.6
	C-Cr (Å)	2.0	3.2	4.8

Two different pathways were also tested for the subsequent C-H bond activation of the bound propyl intermediate to form propylene (see Figure 4.4.1 and 4.4.2). The first path proceeds via hydrogen abstraction of the terminal C-H bond by an adjacent O site (2nd H-O pathway), as was found for the α-Al_2O_3 surface. The second path proceeds instead via a direct insertion of Cr (to which the propyl is bound) into the terminal C-H bond of the propyl to form a strong Cr-H bond as was suggested by previous studies, and directly releases the propylene product. [28, 57] The 2nd H-O path was calculated to have a lower barrier at 164.0 kJ/mol than the 2nd H-Cr path which was 202.6 kJ/mol (see Table 4.4). The first path appears to proceed by a hydrogen abstraction reaction via the vicinal oxygen on the Cr_2O_3 surface. In the second path, propyl desorbs from the Cr site firstly and the Cr site inserts into the terminal C-H bond of propyl, so the activation energy is higher than the 2nd H-O path due to the strong binding of propyl on Cr site (-246.0 kJ/mol). The reaction energy in the 2nd H-Cr path is only a little higher than that in the 2nd H-O path though, since the 2nd H is stabilized by the strong Cr-H bond of -78.2 kJ/mol in comparison with the O-H bond of 82.0 kJ/mol.

A Bader charge analysis was carried out to examine the 2nd C-H bond activation. The results which are shown in Figure 4.5 are indicative of a hydrogen abstraction reaction as there is electron transfer from the H to oxide substrate (-0.15 e) upon deprotonation. Significant electron transfer into the Cr_2O_3 surface is not favorable and in part is responsible for the higher activation energy. In the second path the activation proceeds by a hydride transfer as the propylene directly desorbs and generates a Cr^{d+}-$H^{\delta -}$ intermediate. As such there is a charge flow from the substrate to the hydrogen which changes from -0.17 e in the reactant state to -0.50 e in the product. The total charge injection from propane to the substrate after this step is positively 0.11 e.

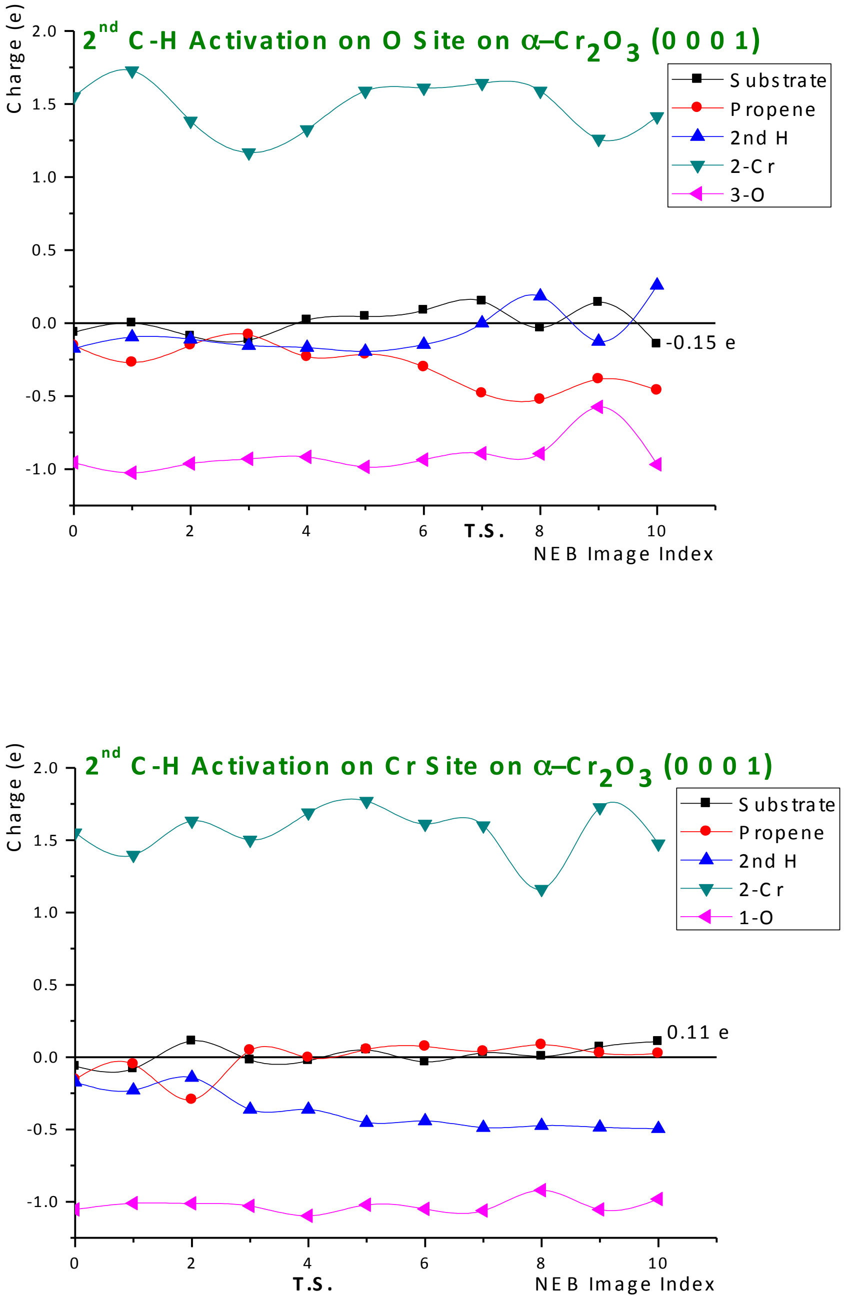

Figure 4.5 Bader charge analysis for different pathways for the activation of the terminal C-H bond of the bound propyl intermediate: a) the H-O pathway and b) the H-Cr pathway.

4.3 Product Desorption and Reaction Energy Profile of Propane Dehydrogenation on the α-Cr_2O_3 Surface

In the H-O pathway, the propylene that forms upon as a result of the hydrogen abstraction can desorb but this is requires an energy 175.6 kJ/mol. As such the overall apparent barrier starting from the gas phase or weakly adsorbed propane of 334.8 kJ/mol. This increases further to 371.3 kJ/mol if we consider the removal of H_2 via H-H recombination. The recombination of H_2 from two O sites proceeds in two steps. In the first step, H diffuses from an O site to the 2-Cr site where it can then pick up an electron and recombine with a second H+ to form H_2 which desorbs from the surface. The path is very similar to that presented for the desorption of H_2 from the α-Al_2O_3 surface (see Figure 4.6). The activation barrier for the diffusion of H from an O site to a Cr site is higher than that for the second C-H activation and such it sets the overall barrier for H-H recombination (36.5 kJ/mol), which is quite low due to the weak bindings of H. The overall apparent barrier for propane dehydrogenation from the adsorbed state was calculated to be 382.1 kJ/mol (see Figure 4.7), which indicates that α-Cr_2O_3 is inactive for PDH via the 2nd H-O pathway.

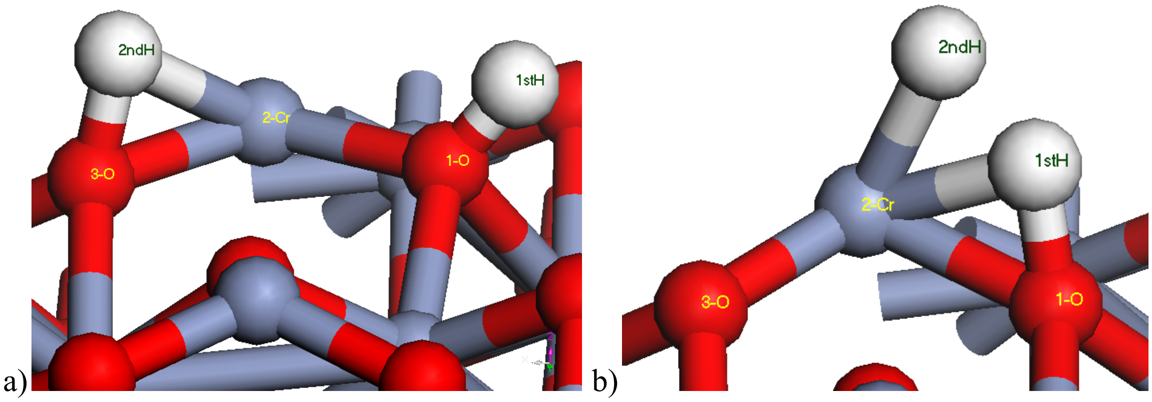

Figure 4.6 a) The transition state for the first step in the recombinative desorption of H_2 involves the transfer of H from an O on the Cr_2O_3 surface to a Cr site vicinal to a second surface H which is followed by subsequent formation of the H-H bond and its desorption as H_2 from the α-Cr_2O_3 (0 0 0 1) surface; b) The 2nd TS for H_2 recombination from two hydrogens from the O sites/TS of H_2 recombination from neighboring Cr-O pair on α-Cr_2O_3 (0 0 0 1) surface.

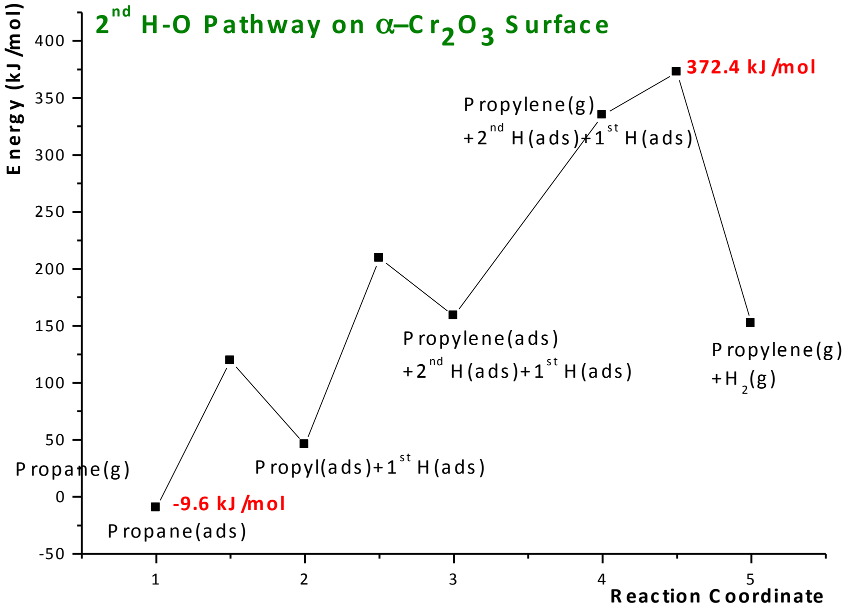

Figure 4.7 DFT calculated reaction energy profile of 2^{nd} H-O pathway on α-Cr_2O_3 (0 0 0 1) surface

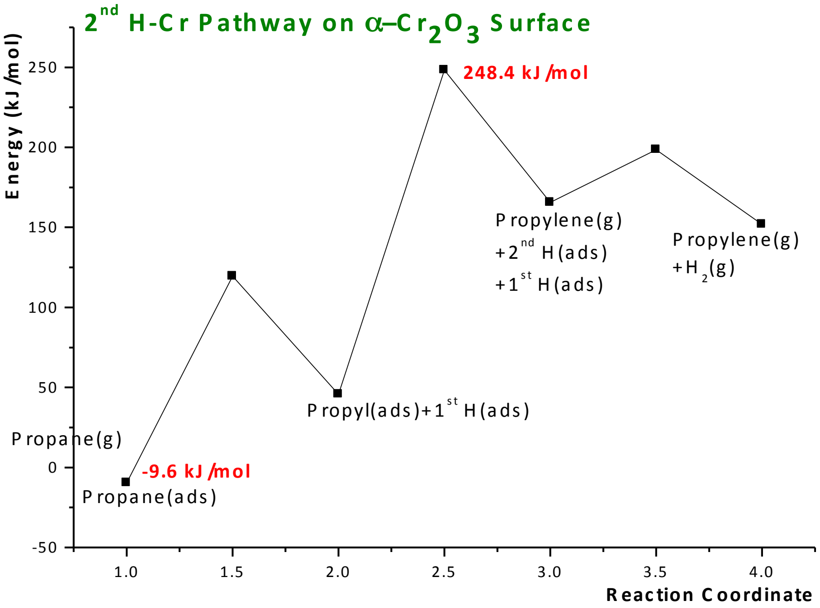

Figure 4.8 DFT-calculated reaction energy profile of 2^{nd} H-Cr pathway on α-Cr_2O_3 (0 0 0 1) surface

In the H-Cr pathway, the propyl intermediate is activated via metal atom insertion which involves a metal atom insertion into the C-H bond resulting in an intrinsic barrier of 202.6 kJ/mol and an overall barrier from the gas phase of 248.4 kJ/mol. The barrier for the H-H recombination is quite low at 32.8 kJ/mol, and the TS is the same as the 2^{nd} TS in the H-H recombination from two O sites (see Figure 4.6 b). This step falls below the previous step in energy as is shown Figure 4.8 and as such does not contribute to the overall activation barrier. The results here indicate that the activation of propane over the vicinal O-Cr pair is favored on this surface, without the involvement of neighboring O site.

4.4 Conclusions for α-Cr_2O_3 Surface

The overall activation barrier for propane dehydrogenation over α-Cr_2O_3 (248.4 kJ/mol) is measured with respect to the gas phase propane since the C-H activation steps are endothermic, and is lower than those calculated on α-Al_2O_3 (332.5 kJ/mol, 379.4 kJ/mol, 338.3 kJ/mol on three α-Al_2O_3 facets respectively), indicating that α-Cr_2O_3 is more active than α-Al_2O_3. PDH on α-Al_2O_3 is significantly hindered by the very strong binding of H and other reaction intermediates on the surface as well as high intrinsic activation barriers that result from unfavorable reaction sites. On α-Cr_2O_3 surface, although Cr binds propyl strongly, O site bind H weakly enough to avoid deep energy wells along the overall energy profile, with the lowest point being -9.6 kJ/mol. Moreover, the weak binding of H on O results in low intrinsic barrier for the recombinative desorption of H_2 from the surface. As such, the overall barrier is dictated by the intrinsic barrier for the 2nd C-H activation step which is not extremely high.

Bader charge transfer analysis showed that that there is a significant charge transfer (-0.89 e) from propane into the α-Al_2O_3 surface upon the activation of C-H bonds whereas the charge transfer involved in the C-H activation on α-Cr_2O_3 was significantly less and the substrate even loses a small amount of negative charge (-0.11 e) to propane. The results indicate that the more active surfaces for PDH are those which minimize the overall charge transfer, which is consistent with the ideas that the active sites are weak Lewis acid-Lewis base pairs [25, 63].

Chapter 5 Comparison between α-Al_2O_3, α-Cr_2O_3 and ZrO_2

The results for the activation of propane over the crystalline α-Al_2O_3 and α-CrO_2 surfaces presented in Chapters 3 and 4, respectively, are compared in this chapter with previous results over ZrO_2 carried out by Dr. Lijun Xu, a postdoctoral research assistant in our group to understand the influence of the oxide on the alkane dehydrogenation. In addition, we compare the influence of O-vacancies and the degree of surface hydroxylation for the α-Al_2O_3 and α-ZrO_2 surfaces. Previous studies suggest that hydroxylated and hydrated α-Cr_2O_3 surfaces do not form and as such they were not examined. The comparisons in this chapter predominantly focus on the changes that occur for PDH over the dry crystalline forms of the α-Al_2O_3, α-Cr_2O_3 and ZrO_2 surfaces.

Previous theoretical results for propane dehydrogenation over ZrO_2 carried out by Xu indicate that the dehydrogenation of propane can proceed over the monoclinic (-1 1 1) facet of ZrO_2, termed m-ZrO_2 (see Figure 5.1) [64].

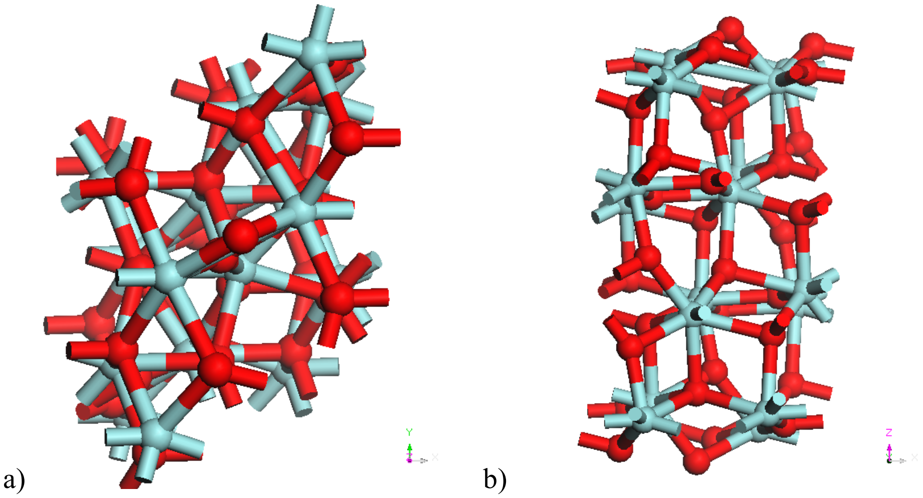

Figure 5.1 The monoclinic (-1 1 1) surface structure of ZrO_2. [64]

a) Top view and b) Side view.

Notes: The blue spheres refer to Zr whereas the red spheres refer to the O atoms.

5.1 Comparison between Reaction Mechanism and Energetics

In Chapter 3, we showed that PDH appears to proceed over adjacent O-Al-O sites, with 1st C-H activation on the Al-O pair whereas the 2nd C-H activation occurs at a second O site. The atomic hydrogen products that form on the a-Al_2O_3 surface bind to the two O sites can subsequently recombine and desorb from the surface as H_2. The most favored path over the α-Cr_2O_3 proceeds over a single Cr-O site pair. The reaction proceeds by the heterolytic activation of the secondary C-H bond of propane at the Cr-O site pair. This is followed by the subsequent Cr insertion and activation of the primary C-H bond of the bound alkyl intermediate to form propylene that desorbs from the surface. The resulting atomic H species that form on O* and Cr* sites recombine and desorb as H_2. The results over m-ZrO_2 and t-ZrO_2 are very similar in that the 1st C-H activation proceeds heterolytically over the Zr-O site pair whereas the activation of the 2nd C-H bond proceeds via a Zr insertion thus resulting in propylene that desorbs from the surface and a hydrogen that bound to the Zr. The Zr-H(-) recombines with the O-H(+) in a heterolytic manner to form H_2 over the Zr-O pair. [60]

In summary, the 1st C-H activation on all of the surfaces examined (α-Al_2O_3, α-Cr_2O_3 and ZrO_2) occurs via a heterolytic splitting of the C-H bond over the metal-oxygen substrate bond to form metal-alkyl and H-O products. The 2nd C-H activation proceeds via a metal site insertion into the primary C-H bond of the alkyl intermediate to form propylene which subsequently desorbs and metal-H bond over both the α-Cr_2O_3 and ZrO_2 surfaces. The desorption of hydrogen from these surfaces involves the heterolytic recombination from the H(-) and H(+) to from H_2 which desorbs from the surface.

The reaction energy profile for the PDH over the α-Al_2O_3 surface (refer to Figure 3.8) proceeds via C-H activation resulting in a very low energy well which ultimately makes it very difficult to remove the resulting hydrogens from the surface thus leading to an activation barrier of 332.9 kJ/mol over α-Al_2O_3. The results on α-Cr_2O_3, however, are rather different as there is no deep well that forms during C-H activation or high barrier for H-H recombination as the highest energy TS is that for the 2nd C-H activation. The overall barrier with respect to the adsorbed propane state on α-Cr_2O_3 was calculated to be 258.0 kJ/mol (refer to Figure 4.8). The results for m-ZrO_2 and t-ZrO_2 indicate that there are no deep energy wells or high energy peak states and that the overall barrier is also slightly decreased [60].

In order to explore the reasons for the different reactivities of the oxides discussed here, we examined the reaction sites' binding abilities as well as the electronic properties of the substrates.

5.2 Comparison between Binding Abilities of Reaction Sites

The results presented on all of the different surfaces that we have explored thus far indicate that the resulting H-O bond strength that forms as a result of C-H activation is an important indicator of catalytic activity in PDH reaction cycle. Weak O-H bonds do not appear to be able to stabilize the proton that results in the transition state whereas strong O-H bonds lead to very higher barriers for the recombinative desorption of H_2 from the surface. By comparing the results over the ZrO_2 surfaces studied by Dr. Xu (see Table 5.1) together with those calculated herein over the α-Al_2O_3 and the α-Cr_2O_3 surfaces, we find that the apparent activation barriers for the PDH reaction are lower on Cr_2O_3 and ZrO_2 surfaces as they have weaker H-O bonds; whereas the reactions over α-Al_2O_3 result in much higher activation energies due to the very strong H-O binding.

Table 5.1 Comparison between binding strengths of O sites for H on different surfaces

Surface	**α-Al_2O_3**	**α-Cr_2O_3**	**m-ZrO_2**
H Binding Energy on O (kJ/mol)	-108.1	82.0	75.3
Total Barrier (kJ/mol)	332.9	257.6	<230

The correlation between the H binding and overall apparent activation energy on Al_2O_3 surface is due to the fact that the strong binding of H on O sites leads to the formation of a very stable product of propylene plus two H* as noted by the deep well on the potential energy surface reactions and a high activation energy for the intrinsic H-H recombination. So while the strong H binding facilitates the initial C-H activation, it leads to the formation of a very stable state which prevents the propylene and hydrogen products from leaving catalyst surfaces, thus blocking the active sites. The PDH reactions on Cr_2O_3 and ZrO_2 surfaces, on the other hand, result in weak H-O surface bonds and more endothermic reaction energies, so there are no deep energy wells within the reaction energy profile. Furthermore, the weak binding of H to the surface also acts to facilitate the more rapid desorption of H_2, thus the recombination of H_2 does not contribute much to the overall barrier.

5.3 Comparison between Electronic Properties of Substrates

By comparing all four of the systems that we studied, we noted a correlation between the lower activation barriers and lower charge transfer between propane and the oxide surface. In order to compare with the results on the ZrO_2 surfaces [60], we compare our findings shown in Table 5.2.

Table 5.2 Comparison of the charge transfer into the substrate between different surfaces

Surface	**α-Al_2O_3**	**α-Cr_2O_3**	**m-ZrO_2**
Obtained Charge (e)	-0.89	0.11	-0.17
Total Barrier (kJ/mol)	332.9	257.6	< 230

The "Obtained Charge" term reported in Table 5.2 refers to the surface charge obtained from reactants after the 2nd C-H activation. It shows that α-Al_2O_3 prefers to receive a larger amount of negative charge from reactants, while the others prefer weaker charge transfer flows between reactants and substrates. For α-Cr_2O_3, the substrate even loses a little negative charge to the reactants, indicating that it is the weakest electron acceptor among these oxides.

The changes in the activation barrier over the different oxides also appear to be related to some extent to the coordination state of surface sites. On the ZrO_2 surfaces, the Zr sites tend to have only two O ligands (see Figure 5.1) compared to bulk Zr which is coordinated to 8 O sites; while on both α-Al_2O_3 and α-Cr_2O_3 surfaces, the surface metal sites are missing over half of the 6 O ligands of the bulk metal sites. The ZrO_2 surfaces are thus the most saturated surfaces in terms of the coordination state of surface site.

The differences in reactivity and bonding also tend to correlate with changes in oxide properties such as melting point. The ZrO_2 surfaces have the highest melting points (2988 K), and α-Cr_2O_3 has a higher melting point than α-Al_2O_3 (2708 K vs 2345 K). Higher melting points typically result in stronger metal-oxygen bonds and materials with highly saturated electron density. This is consistent with the findings that the surface sites on ZrO_2 having the highest saturation density. While ZrO_2 has the highest saturation density, it is a better electron acceptor than α-Cr_2O_3 in the C-H activation of propane. The α-Al_2O_3 is the most unsaturated oxide, which is consistent with the strongest electron acceptability of α-Al_2O_3 in this reaction.

5.4 Summary and Potential Opportunities in Oxide Complexes

The results reported herein suggest that the site-specific H-binding energies and electronic properties of the α-Al_2O_3, α-Cr_2O_3 and ZrO_2 surfaces act to control C-H bond activation in propane. Weaker H-binding energies and lower electron acceptability tend to favor propane dehydrogenation over the refractory oxide surfaces studied. There is a limit, however, on the strength of the O-H bond, as oxides with too weak of an O-H bonds result in much higher reaction energies for the 1st C-H activation which increases the energy for the 2nd C-H activation TS. This is consistent with the higher reaction energy and apparent activation barriers reported on the α-Cr_2O_3 surface. The strong O-H bonds that form on the α-Al_2O_3 and the weak O-H bonds that result on the α-Cr_2O_3 surface provide guidelines for the optimal O-H bond strength that will minimize deep energy wells and high energy peaks in the energy profile.

Similarly, the optimal oxides are one that have weak electron acceptability but still are able to accept some charge. The electron acceptability of α-Cr_2O_3 appears to be a little too weak as it loses negative charges even to the reactants in the activation of C-H bonds. The weak electron acceptability is related to the weak binding of H on O sites. Therefore, a moderately weak electron acceptability might correspond to the moderate binding property, and might be helpful to the overall activity.

The CrO_x/α-Al_2O_3 catalysts examined by UOP provide mixed Cr and Al oxides which may provide mixed Cr-O-Al sites and unique reactivity over the pure crystalline α-Cr_2O_3 and α-Al_2O_3 phases. [23, 56] The Cr-O-Al bonds which are comprised of the stronger Cr-O bonds and weaker O-Al bonds may provide more reactive O-H bond strengths or may be able to be tuned to provide optimal O-H bond strengths. The electron acceptability for these mixed systems will likely lie somewhere between the strong acceptability of α-Al_2O_3 and the weak acceptability of α-Cr_2O_3.

We therefore focus on the mixed Cr-Al oxide complex structures in the next-stage few chapters and further probe the correlations between binding properties/electronic properties and catalytic activities by tuning the structure and composition of Al and Cr oxide species at the surface, aiming to build up a more thorough geometric/electronic structure-activity relationship for the refractory oxides.

Chapter 6 PDH on Cr/α-Al_2O_3 Complexes

6.1 Introduction

The active Cr sites in the commercial CrO_x/Al_2O_3 catalyst for propane dehydrogenation are thought to be particular Cr(III) centers. [23, 57, 60, 65] There are three types of Cr(III) sites believed to be formed with increased Cr loadings: the first are single Cr(III) centers anchored to the Al_2O_3 substrate; the second are Cr(III) sites within amorphous Cr_2O_3 clusters attached to Al_2O_3 surface; and the third are Cr sites within the crystalline α-Cr_2O_3 which do not chemically interact with Al_2O_3 substrate. [28, 57, 60] We have already discussed PDH over the α-Cr_2O_3 surfaces in Chapter 4. We will examine PDH over the supported Cr(III) and the amorphous Cr_2O_3 clusters in this chapter and the next. The commercial CrO_x/Al_2O_3 catalyst typically uses γ-Al_2O_3 as the support [8]. In the UOP's experiments, α-Al_2O_3 was used as a support in order to probe a range of different refractory oxides [20]. As such, we have examined both the grafted Cr complex and the amorphous Cr_2O_3 clusters on the α-Al_2O_3.

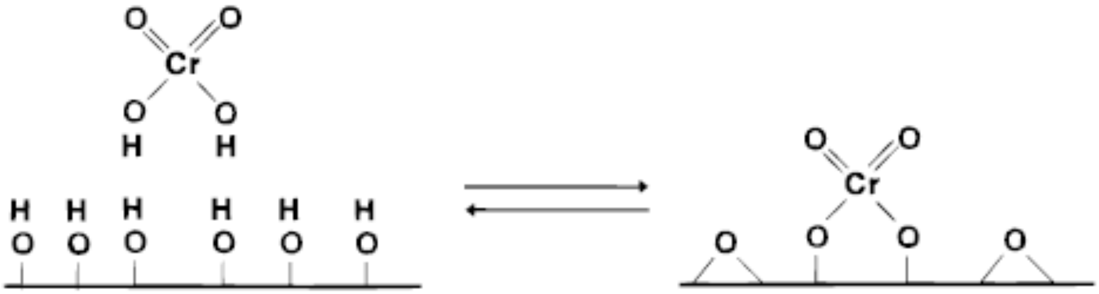

Figure 6.1 The dehydration of chromate complexes on fully hydroxylated Al_2O_3 surface

The grafted Cr(III) is derived experimentally from reduction of the grafted Cr(VI) onto an alumina support. This involves a reactive dehydration of the chromate complexes and hydroxyl groups on Al_2O_3 surface during the catalyst preparation process (see Figure 6.1), which anchors the Cr complex to the Al_2O_3 surface via two Cr-O-Al bridge bonds. [23]

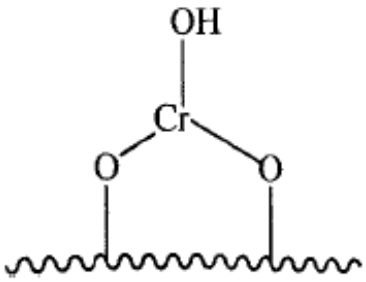

Figure 6.2 The two-bridge Cr(III) center formed after reduction of grafted Cr(VI) [23]

The two-bridge grafted Cr(III) (see Figure 6.2) is then formed after the reduction of grafted Cr(VI) by propane and H_2 in PDH reaction, with two Cr(III)-O-Al bridge bonds and a third hydroxyl ligand pointing outward. [23, 57, 66] The hydroxyl group on the two-bridge Cr(III) center can subsequently react with hydroxyl groups on the Al_2O_3 surface, leading to a three-bridge Cr(III) center comprised of three Cr(III)-O-Al bridge bonds [19]. The formation mechanism for this structure is illustrated in Figure 6.3.

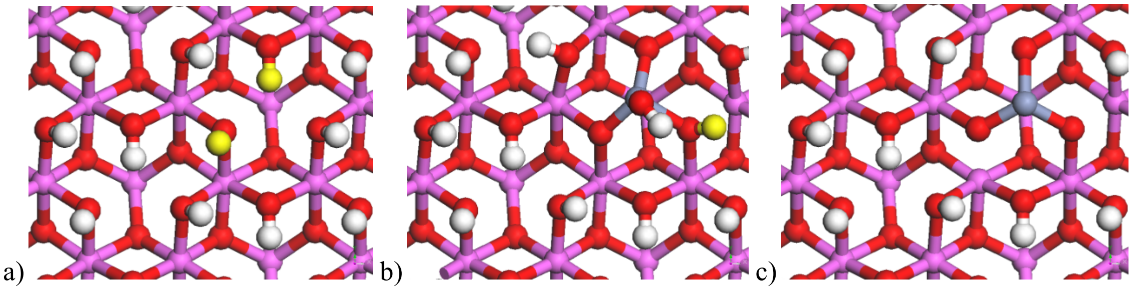

Figure 6.3 The formation process for the three-bridge grafted Cr(III) center on the fully hydroxylated α-Al_2O_3(0 0 0 1) surface involves:

a) The reaction of the fully hydroxylated α-Al_2O_3 surface with two hydroxyl groups (Yellow) and a chromate complex (not shown) to form b);
b) The formation of two-bridge Cr(III) center after surface hydroxyl reacts with chromate and the reduction of Cr(VI);
c) The formation of the three-bridge Cr(III) center after further dehydration of the two-bridge Cr(III) with the surface hydroxyl group (Yellow-colored in b).

The reported literature indicates that the Cr(III) center can be in monomer, dimer or trimer forms [67-71] whose structures are shown in Figure 6.4, where the three-bridge Cr(III) center is coordinated to 3 O sites in the 2nd layer. The OH sites on the fully hydroxylated α-Al_2O_3 substrate were found to be inactive for PDH in our study discussed in Chapter 3. So the potential reaction sites for the 1st C-H activation are still considered to be the adjacent Cr-O pairs; for the 2nd C-H activation, the Cr site, the adjacent O, and the nearby OH are all possibly involved in the reaction.

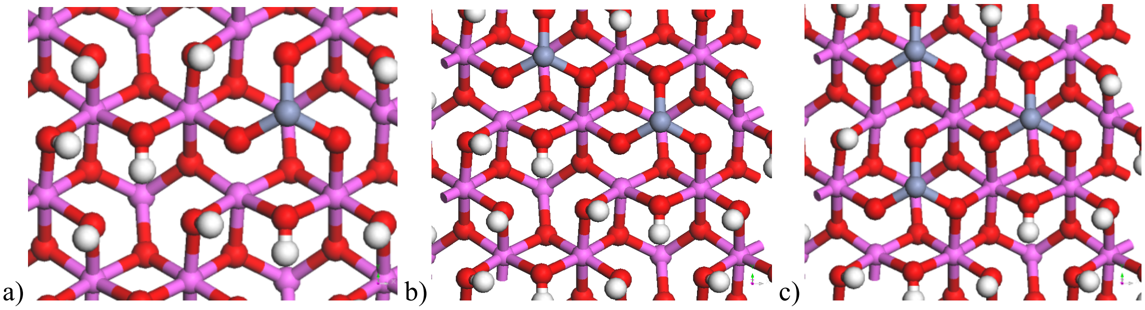

Figure 6.4 Monomer, dimer and trimer Cr/α-Al_2O_3 complexes: a) monomer, b) dimer and c) trimer.

6.2 Adsorption of Reactants, Intermediates and Products onto Cr/α-Al_2O_3 Complexes

The chemical nature and reactivity of the surface was first explored by examining the chemisorption of the different reactants, intermediates and products on the different sites on the Cr/α-Al_2O_3 surfaces. The binding energies for H and propyl intermediates on the O, OH and metal sites were calculated at each of these sites on the monomer, dimer and trimer Cr complexes on the α-Al_2O_3 surface and compared with the previous results for the α-Cr_2O_3, the dry and the fully-hydroxylated α-Al_2O_3 surfaces. The results reported in Table 6.1 show that the binding energies of H on the Cr sites on monomer, dimer and trimer Cr/α-Al_2O_3 complexes increase from -56.0 to -58.9 to -61.8 kJ/mol as the number of Cr nearest neighbors increases from 0 to 1 to 2. These energies, however, are nearly 20 kJ/mol weaker than the H-Cr binding energies on the α-Cr_2O_3 surface (-78.2 kJ/mol). In comparison, the H-Al binding energy on α-Al_2O_3 was calculated to be unbound (180.4 kJ/mol).

The H binding energies on the O site vicinal to the Cr were calculated to be -3.9 kJ/mol for both the monomer and dimer Cr complexes and +7.9 kJ/mol for the trimer Cr complex. These moderate binding energies on the Cr/α-Al_2O_3 are much weaker than the H-O binding energies on the unmodified α-Al_2O_3 surface (-108.1 kJ/mol) but much stronger than those on the α-Cr_2O_3 surface (+82 kJ/mol) which are unbound. These O sites on the Cr/Al_2O_3 are made up of Cr-O-Al bonds and as such provide moderate H-O binding energies. Similar changes in the H-binding energies were also calculated at the OH sites on the Cr/Al_2O_3. The H-binding energies at the OH sites on the monomer, dimer and trimer Cr/Al_2O_3 complexes were calculated to be -60.8, -54.0, and -34.7 kJ/mol, which are weaker than those on the OH sites of fully-hydroxylated α-Al_2O_3 (-70.4 kJ/mol). The decrease in the binding energy with increasing Cr content indicates that the binding energies can be tuned by altering the number of neighboring Cr and Al centers.

As was discussed in Chapter 5, the moderate binding of H to the O site should help to lower the barriers for hydrogen removal and increase the activity for PDH over both the α-Cr_2O_3 and hydroxylated α-Al_2O_3 surfaces.

Table 6.1 Adsorptions of reactants, intermediates and products onto Cr/α-Al_2O_3 complexes ("Monomer/Dimer/Trimer Cr" in the table) in comparison with α-Cr_2O_3, fully hydroxylated α-Al_2O_3 ("Fully Al_2O_3" in the table) and dry α-Al_2O_3 ("α-Al_2O_3" in the table)

***E**_{ads}* (kJ/mol)	**Monomer Cr**	**Dimer Cr**	**Trimer Cr**	**α-Cr_2O_3**	**Fully Al_2O_3**	**α-Al_2O_3**
H-O	-3.9	-3.9	7.7	82.0	N/A	-114.8
H-OH	-60.8	-54.0	-34.7	N/A	-70.4	N/A
H-Metal	-56.0	-58.9	-61.8	-78.2	N/A	180.4
Propyl-Metal	-232.5	-233.5	-236.4	-246.0	-118.9 (Propyl-OH)	-31.8

Note: N/A in this table corresponds to the situation that there is no such site on the surface.

A closer comparison of the H binding energies on the Cr, O and OH sites over the different Cr complexes supported on α-Al_2O_3 indicates that the changes are not very large. It does, however, appear to be a general trend that the binding energies to the Cr become stronger with increasing Cr content, while bindings to the O and OH sites become somewhat weaker with increasing Cr content.

6.3 1st C-H Activation of Propane on Different Cr/α-Al_2O_3 Complexes

The activation of the initial C-H bond of propane at its secondary position over the Cr-O pair of the monomeric Cr/α-Al_2O_3 occurs in a heterolytic manner similar to that on the α-Cr_2O_3 surface. The activation barrier for C-H activation on the Cr-O site on the Cr/α-Al_2O_3 surface, however, is only 91.6 kJ/mol (see Table 6.2), whereas that on Cr-O site pair on the α-Cr_2O_3 surface was calculated to be 119.6 kJ/mol. Similarly the overall reaction energy was calculated to be more exothermic with an energy of -36.3 kJ/mol on the Cr/α-Al_2O_3 verses +45.4 kJ/mol on α-Cr_2O_3.

The more favorable activation and reaction energies are the result of the stronger hydrogen binding energy on the Cr center (-3.9 kJ/mol for Cr/α-Al_2O_3 vs +82.0 kJ/mol on α-Cr_2O_3) and similar propyl-O binding energy (-232.5 kJ/mol for Cr/α-Al_2O_3 vs -246.0 kJ/mol for α-Cr_2O_3). The transition state structures and the mechanism appear to be quite similar (see Figure 6.5.2) on the dimer and trimer complexes as compared to that on the monomer. The calculated reaction energies and activation barriers are also close to each other among different complexes (see Table 6.2).

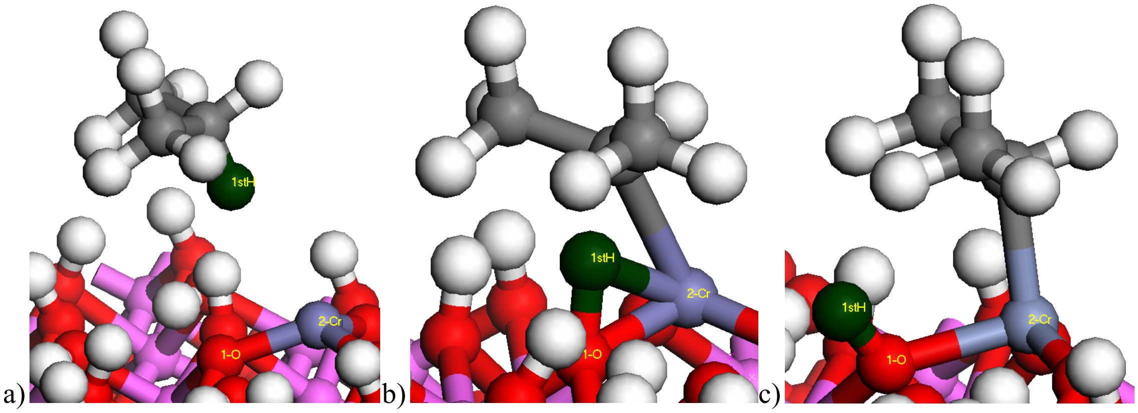

Figure 6.5.1 The activation of the 1st C-H bond of propane at the secondary position over a neighboring O-Cr site pair on monomer Cr/α-Al_2O_3 surface. The structures of the a) reactant, b) transition and c) product states.

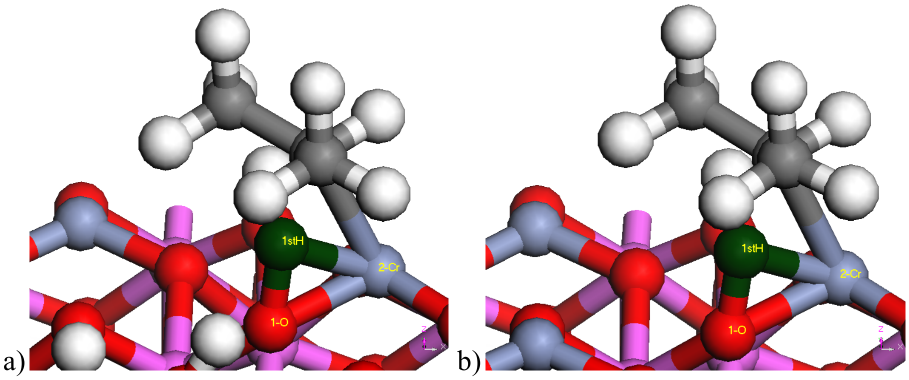

Figure 6.5.2 The transition state for the activation of the 1st C-H bond of propane at the secondary position over a neighboring O-Cr site pair on the dimer and trimer Cr/α-Al_2O_3 complexes. The transition state structure and the activation barrier for: a) the dimer complex and b) the trimer complex.

Table 6.2 Energetics comparison between monomer, dimer and trimer Cr/α-Al_2O_3 complexes for the 1st C-H activation of propane

Cr/α-Al_2O_3 Complex	**E_{rxn} (kJ/mol)**	**E_{act} (kJ/mol)**
Monomer	-36.3	91.6
Dimer	-32.7	83.8
Trimer	-18.5	83.9

The results from a Bader charge analysis (see Figure 6.6) confirmed that the reaction proceeds via a heterolytic mechanism involving the formation of a propyl anion and a H-cation in the TS as was found over the other refractory oxide complexes examined.

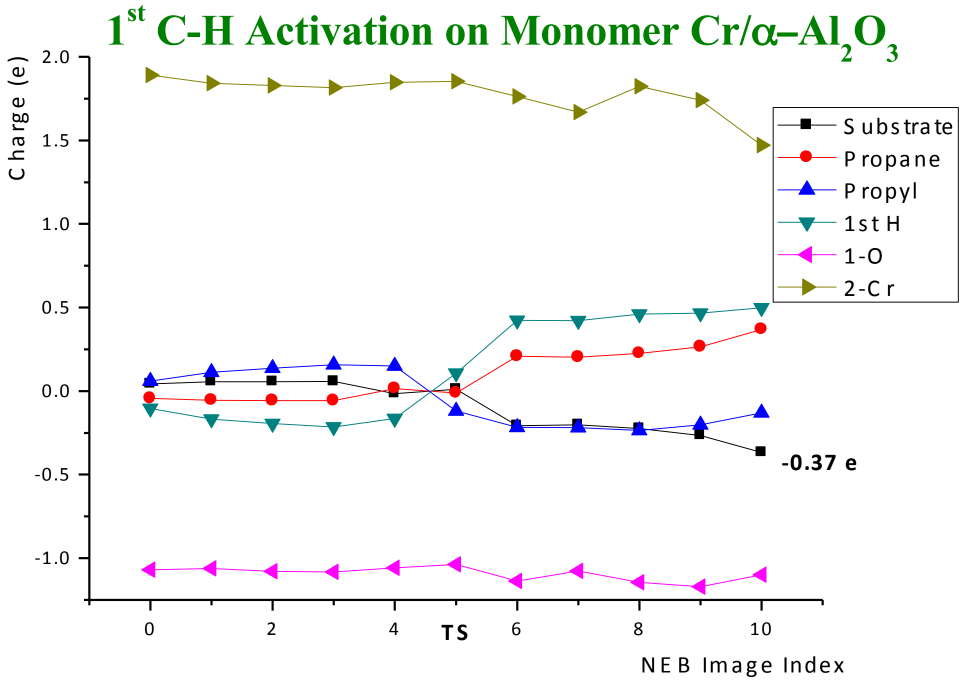

Figure 6.6 Bader charge analysis of the 1st C-H activation on a neighboring Cr-O pair on monomer Cr/α-Al_2O_3 complex

6.4 2^{nd} C-H Activation of Propane on Monomer Cr/α-Al_2O_3 Complex

The 2^{nd} C-H activation which involves the activation of the primary C-H bond of the adsorbed propyl intermediate can occur on the Cr site or on a vicinal O or OH site. The activation of the C-H bond of the propyl at the Cr site (2^{nd} H-Cr) proceeds by the Cr insertion into one of the primary C-H bonds to form propylene which directly desorbs into the gas phase (see Figure 6.7.2 and Table 6.4). The intrinsic activation barrier and the overall reaction energy were calculated to be 217.1 kJ/mol and 109.6 kJ/mol, respectively (see Table 6.3). The high barrier and reaction energy are similar to those found for the 2^{nd} C-H activation over the Cr site on α-Cr_2O_3 surface. While the barrier and overall energy for this intrinsic C-H activation step appear to be somewhat high, it should be noted this step involves not only the activation of the C-H bond, but also the activation of the Cr-C bonds and the direct desorption of propylene.

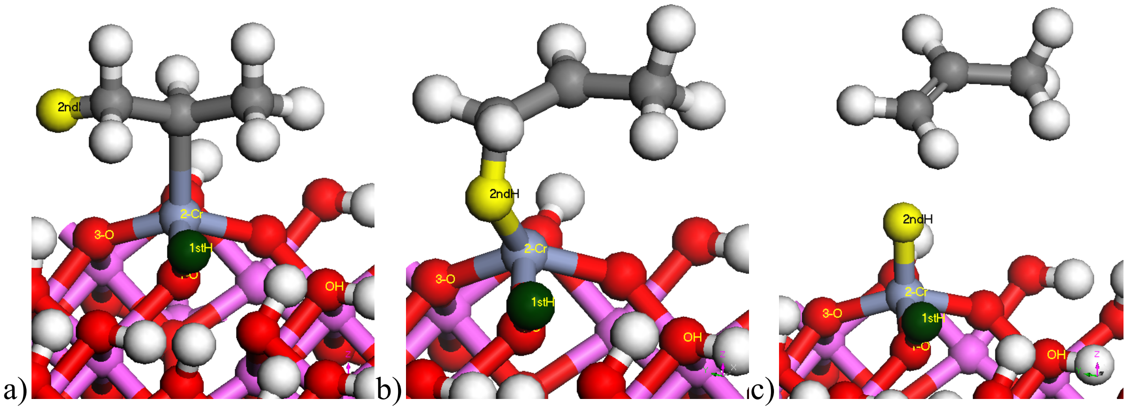

Figure 6.7.1 The activation of the adsorbed propyl intermediate at the primary C-H bond at the Cr site on monomer Cr/α-Al_2O_3 complex. The structures of the: a) reactant, b) transition and c) product states.

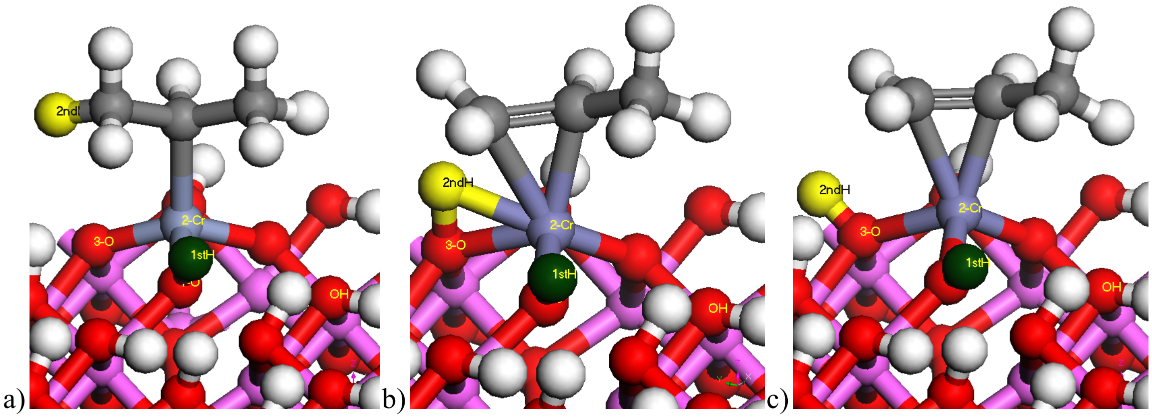

Figure 6.7.2 The activation of the adsorbed propyl intermediate at the primary C-H bond at the adjacent O site on monomer Cr/α-Al_2O_3 complex. The structures of the a) reactant, b) transition and c) product states.

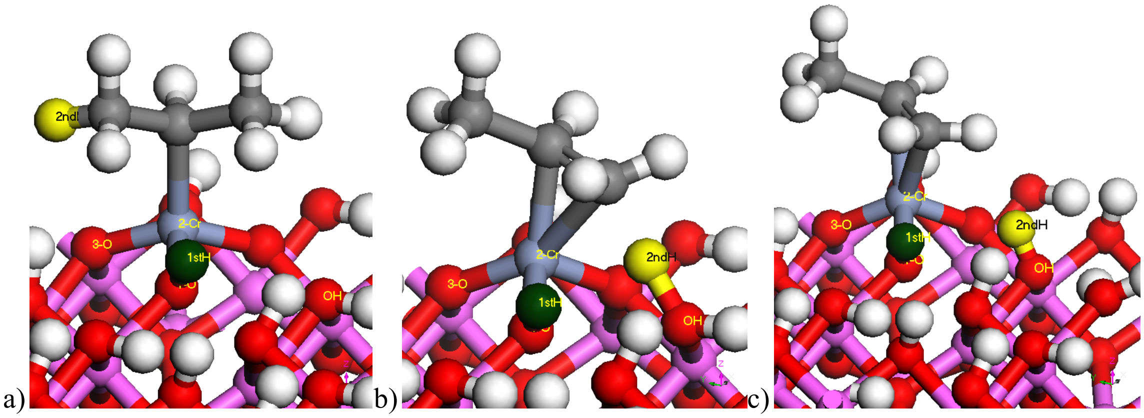

Figure 6.7.3 The activation of the adsorbed propyl intermediate at the primary C-H bond at the surrounding OH group on monomer Cr/α-Al_2O_3 complex. The structures of the: a) reactant, b) transition and c) product states.

Table 6.3 Energetics comparison between different paths for the primary C-H activation of propyl on the monomer Cr/α-Al_2O_3 complex

Path	E_{rxn} **(kJ/mol)**	E_{act} **(kJ/mol)**
2nd H-Cr Path	109.6	217.1
2nd H-O Path	74.3	167.9
2nd H-OH Path	-5.8	115.8

Table 6.4 Evolution of bond distances in different paths of the primary C-H activation of propyl on the monomer Cr/α-Al_2O_3 complex

Path	**Bond Distance**	**Reactant**	**TS**	**Product**
2nd H-Cr Path	**2nd H-Cr (Å)**	3.2	1.7	1.6
	C-Cr (Å)	2.0	2.9	4.7
2nd H-O Path	**2nd H-O (Å)**	3.0	1.2	1.0
	C-Cr (Å)	2.0	2.0	2.1
2nd H-OH Path	**2nd H-OH (Å)**	3.1	1.2	1.0
	C-Cr (Å)	2.0	2.0	2.1

The activation of the C-H bond of the bound propyl intermediate can also occur at a vicinal O or a vicinal OH site. The activation at a vicinal O center proceeds with an intrinsic barrier of 167.9 kJ/mol and an overall reaction energy of 74.3 kJ/mol. While the barrier and the overall energy at this site is lower than that at the Cr site, it does not include the energy of 170 kJ/mol required to desorb the strongly held propylene. The activation of the 2nd C-H bond can also occur at a vicinal OH site. The intrinsic activation barrier and overall reaction energy at the OH site were calculated to be rather favorable at 115.8 kJ/mol and -5.8 kJ/mol, respectively due to the strong binding of H to the OH site. The desorption of the resulting propylene that forms on Cr requires over 143 kJ/mol thus significantly increasing the overall activation barrier. The different pathways for the 2nd C-H activation on the monomer complex are shown from Figure 6.7.1 to 6.7.3.

Bader charge analyses show that the electronic state of the substrate in the product state is different among these three paths: in the 2nd H-Cr pathway the substrate gains the smallest amount of negative charge (-0.16 e); while in the 2nd H-O pathway and the 2nd H-OH pathway the substrate picks up -0.35 e and -0.47 e respectively (see Figure 6.8.1 to 6.8.3). So from the aspect of charge transfer as discussed in Chapter 5, the 2nd H-Cr pathway is also the most favored path since it has the weakest negative charge transfer from the reactants to the substrate.

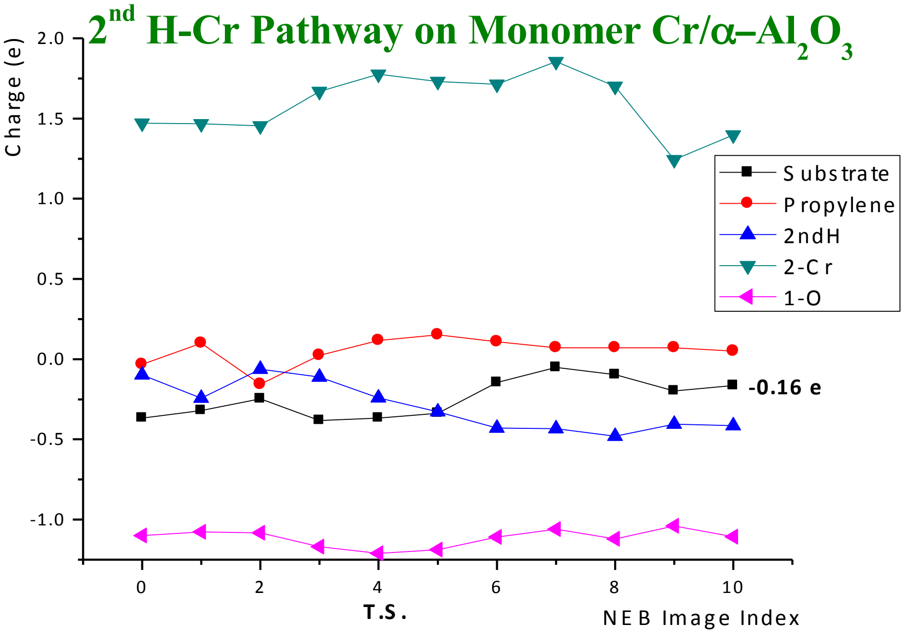

Figure 6.8.1 Bader charge analysis of the 2nd H-Cr pathway for the 2nd C-H activation on monomer Cr/α-Al_2O_3 complex. The charges on the substrate, propylene, 2nd H, 2-Cr and 1-O are shown in black, red, blue, green and purple, respectively.

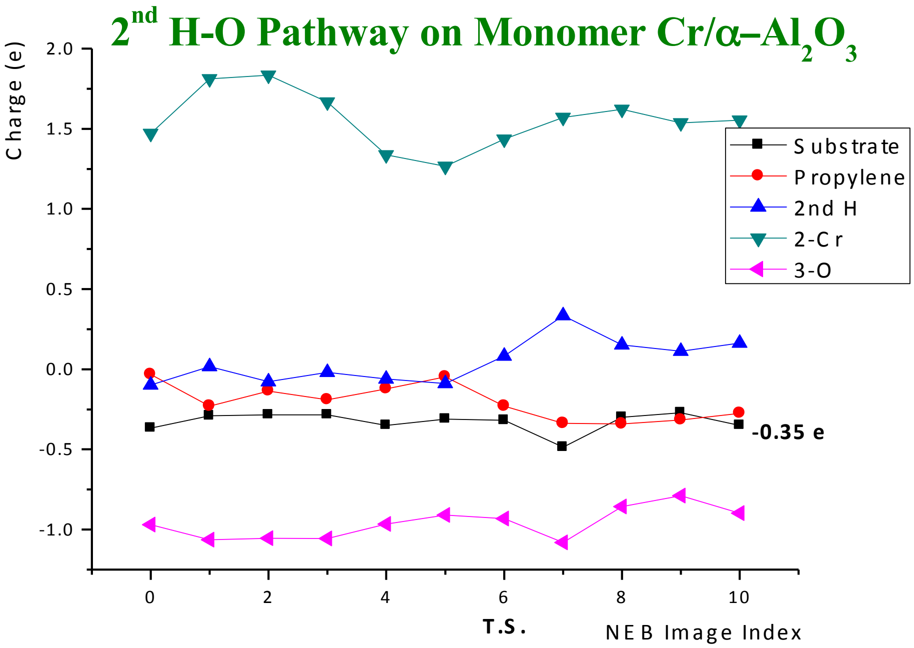

Figure 6.8.2 Bader charge analysis of the 2nd H-O pathway for the 2nd C-H activation on monomer Cr/α-Al_2O_3 complex. The charges on the substrate, propylene, 2nd H, 2-Cr and 3-O are shown in black, red, blue, green and purple, respectively.

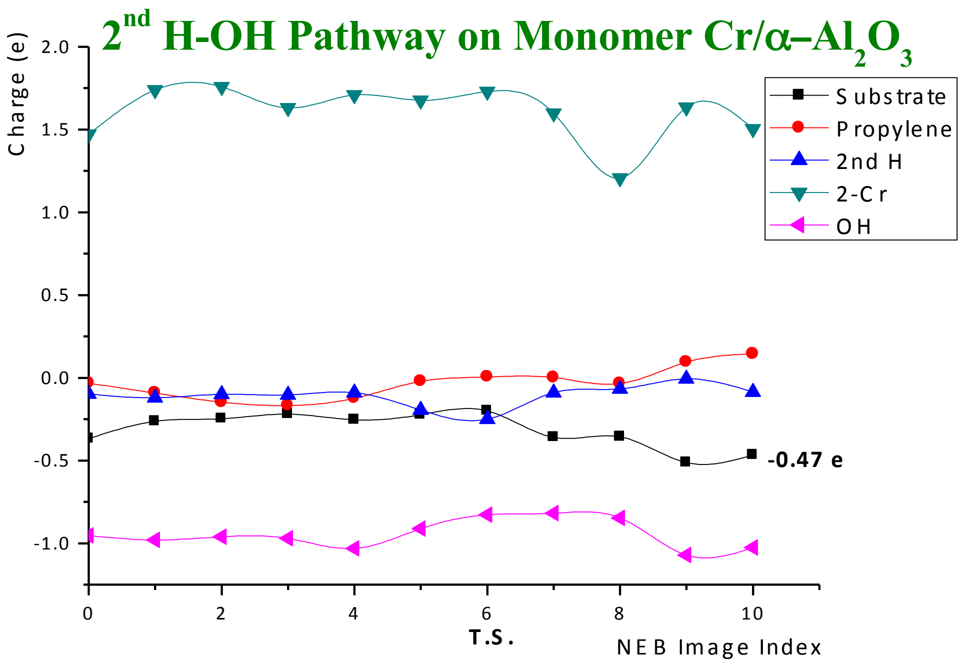

Figure 6.8.3 Bader charge analysis of the 2nd H-OH pathway for the 2nd C-H activation on monomer Cr/α-Al_2O_3 complex. The charges on the substrate, propylene, 2nd H, 2-Cr and OH are shown in black, red, blue, green and purple, respectively.

6.5 Product Desorption and Reaction Energy Profiles of Propane Dehydrogenation on Monomer Cr/α-Al_2O_3 Complex

The DFT calculated reaction energy profiles for the overall catalytic cycles for propane dehydrogenation for the 2nd H-Cr, H-O and H-OH paths shown in Figure 6.9.1-6.9.3 are similar to the reaction energy profile for PDH over α-Cr_2O. The desorption of propylene for both the 2nd H-O and H-OH paths are rather high in energy (143.5 kJ/mol for H-O path and 143.2 kJ/mol for the H-OH path) (see Figure 6.9.2 and 6.9.3). The overall energy level for the 2nd H-Cr pathway, on the other hand, includes the desorption of propylene, and since the subsequent H-H recombination is rather easy, it provides a direct measure of the apparent activation energy (see Figure 6.9.1). Summarized in Table 6.4, the 2nd H-Cr pathway has the lowest overall barrier (***E****ovr-act* in Table 6.4) at 217.2 kJ/mol, while the 2nd H-O and the 2nd H-OH pathways require higher overall barriers of 320.2 kJ/mol and 264.2 kJ/mol, respectively.

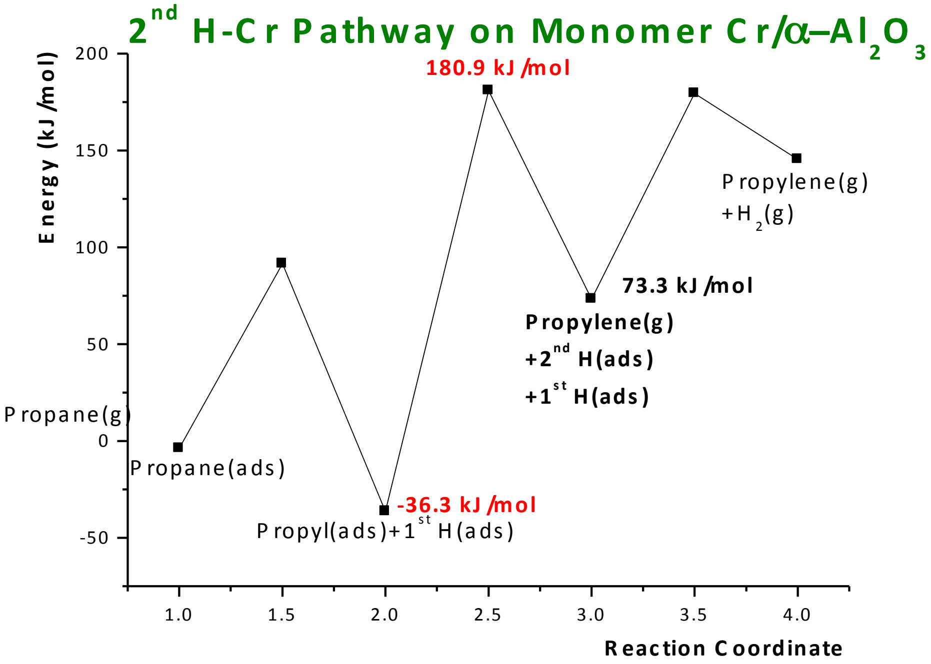

Figure 6.9.1 DFT-calculated reaction energy profile of 2nd H-Cr pathway on neighboring O-Cr pair on monomer Cr/α-Al_2O_3 complex

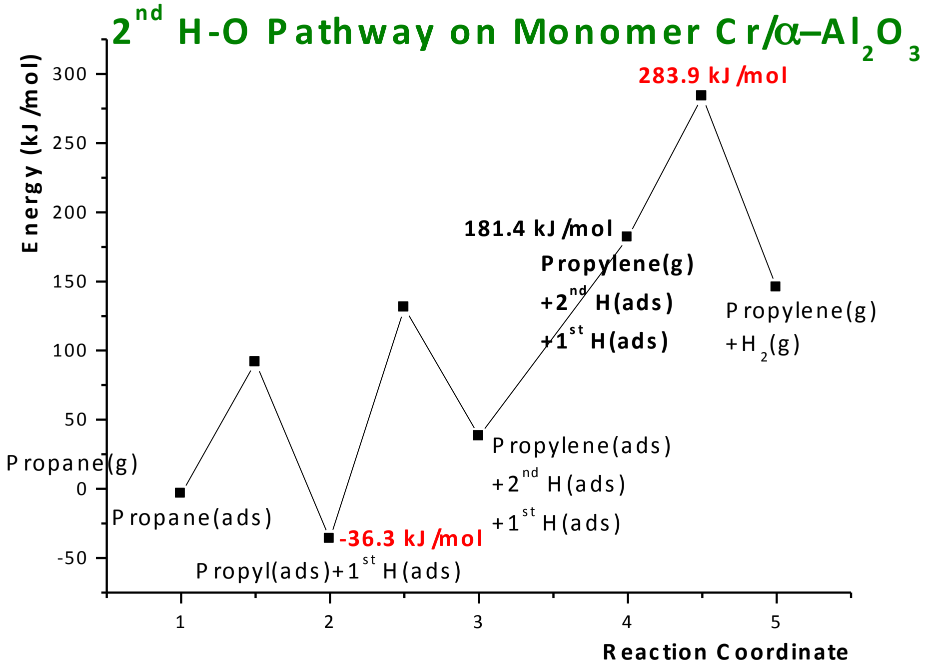

Figure 6.9.2 DFT-calculated energy profile of the 2nd H-O pathway on two O sites on monomer Cr/α-Al_2O_3 complex

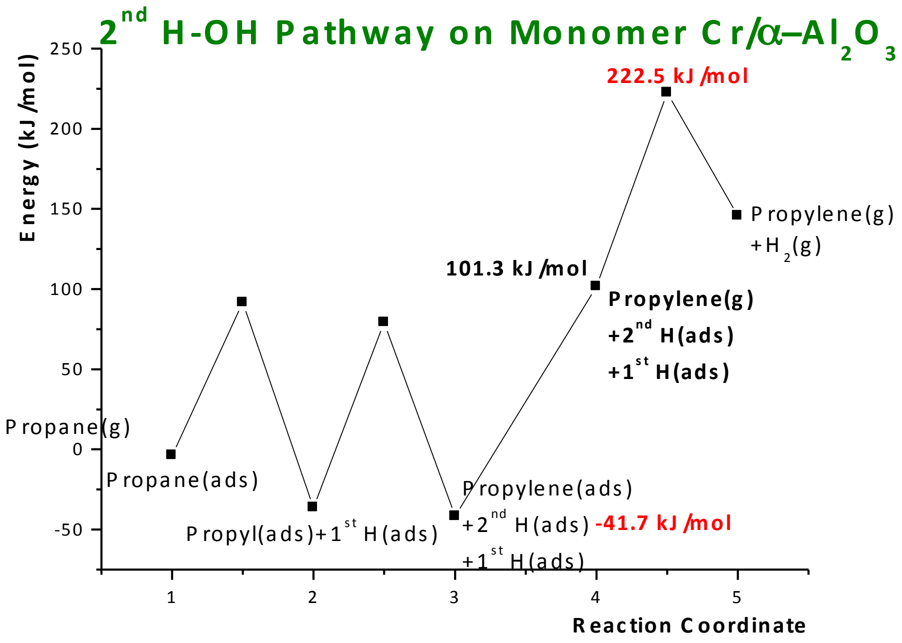

Figure 6.9.3 DFT-calculated reaction energy profile of the 2nd H-OH reaction pathway on monomer Cr/α-Al_2O_3 complex

Table 6.5 Energetics comparison between different paths for propane dehydrogenation on monomer Cr/α-Al_2O_3 complex

Path	$E_{ovr-act}$ **(kJ/mol)**	E_{rxn} **(H_2 Splitting) (kJ/mol)**
2nd H-Cr Path	217.2	-72.4
2nd H-O Path	320.2	41.5
2nd H-OH Path	264.2	-31.8

Comparing the states after propylene desorption (marked by “Propylene (g) + 2nd H (ads) + 1st H (ads)” from Figure 6.9.1 to 6.9.3), the 2nd H-Cr pathway also has the lowest energy (73.3 kJ/mol vs 181.4 kJ/mol for 2nd H-O path vs 101.3 kJ/mol for 2nd H-

OH path). The overall reaction starting from propane in the gas phase to this state involves the dissociative removal of two H atoms from the gas phase propane to form two hydrogen atoms bound to the Cr/α-Al_2O_3 surface. From this aspect, the energies should show similar trends to those found for the splitting of H-H bond of H_2 to form two surface hydrogen atoms (-72.4 kJ/mol for the H-Cr vs 41.5 and -31.8 kJ/mol for the H-O and H-OH paths) as is shown in Table 6.5 and Figure 6.10. The recombination activation energies for the adsorbed H* in the H-Cr, H-O and H-OH paths are similar to one another (106.4 kJ/mol vs 101.9 kJ/mol vs 108.5 kJ/mol) and are the activation energies for the reverse reaction of H_2 dissociation reported in Figure 6.10.

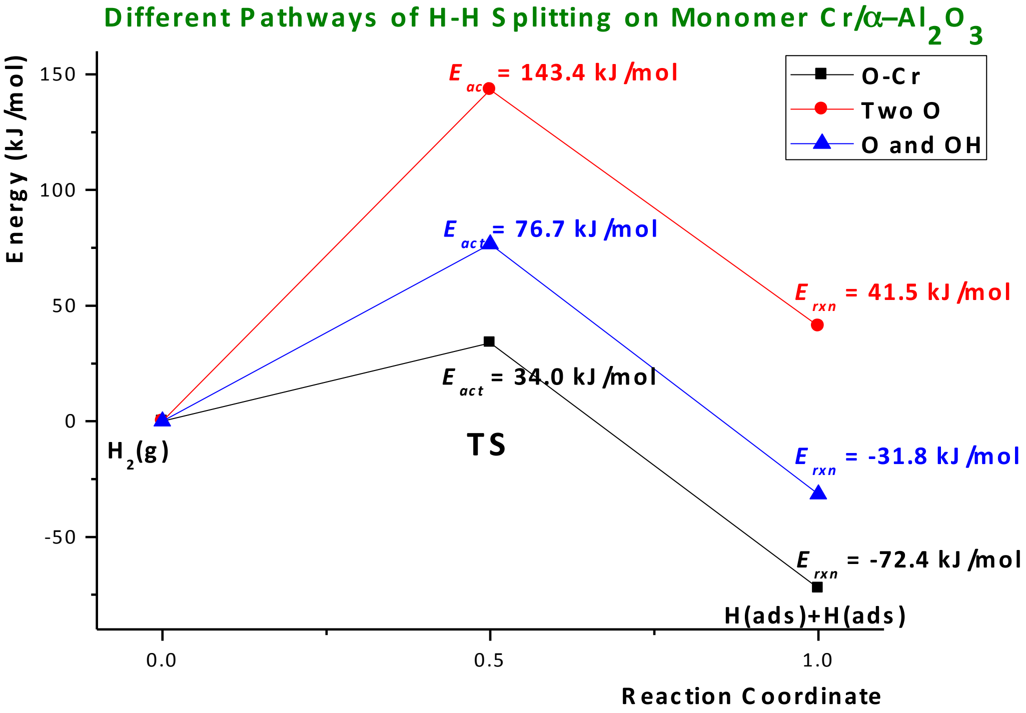

Figure 6.10 Different H-H splitting pathways on monomer Cr/α-Al_2O_3 complex

More generally, as long as propyl binds to the same Cr site in the 1st step, the contribution from Cr-C bond formation as a result of propyl binding in the 1st C-H activation and Cr-C bond breaking that results from the 2nd C-H activation and propylene desorption would be similar, so then the preference for different pathways can be understood from the activation of H_2 and H-H recombination.

6.6 Reaction Energy Profiles of Propane Dehydrogenation through Different Paths on Dimer and Trimer Cr/α-Al_2O_3 Complexes

The reaction energy profiles and PDH activity for the dimer and trimer Cr/α-Al_2O_3 complexes are very similar to those presented here for the monomer Cr/α-Al_2O_3 complex. The overall reaction energy profiles for the 2nd H-Cr, H-O and H-OH paths the dimer and trimer complexes are shown in Figure 6.11.1 and 6.11.2. It is also apparent that similar to the monomer case, the 2nd H-Cr pathway's preference is consistent with the energy preference at the point of "Propylene (g) + 2nd H + 1st H" marked in the figures, since the activation energies for H-H recombination are similar in these three different pathways.

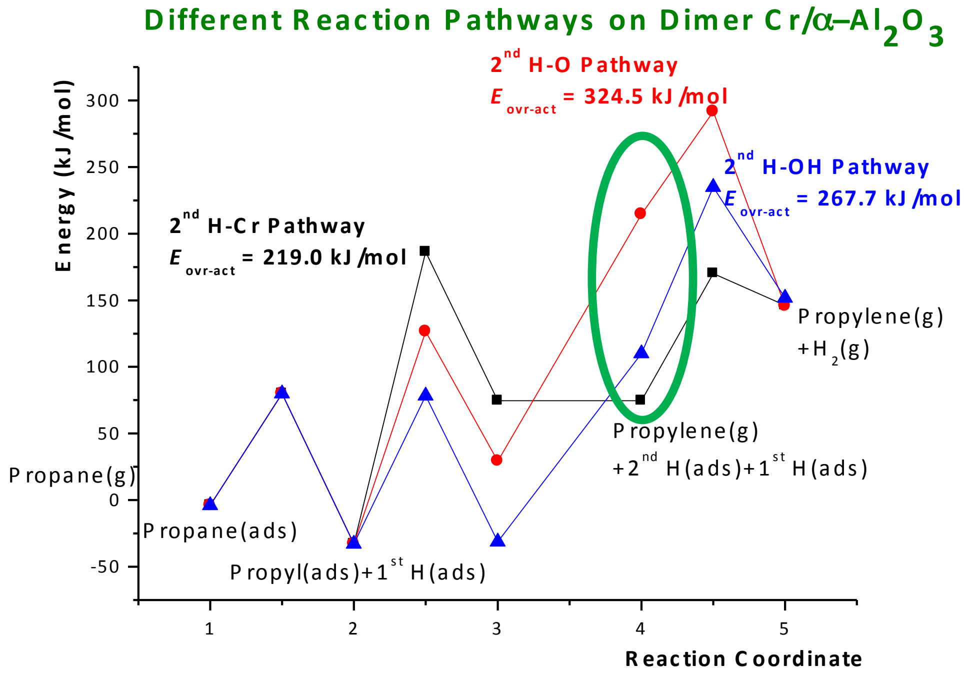

Figure 6.11.1 Energy profiles of different reaction pathways on dimer Cr/α-Al_2O_3 complex

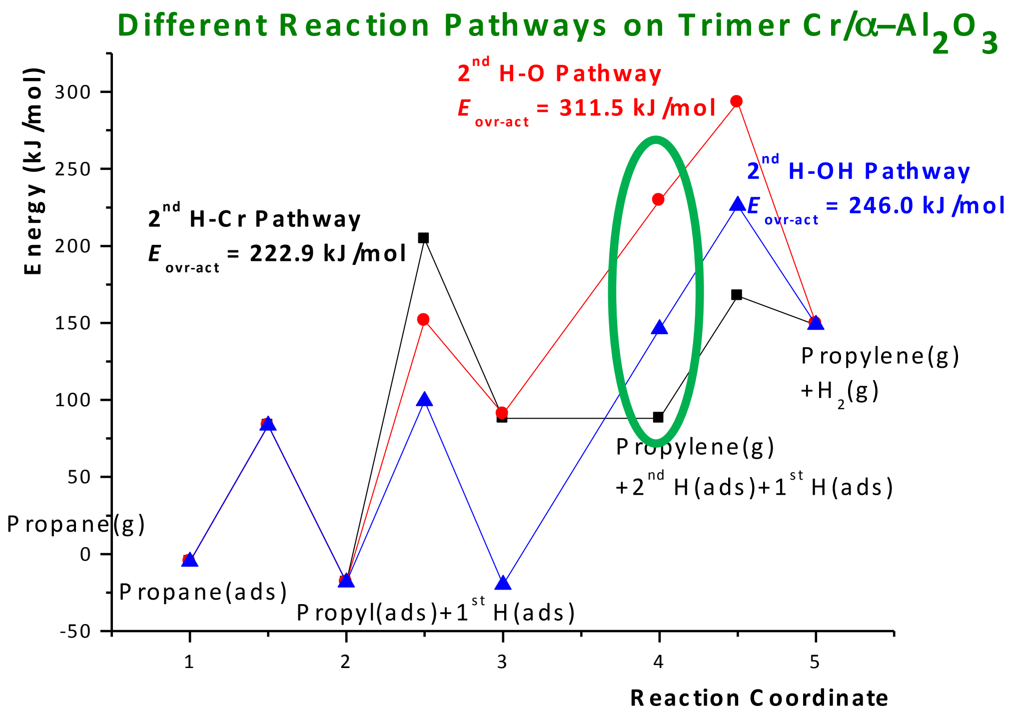

Figure 6.11.2 Energy profiles of different reaction pathways on trimer Cr/α-Al_2O_3 complexes

From the bader charge analysis results of 2nd H-Cr pathway (see Figure 6.12.1 and 6.12.2), the dimer and trimer Cr/α-Al_2O_3 complexes are further weaker electron acceptors than the monomer complex (Charge injection from propane: -0.16 e for monomer vs -0.04 e for dimer vs 0.02 e for trimer), and the trimer complex even loses a little electron to propane. The difference in charge transfer is small among these three complexes, but there seems to be a trend that the electron affinity of the Cr/α-Al_2O_3 complexes becomes weaker with the increase of Cr extent, which is consistent with the weak electron affinity of pure α-Cr_2O_3 surface who loses 0.11 e to propane during PDH reaction.

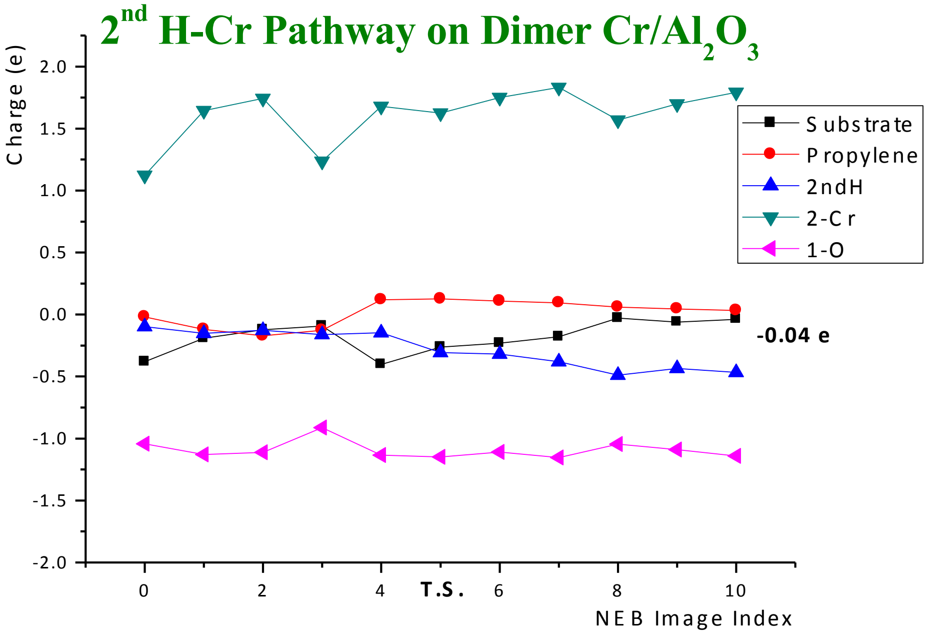

Figure 6.12.1 Bader charge analysis of the 2nd H-Cr pathway for the 2nd C-H activation on dimer Cr/α-Al_2O_3 complex. The charges on the substrate, propylene, 2nd H, 2-Cr and 1-O are shown in black, red, blue, green and purple, respectively.

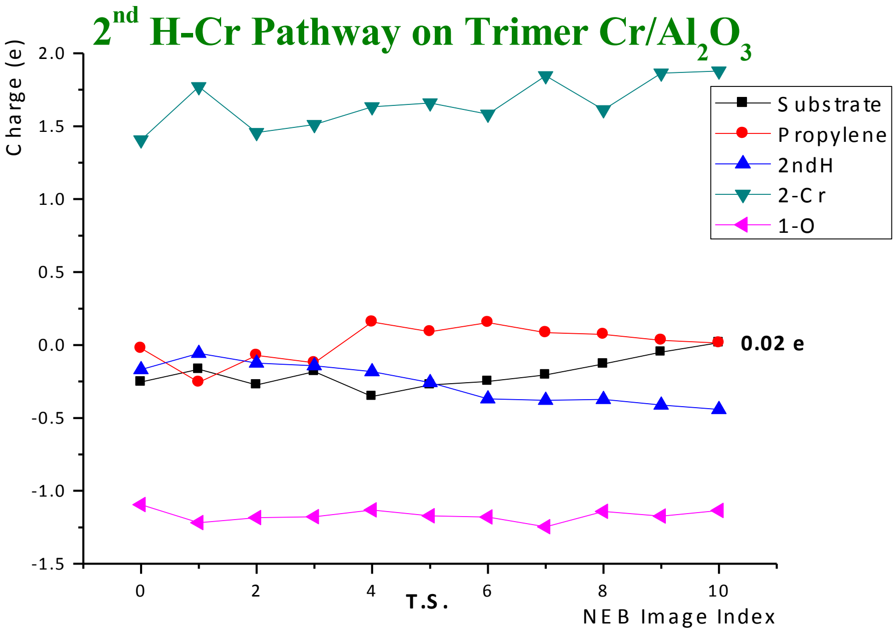

Figure 6.12.2 Bader charge analysis of the 2nd H-Cr pathway for the 2nd C-H activation on trimer Cr/α-Al_2O_3 complex. The charges on the substrate, propylene, 2nd H, 2-Cr and 1-O are shown in black, red, blue, green and purple, respectively.

6.7 Conclusions

The results from a detailed density functional theoretical calculations for elementary steps involved in propane dehydrogenation over α-Cr_2O_3 and monomeric CrO_x complexes on Al_2O_3 indicate that the 2nd H-Cr and H-O paths have significantly lower overall barriers (217.1 kJ/mol vs 257.6 kJ/mol, and 320.3 kJ/mol vs 382.1 kJ/mol respectively) on Cr/α-Al_2O_3 complexes than on the α-Cr_2O_3 surface.

The reaction mechanism involved in the activation of propane as well as the propyl intermediate that occur over the Cr-O sites appears to be quite similar for PDH over the α-Cr_2O_3 and over the monomer, dimer and trimer CrO_x clusters on the Al_2O_3 surface.

The resulting differences are related to binding of H which is weakly bound (-3.9 kJ/mol) to the O sites on the Cr/α-Al_2O_3 complex and unbound (+82.0 kJ/mol) on the O-sites on the α-Cr_2O_3 surface; the binding strengths of propyl and H on Cr sites of Cr/α-Al_2O_3 complexes are similar to those on α-Cr_2O_3 and are quite strong.

The results here taken together with the results in Chapter 3 which shows that the strong H-binding on the α-Al_2O_3 (-114.8 kJ/mol) and fully–hydroxylated α-Al_2O_3 surfaces (-70.4 kJ/mol) and inactivity on these surfaces indicate that highest catalytic activity for propane dehydrogenation requires sites with moderate H-binding energies that can activate C-H bonds and still allow for hydrogen desorption. Small Cr clusters results in the formation of Al-O-Cr sites which have weak H binding as opposed to the very strong H-binding to the O-sites on α-Al_2O_3 and the unbound H on O sites on α-Cr_2O_3.

The Cr complexes bound to the α-Al_2O_3 also lead to surfaces that result in slight negative charge gain or lose after the 2nd C-H activation (-0.16 e to +0.02 e), as compared to the α-Cr_2O_3 surface which loses 0.11 e to the reactants and the α-Al_2O_3 surfaces which gain negative charges from -0.61 e to -0.98 e. Therefore, the charge transfer properties of Cr/α-Al_2O_3 complexes seems to be in a moderate range compared to crystalline α-Al_2O_3 and α-Cr_2O_3, thus allow for greater overall activity.

Chapter 7 PDH on Amorphous Cr_2O_3/α-Al_2O_3 Complex

7.1 Introduction and Amorphous Cr_2O_3/α-Al_2O_3 Complex Structures

In addition to the Cr sites on crystalline α-Cr_2O_3 and the monomeric chromium clusters on α-Al_2O_3 that were discussed in chapters 4 and 6, amorphous Cr_2O_3 clusters anchored to α-Al_2O_3 may also be active for propane dehydrogenation. There are no reported structures for amorphous Cr_2O_3 clusters on Al_2O_3 reported in the literature. We have therefore used simulated annealing and ab initio molecular dynamics to find the lowest energy structures to model Cr_2O_3 clusters on the surface of α-Al_2O_3. Similar simulated annealing and MD simulations have been used to build models for other amorphous metal oxides [72-75].

We start by first cutting out a series of Cr_2O_3 clusters from the bulk crystalline α-Cr_2O_3, as models of the amorphous clusters. These clusters were subsequently optimized by using simulated annealing to find their lowest energy forms. Simulated annealing was carried by: 1) slowly heating the clusters from 0 K to 2710 K (melting point of α-Cr_2O_3 is 2708 K) over 100 steps of ionic relaxation, 2) holding the temperature constant at 2710 K for 500 steps of ionic relaxation and 3) slowly cooling the overall system down from 2710 K to 0 K over 1000 steps of ionic relaxation. In this way, stable amorphous Cr_2O_3 clusters with different sizes (2, 3, 4, 5 and 6 Cr_2O_3 units) were obtained (see Figure 7.1).

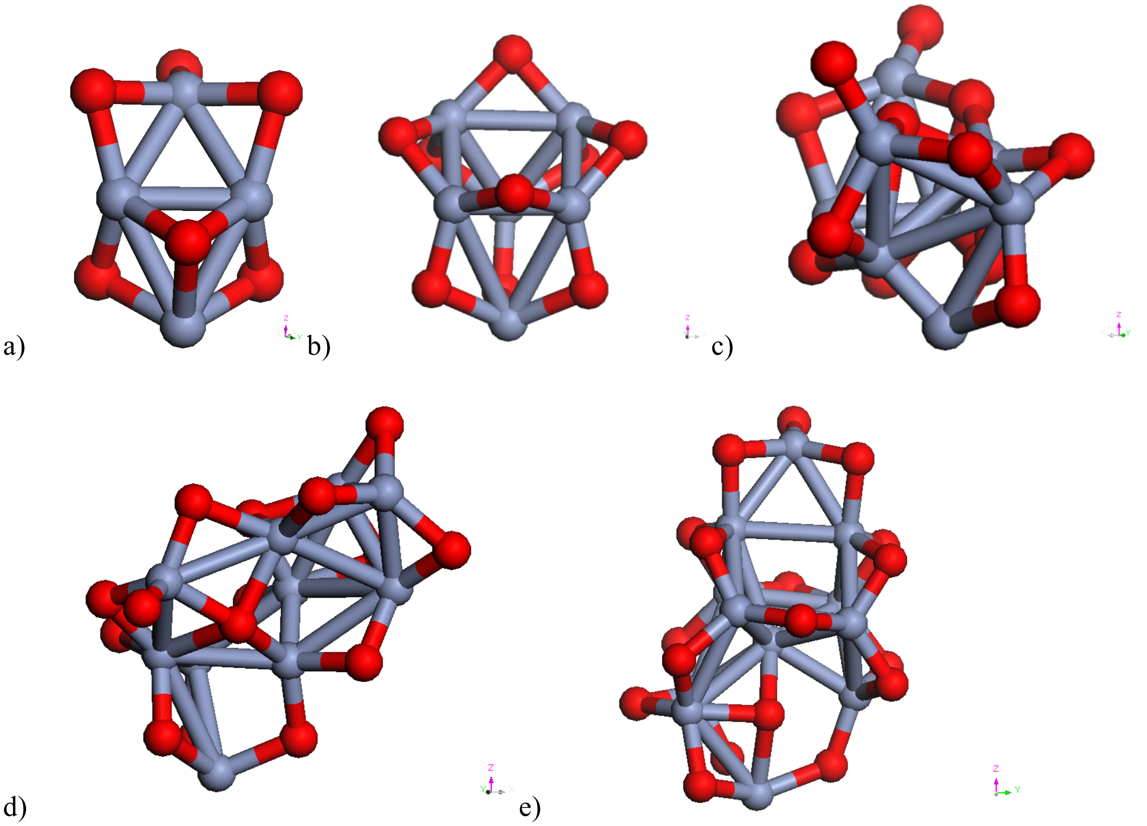

Figure 7.1 Calculated structures for amorphous Cr_2O_3 clusters obtained via ab initio molecular dynamics simulating annealing.

a) $2Cr_2O_3$ cluster, b) $3Cr_2O_3$ cluster, c) $4Cr_2O_3$ cluster,

d) $5Cr_2O_3$ cluster and e) $6Cr_2O_3$ cluster.

Compared to the crystalline α-Cr_2O_3 (0 0 0 1) surface, the Cr sites in these amorphous clusters can be slightly more coordinatively saturated. In α-Cr_2O_3, the surface Cr sites are bound to oxygens, while the Cr sites in the cluster are bound to three or four oxygens and in addition they are also coordinated to other Cr sites. The O atoms on α-Cr_2O_3 surface sit in 3-fold Cr sites where they are coordinated to three Cr ligands. The oxygen sites on the Cr_2O_3 clusters, on the other hand, reside at 2-fold bridge sites, and in some cases they are only bound to a single Cr site (See Figure 7.1 a), c), d), and e)). While the Cr sites on the amorphous Cr clusters are more coordinatively saturated than those on the α-Cr_2O_3 surface, the O sites are coordinatively unsaturated. These differences in the coordination states of the Cr and O sites on the amorphous clusters and the crystalline α-Cr_2O_3 will therefore likely result in different electronic properties, adsorption energies and reactivity.

Table 7.1 DFT-optimized Cr-O bond lengths of amorphous Cr_2O_3 clusters

	2Cr_2O_3	**3Cr_2O_3**	**4Cr_2O_3**	**5Cr_2O_3**	**6Cr_2O_3**
Cr-O Bond Length (Å)	1.6 – 2.0	1.7 – 1.9	1.6 – 2.2	1.6 – 2.2	1.6 – 2.1

To simulate the amorphous Cr_2O_3/α-Al_2O_3 complexes, the clusters must be anchored to the Al_2O_3 substate. As shown in Figure 7.2, the optimized clusters are bound to the fully hydroxylated α-Al_2O_3 surface via bonds between a Cr site on Cr_2O_3 clusters and three terminal hydroxyl groups on the substrate, thus resulting in an octahedral-type configuration at the Cr sites.

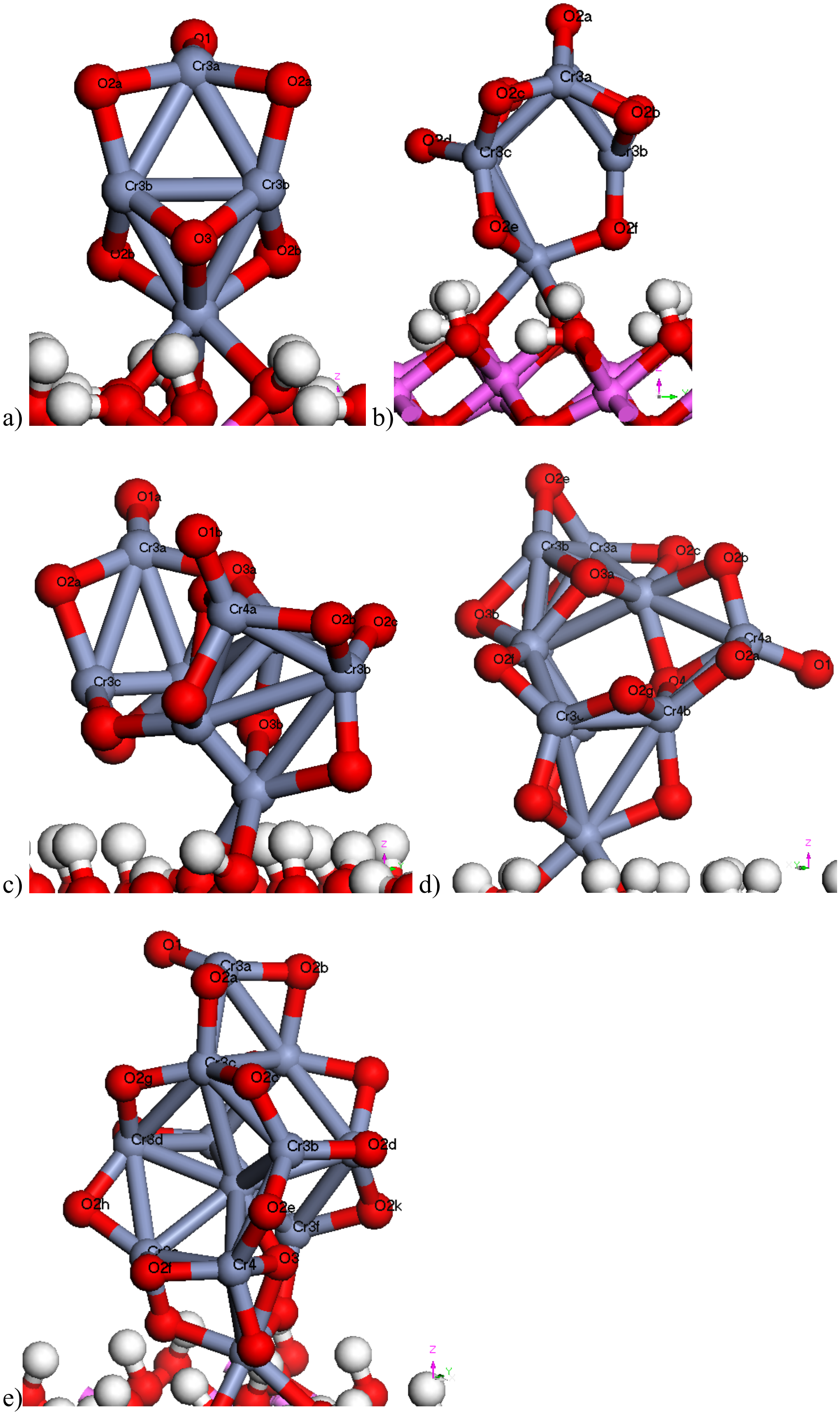
O1
Cr3a
O2a
O2a
Cr3b
Cr3b
O3
O2b
O2b
a)
O2a
Cr3a
O2c
O2b
O2d
Cr3c
Cr3b
O2e
O2f
b)
O1a
O1b
Cr3a
O3a
O2a
Cr4a
O2b
O2c
Cr3c
Cr3b
O3b
c)
O2e
Cr3b
Cr3a
O2c
O2b
O3a
O3b
Cr4a
O2a
O1
O2f
O2g
O4
Cr3c
Cr4b
d)
O1
Cr3a
O2a
O2b
Cr3c
O2g
O2c
Cr3d
Cr3b
O2d
O2h
O2e
O2k
Cr3f
O2f
Cr4
O3
e)

Figure 7.2 DFT-optimized amorphous Cr_2O_3 clusters bound to fully hydroxylated α-Al_2O_3 substrate. a) $2Cr_2O_3$/α-Al_2O_3, b) $3Cr_2O_3$/α-Al_2O_3, c) $4Cr_2O_3$/α-Al_2O_3, d) $5Cr_2O_3$/α-Al_2O_3 and e) $6Cr_2O_3$/α-Al_2O_3.

The bond lengths for the optimized supported clusters which are summarized in Table 7.2 are similar to those in Cr_2O_3 clusters.

Table 7.2 DFT-optimized bond lengths for the Cr_2O_3 complexes bound to the α-Al_2O_3

	$2Cr_2O_3$	**$3Cr_2O_3$**	**$4Cr_2O_3$**	**$5Cr_2O_3$**	**$6Cr_2O_3$**
Cr-O Bond length (Å)	1.6 – 2.0	1.7 – 1.9	1.6 – 2.2	1.6 – 2.2	1.6 – 2.1

7.2 Adsorption of the Hydrogen and Propyl Intermediates in Propane Dehydrogenation on Amorphous Cr_2O_3/α-Al_2O_3

The adsorption of the primary reactants, intermediates and products in propane dehydrogenation were examined at the different possible Cr and O sites on the amorphous Cr_2O_3. These sites are labeled by the Cr and O sites followed by the coordination number of the neighboring O and Cr sites, respectively. The letter that follows the coordination number represents the different positions of the sites with the same coordination number.

7.2.1 Adsorption of the Hydrogen and Propyl Intermediates on $2Cr_2O_3/\alpha\text{-}Al_2O_3$

In the $2Cr_2O_3/\alpha\text{-}Al_2O_3$ system, the symmetric cluster $2Cr_2O_3$ is comprised of a single 1-fold O-site, two pairs of 2-fold O-sites, and one 3-fold O sites along with two pairs of 3-fold Cr sites (see Figure 7.2 a)). The adsorption energies for hydrogen and propyl intermediates were examined at each of these sites. The results are reported in Table 7.3.1 and 7.3.2.

The binding of H at the O sites becomes weaker as the O coordination number increases. This is expected as the O site becomes more saturated with more Cr ligands. Hydrogen can bind to two different 2-fold O sites: the O2a site at the upper layer of the surface, and the O2b site in the lower layer closer to the substrate. The calculated binding energies of H at these sites are similar to one another with a small difference of 2.9 kJ/mol. This indicates that the distance from the Al_2O_3 substrate does not have a strong influence on these two 2-fold O sites.

Although the two 3-fold Cr sites (Cr3a-top layer and Cr3b-bottom layer) reside in different layers, they have similar H and propyl binding energies as reported in Table7.2. The H binding energies on Cr3a and Cr3b were both calculated to be -1.9kJ/mol and the propyl binding energies were -170.9 and -168.8 kJ/mol, respectively. So the influence of the Cr distance from Al_2O_3 substrate appears to be weak as well.

Table 7.3.1 DFT-calculated H and propyl intermediate binding energies on the O sites of amorphous $2Cr_2O_3/\alpha\text{-}Al_2O_3$

	H-O1	**H-O2a**	**H-O2b**	**H-O3**
$\boldsymbol{E_{ads}}$ **(kJ/mol)**	-38.6	1.0	-1.9	69.5

Table 7.3.2 DFT-calculated H and propyl intermediate binding energies on the Cr sites of amorphous $2Cr_2O_3/\alpha\text{-}Al_2O_3$

	H-Cr3a	**H-Cr3b**
$\boldsymbol{E_{ads}}$ **(kJ/mol)**	-1.9	-1.9
	Propyl-Cr3a	**Propyl-Cr3b**
$\boldsymbol{E_{ads}}$ **(kJ/mol)**	-170.9	-168.8

7.2.2 Adsorption of the Hydrogen and Propyl Intermediates on $3Cr_2O_3/\alpha\text{-}Al_2O_3$

The $3Cr_2O_3/\alpha\text{-}Al_2O_3$ is a symmetric structure where all of its O sites are 2-fold and all its Cr sites are 3-fold (see Figure 7.2 b)). For O sites, there are four layers in total with 6 different types of O sites: the O2a site is the only atop site; the O2b and the O2c sites are both symmetric O sites that reside in the 2nd layer; the O2d site is the only site in the 3rd layer; the symmetric O2e and non-symmetric O2f sites are in the bottom layer. For Cr sites, there are two layers with 3 types of Cr sites in total: Cr3a is a symmetric site that resides in the 1st layer; Cr3b is a symmetric site in the 2nd layer, and Cr3c is an asymmetric site that also resides in 2nd layer.

Table 7.4.1 DFT-calculated binding energies for H and propyl intermediates on O sites of amorphous $3Cr_2O_3/\alpha\text{-}Al_2O_3$

	H-O2a	**H-O2b**	**H-O2c**	**H-O2d**
$\boldsymbol{E_{ads}}$ **(kJ/mol)**	56.0	20.1	26.7	51.1

Table 7.4.2 DFT-calculated binding energies for H and propyl intermediates on Cr sites of amorphous $3Cr_2O_3/\alpha\text{-}Al_2O_3$

	H-Cr3a	**H-Cr3b**	**H-Cr3c**
$\boldsymbol{E_{ads}}$ **(kJ/mol)**	39.6	28.9	23.2
	Propyl-Cr3a	**Propyl-Cr3b**	**Propyl-Cr3c**
$\boldsymbol{E_{ads}}$ **(kJ/mol)**	-120.6	-120.6	-118.7

Hydrogen does not appear to bind favorably to any of the O sites as the energies are all positive. The binding of hydrogen to the O2b and O2c sites is more favorable than the binding to the O2a and O2e sites. This is likely due to the fact that O2b and O2c sites bind to Cr centers that have more O neighbors than those for the O2a and O2d sites. As such they compete for electron density from the Cr sites with more O sites and are less saturated in electron density, thus lead to stronger H-binding energies than the O2a and O2d sites. The results of Bader charge analysis are consistent with this idea showing that the charge on O2b and O2c sites is about -0.80 e, while that on O2a site and O2d site is -0.88 e and -0.91 e respectively. The O2e and O2f sites in the bottom layer do not appear to bind H due to strong steric effect from substrate hydroxyl groups.

Hydrogen appears to favorably bind to all of the different Cr3 sites as is shown in Table 7.4.2. The calculated H-binding energies on all of the different Cr3 sites are very similar ranging from -118.7 to -120.7 kJ/mol. This indicates a weak influence of the position relative to the Al_2O_3 substrate and is consistent with the cases on $2Cr_2O_3$/α-Al_2O_3.

7.2.3 Adsorption of Hydrogen and Propyl Intermediates on $4Cr_2O_3$/α-Al_2O_3, $5Cr_2O_3$/α-Al_2O_3 and $6Cr_2O_3$/α-Al_2O_3

For clusters larger than $3Cr_2O_3$, there are many more types of possible reaction sites. Some of these sites are combined based on their coordination numbers in the following tables of adsorption behavior.

The adsorption or binding of H to the O sites drops significantly with increasing the O coordination number (see Table 7.5.1). Hydrogen binds favorably to the 1-fold O sites with binding energies that range from -56.0 to -16.3 kJ/mol. Hydrogen binding energy on the 1-fold O sites was found to be stronger for the O1 coordinated to 4-fold Cr site (-56.0 kJ/mol) verses the O1 coordinated to 3-fold Cr site (-16.3 kJ/mol), since the O1 coordinated to Cr4 picks up less electron density than the O1 coordinated to Cr3 and thus more unsaturated. The H binding energies on the O2 and O3 sites on the other hand are unfavorable ranging from +3.9 to +27 kJ/mol for the O2 sites and +28.8 kJ/mol for the O3 sites.

Table 7.5.1 DFT-calculated binding energies for H and propyl intermediates on O sites of amorphous $4Cr_2O_3/\alpha\text{-}Al_2O_3$

	H-O1 Sites	**H-O2 Sites**	**H-O3**
E_{ads} **(kJ/mol)**	-56.0 – -16.3	3.9 – 27.0	28.8

Table 7.5.2 DFT-calculated binding energies for H and propyl intermediates on Cr sites of amorphous $4Cr_2O_3/\alpha\text{-}Al_2O_3$

	H-Cr3a	**H-Cr3b**	**H-Cr3c**
E_{ads} (kJ/mol)	-8.7	35.7	97.5
	Propyl-Cr3a	**Propyl-Cr3b**	**Propyl-Cr3c**
E_{ads} (kJ/mol)	-177.5	-110.0	-71.4

Hydrogen and propyl binding energies at the Cr sites were found to be the strongest at the Cr3a site. This Cr site is bound to a terminal oxygen as well as bridging oxygen centers. The terminal O site is more unsaturated than O2 and O3 sites, so it would pick up more electron density from the Cr3a site. As a result the Cr3a site is more unsaturated and binds the H and propyl intermediates more strongly. The Cr3b site binds propyl and H more strongly compared with the Cr3c site. The reason might be that two of its O2 ligands are bound to the two 4-fold Cr sites respectively, so with more O competitors these two O2 ligands are more unsaturated than the O2 ligands of Cr3c site, leading to more unsaturated Cr3b site than Cr3c site.

For the two 4-fold Cr sites in this cluster, one of them is not available for propyl to bind due to strong steric effects, and the other Cr4 site would not be bound to one of its O ligands in adsorption tests, resulting in binding strengths similar to the Cr3c site.

Table 7.6.1 DFT-calculated binding energies for H and propyl binding at the O sites on amorphous $5Cr_2O_3/\alpha\text{-}Al_2O_3$

	H-O1	**H-O2 Sites**	**H-O3**
E_{ads} **(kJ/mol)**	-58.5	-59.0 – 24.4	46.3

Table 7.6.2 DFT-calculated binding energies for H and propyl groups at Cr sites of amorphous $5Cr_2O_3/\alpha\text{-}Al_2O_3$

	H-Cr3a	**H-Cr3b**	**H-Cr**
E_{ads} **(kJ/mol)**	-4.5	-18.4	18.2
	Propyl-Cr3a	**Propyl-Cr3b**	**Propyl-Cr4**
E_{ads} **(kJ/mol)**	-168.3	-176.8	-101.3

The results reported for the 5-fold coordinated O sites on $5Cr_2O_3/\alpha\text{-}Al_2O_3$ show the general trend of weaker H binding with the increasing coordination number of the O binding site (see Table 7.6.1). Among the 2-fold O sites, the two O sites sharing the same Cr site with the 1-fold O site have the strongest H binding, as these two O sites pick up less electron density from Cr under the influence of the terminal O site. The O2 site that sits at the top of the cluster has the weakest H binding energy among the bridging (2-fold) O sites. This site is similar to the top O2 site in the $3Cr_2O_3/\alpha\text{-}Al_2O_3$ system (see Table 7.4.1) as it is the most saturated O2 site with the lowest number of competing O sites. For the rest of the O2 sites, there is no significant difference with the range of H binding energy narrowly distributed from -14.2 to 10.8 kJ/mol.

In analyzing the binding at the Cr sites on the $5Cr_2O_3/\alpha\text{-}Al_2O_3$ system, the two 3-fold sites along with the single 4-fold Cr site appear to be the most likely reaction sites, as the steric interactions are significantly weaker at these sites than at other sites.. Among these, the two 3-fold Cr sites have similar binding properties, since they have similar surrounding environment. The binding of hydrogen at the two 3-fold Cr sites is stronger than that at the 4-fold Cr sites, which is consistent with the previous noted trend of decreasing binding energy with increasing coordination number of the O sites.

The $6Cr_2O_3/\alpha\text{-}Al_2O_3$ system contains only one O1 site and one O3 site; the remaining O sites are all 2-fold. For the Cr sites, there is only one 4-fold site. The remaining Cr sites are 3-fold.

Table 7.7.1 DFT-calculated binding energies for H at the O sites of amorphous $6Cr_2O_3/\alpha\text{-}Al_2O_3$

	H-O1	**H-O2 Sites**	**H-O3**
E_{ads} (kJ/mol)	-48.0	-66.9 – 46.3	21.8

Table 7.7.2 DFT-calculated binding energies for H and propyl intermediates at the Cr sites of amorphous $6Cr_2O_3/\alpha\text{-}Al_2O_3$

	H-Cr3a	**H-Other Cr3 Sites**	**H-Cr4**
E_{ads} (kJ/mol)	-11.2	107.2 – 135.7	77.5
	Propyl-Cr3a	**Propyl-Other Cr3 Sites**	**Propyl-Cr4**
E_{ads} (kJ/mol)	-195.9	-49.9 – -23.1	-76.1

As in previous $Cr_2O_3/\alpha\text{-}Al_2O_3$ systems, the H is more weakly held to O sites that have higher coordination numbers (see Table 7.7.1). There is one O2 site (-66.9 kJ/mol), however, that binds H more strongly than the O1 site, as it is coordinated with the 4-fold

Cr site and thus more unsaturated. The higher degree of unsaturation at the 2-fold Cr site supported by a Bader charge analysis which shows that the O2 site is slightly more unsaturated (-0.78 e) than the O1 site (-0.80 e). The two O2 sites that share the same Cr center with the O1 site can also bind H rather strongly. Other than these particular sites, the binding strengths of H on the rest of the 2-fold O sites are narrowly distributed in a moderate range from -15.2 to 28.9 kJ/mol. The only 3-fold O site would break one of its bonds to a Cr ligand thus the resulting binding energy (21.8 kJ/mol) is in the moderate range of O2 sites.

For Cr sites, the Cr3a site coordinated with O1 is more unsaturated and thus has a significantly stronger affinity for both H and propyl. The rest of the Cr3 sites bind H and propyl with similar adsorption strengths as they are in similar surrounding environment. The 4-fold Cr site binds propyl and H more strongly than most of the 3-fold Cr sites, which indicates that this 4-fold Cr site is more unsaturated.

7.2.4 Summary of Adsorption of the Hydrogen and Propyl Intermediates on Amorphous Cr_2O_3/α-Al_2O_3 and Comparison with other Oxides

As discussed in the previous section, the binding of propyl and H to the O and Cr sites, in general, becomes weaker with increases in the coordination number of the active site. In addition, the coordination states of the nearby sites could also affect the binding abilities: For O sites, the binding becomes weaker with decreases in the coordination number of the next-nearest Cr ligands, since with less O competitors it could pick up more negative charge from the Cr ligands and thus is more saturated; For Cr sites, the binding becomes stronger with decreases in the coordination number of the nearest O ligands, since it needs to transfer more negative charge to the O ligands and thus is more unsaturated. The first factor is the main deciding factor in most cases, but sometimes the second factor could be strong enough that the site with higher coordination number has stronger bindings than the site with lower coordination number, such as the O2 site in $6Cr_2O_3/\alpha\text{-}Al_2O_3$ system (see Table 7.7.1) For some sites, the metal-ligand interaction is very weak and can be broken thus resulting in binding energies that are more characteristic of sites with lower coordination numbers.

In general, the position and relative location of O and Cr sites with respect to the Al_2O_3 substrate do not appear to significantly influence the calculated H or the propyl binding energies. On the smaller symmetric $2Cr_2O_3$ and $3Cr_2O_3$ clusters, the sites with same coordination numbers in different positions have similar binding properties. On larger and more complex clusters, the coordination number of active Cr and O sites along with the coordination number or saturation of their ligands is important in controlling the H and propyl binding energies.

The comparison among different amorphous $Cr_2O_3/\alpha\text{-}Al_2O_3$ complexes analyzed here and the $\alpha\text{-}Cr_2O_3$ and $\alpha\text{-}Al_2O_3$ surfaces discussed previously are shown in Table 7.8 below.

Table 7.8 DFT-calculated binding energies for H and propyl intermediates on the amorphous Cr_2O_3/α-Al_2O_3, α-Cr_2O_3, monomer Cr/α-Al_2O_3complex (“Cr/α-Al_2O_3” in table), and α-Al_2O_3 surfaces.

E_{ads} (kJ/mol)	**$2Cr_2O_3$/α-Al_2O_3**	**$3Cr_2O_3$/α-Al_2O_3**	**$4Cr_2O_3$/α-Al_2O_3**	**$5Cr_2O_3$/α-Al_2O_3**	**$6Cr_2O_3$/α-Al_2O_3**	**α-Cr_2O_3**	**Cr/α-Al_2O_3**	**α-Al_2O_3**
H-O1	-38.6	N/A	-56.0 – -16.3	-58.5	-48.0	N/A	N/A	N/A
H-O2	-1.9 – 1.0	20.1 – 56.0	3.9 – 27.0	-59.0 – 24.4	-66.9 – 46.3	N/A	N/A	N/A
H-O3	69.5	N/A	28.8	46.3	21.8	82.0	-3.9	-114.8
H-M	-1.9	23.2 – 39.6	-8.7 – 97.5	-4.5 – 18.2	-11.2 – 135.7	-78.2	-56.0	180.4
Propyl-M	-170.9 – -168.8	-120.6 – -118.7	-177.5 – -71.4	-176.8 – -101.3	-195.9 – -23.1	-246.0	-232.5	-31.8

In comparing the different amorphous Cr_2O_3 clusters on the Al_2O_3 substrate, there does not appear to be an apparent correlation between the cluster size and binding abilities. As the complexity of the Cr_2O_3 clusters increases with increases in cluster size, the range of binding abilities becomes broader for 2-fold O sites and 3-fold Cr sites (which are the major sites in these clusters) due to the different ligand environments.

Compared with the crystalline α-Cr_2O_3 surface, the binding strengths of H on O sites are stronger on Cr_2O_3/α-Al_2O_3, whereas the Cr sites bind both H and propyl more weakly on the Cr_2O_3/α-Al_2O_3 than on the α-Cr_2O_3. This is due to greater degree of unsaturated coordination states of O site and the more saturated coordination states of Cr sites on the Cr complexes than on α-Cr_2O_3. Compared with the monomeric chromia complexes on alumina (Cr/α-Al_2O_3), the 3-fold O sites present on the amorphous chromia complexes bind H more weakly, while the 2-fold and 1-fold O sites present in the amorphous chromia complexes have similar H binding energies or even stronger than those in the monomer complex. The binding energies on the Cr sites for the monomeric Cr/α-Al_2O_3 were calculated to be stronger than amorphous complexes for both H and propyl.

Compared with the crystalline α-Al_2O_3 surface, the binding energies of H to the O-sites were calculated to be significantly weaker on the amorphous chromia complexes, whereas the binding energies for H and propyl on the metal sites were found to be much stronger than those on α-Al_2O_3.

In general, the binding energies for the H and propyl intermediates on the amorphous Cr_2O_3 clusters were found to be much more moderate than those on α-Al_2O_3 and α-Cr_2O_3 surfaces, which is predominantly due to the more moderate coordination states of O sites and Cr sites. The binding energies of H and propyl are rather polarized on the α-Al_2O_3 and α-Cr_2O_3 surfaces, and thus result in either a deep adsorption well or a high C-H activation barrier thus limiting the catalytic turnover for propane dehydrogenation.

The Cr sites on the amorphous chromia clusters have weaker binding abilities than on α-Cr_2O_3 and Cr/α-Al_2O_3, which might be helpful to the 2nd C-H activation since propyl needs to desorb from Cr site firstly. For the O-sites, while they have a wide range of different H-binding energies, they all fall between those found on the α-Al_2O_3 and α-Cr_2O_3 surfaces and close to the moderate binding of H on O sites on monomer Cr/α-Al_2O_3. The more moderate H- and propyl- interactions on the supported Cr complexes therefore suggest that these supported clusters may be more active for carrying out propane dehydrogenation.

7.3 C-H Activation of Propane on Amorphous $Cr_2O_3/\alpha\text{-}Al_2O_3$

7.3.1 Propane Dehydrogenation on Amorphous $2Cr_2O_3/\alpha\text{-}Al_2O_3$

7.3.1.1 1st C-H Activation of Propane on Amorphous $2Cr_2O_3/\alpha\text{-}Al_2O_3$

The activation of the 1st C-H activation on the amorphous $2Cr_2O_3/\alpha\text{-}Al_2O_3$ complex was calculated to preferentially occur over Cr-O site pairs. The Cr-O sites pairs that lie in the lower layers closest to the substrate lead to strong repulsive interactions between the hydroxyl groups at the substrate interface and the reaction intermediates. As such we predominantly focus on C-H activation over the Cr-O site pairs within the outermost layer (at Cr3a).

The outer Cr3a site binds a 1-fold O site (O1) and two symmetric 2-fold O sites (O2a), thus resulting in Cr3a-O1 and Cr3a-O2a site pairs. As shown in Table 7.9, the DFT-calculated reaction energies for the C-H activation of propane over the Cr3a-O1 and Cr3a-O2a sites were endothermic at 41.8 and 52.5 kJ/mol, respectively, which are fairly close to one another. The reaction appears to involve the heterolytic splitting of C-H bond as shown in changes in structure reported in Figure 7.3.1-7.3.2 and Table 7.10 to form a propyl-Cr and O-H intermediates. The detailed Bader charge analysis shown in Figure 7.4 follows the change in charge on the Cr3a, propyl, O2a, H and surface states along the reaction trajectory for the activation of the secondary C-H bond of propane over the Cr3a-O2a site. The results clearly show that propyl and H species become negatively and positively charged respectively as the reaction proceeds. After the 1st C-H activation there is a small degree of electron transfer into the supported Cr_2O_3 cluster.

Table 7.9 DFT calculated activation barriers and reaction energies for the activation of the 1st C-H of propane on different Cr-O pairs on $2Cr_2O_3$/α-Al_2O_3

	Cr3a-O1 Pathway	**Cr3a-O2a Pathway**
E_{act} (kJ/mol)	128.4	125.7
E_{rxn} (kJ/mol)	41.8	52.5

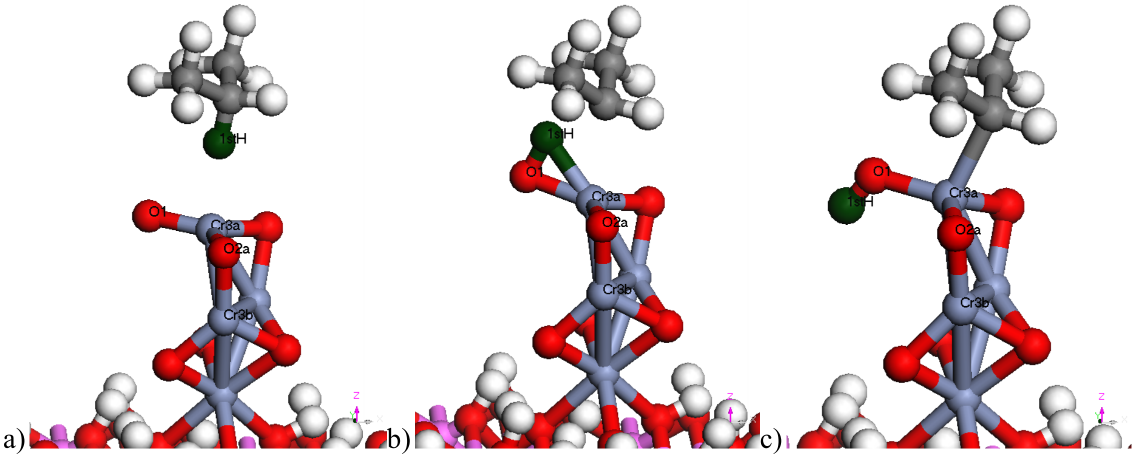

Figure 7.3.1 1st C-H bond activation on Cr3a-O1 pair on amorphous $2Cr_2O_3$/α-Al2O3: a) Reactant, b) TS and c) Product structures.

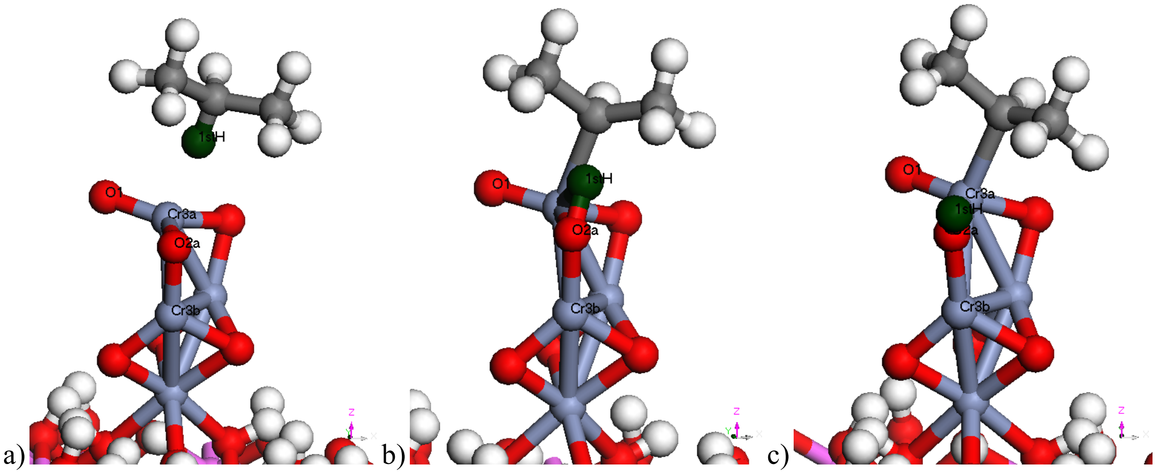

Figure 7.3.2 1st C-H bond activation on Cr3a-O2a pair on amorphous $2Cr_2O_3/\alpha\text{-}Al_2O_3$: a) Reactant, b) TS and c) Product structures.

Table 7.10 Evolution of bond distances during the 1st C-H activation of propane through different paths on amorphous $2Cr_2O_3/\alpha\text{-}Al_2O_3$

Path	**Bond Distance**	**Reactant**	**TS**	**Product**
Cr3a-O1 Path	**1st H-O (Å)**	2.5	1.1	1.0
	C-Cr (Å)	3.2	2.4	2.1
Cr3a-O2a Path	**1st H-O (Å)**	2.6	1.1	1.0
	C-Cr (Å)	3.2	2.3	2.1

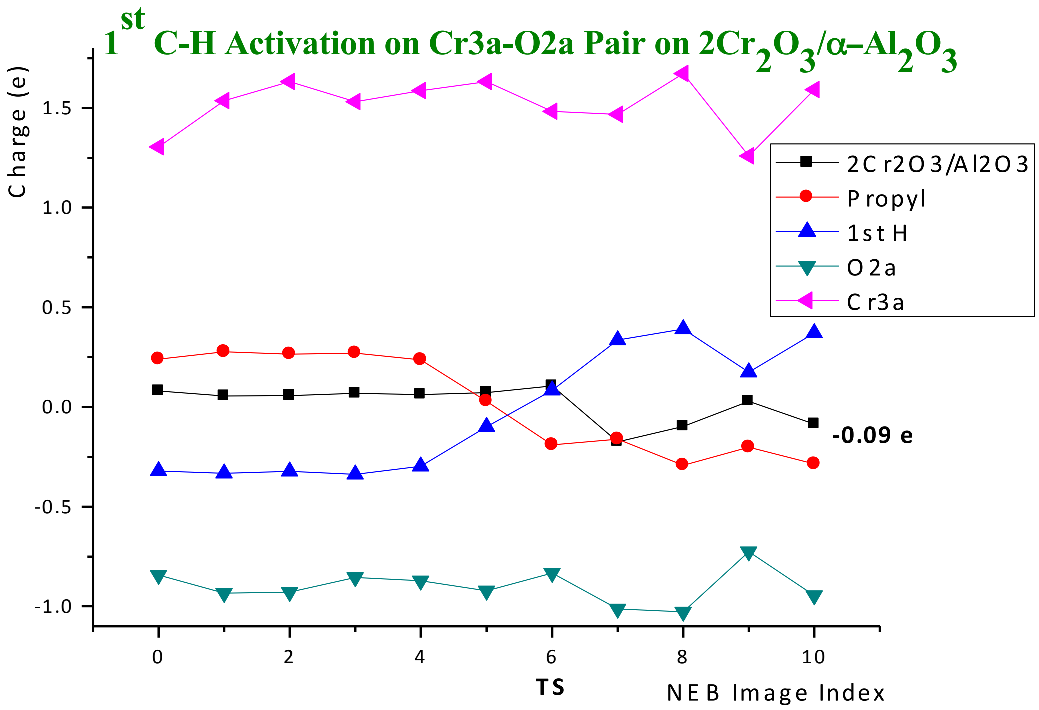

Figure 7.4 Bader charge analysis for the Cr3a, O2a, H and propyl sites for the 1st C-H bond activation over the Cr3a-O2a pair on amorphous $2Cr_2O_3/\alpha\text{-}Al_2O_3$

The activation energies (125.7-128.4 kJ/mol) and the reaction energies (41.8-52.5 kJ/mol) on this cluster are similar to those that were reported for the crystalline $\alpha\text{-}Cr_2O_3$ surface (E_{act} = 119.6 kJ/mol and E_{rxn} = 45.7 kJ/mol) in Chapter 4. This is due to the balance between a weaker binding of propyl on Cr and a stronger binding of H on O than that on the crystalline $\alpha\text{-}Cr_2O_3$ surface. The barrier and overall reaction energy are somewhat higher though than that on the monomer $Cr/\alpha\text{-}Al_2O_3$ system (E_{act} = 91.7 kJ/mol and E_{rxn} = -36.7 kJ/mol) due to the weaker binding of propyl on the Cr site and the similar H binding strength on the O site.

7.3.1.2 2^{nd} C-H Activation of Propane on Amorphous $2Cr_2O_3/\alpha$-Al_2O_3

The activation of the 2^{nd} C-H bond is favored at the Cr site that carried out the 1^{st} C-H activation, which is similar to that reported for the activation of propyl over the α-Cr_2O_3 surface and monomeric Cr/α-Al_2O_3 surfaces. As discussed in Chapter 4, the primary C-H bond of the bound propyl intermediate is activated to release propylene into the gas phase and form a surface hydride on the Cr site (H-Cr) (see Figure 7.4.1 to 7.4.2). This step takes place at the same Cr site for the two Cr-O site pairs considered, and as such this step is essentially the same. This is consistent with the calculated activation energies reported in Table 7.11 and the bond distances reported in Table 7.12simila. The slightly different reaction energies (109.6 kJ/mol vs 84.3 kJ/mol) are probably due to the differences in the stabilization effect of the H species at different O sites and the different distances of propylene from the Cr site in the product (4.4 **Å** vs 5.0 **Å**) shown in Table 7.12.

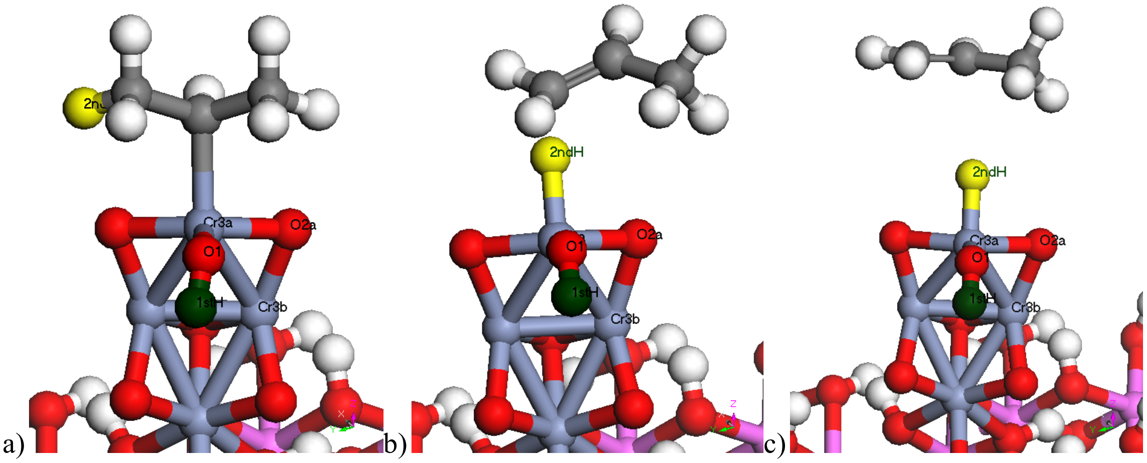

Figure 7.5.1 The activation of the 2^{nd} (terminal) C-H bond of propane on Cr3a-O1 site pair on amorphous $2Cr_2O_3/\alpha$-Al_2O_3: a) Reactant, b) TS and c) Product structures.

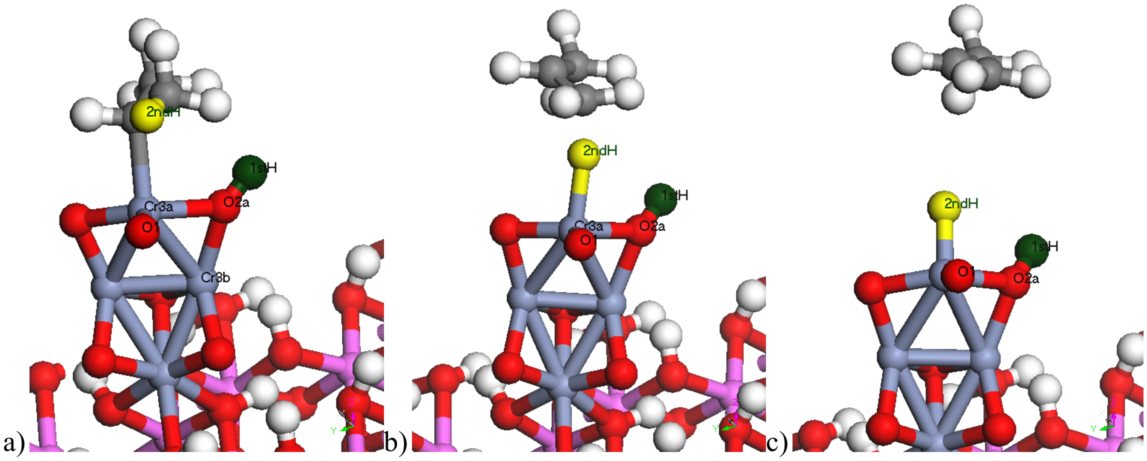

Figure 7.5.2 The activation of the 2nd (terminal) C-H bond of propane on Cr3a-O2a site pair on amorphous $2Cr_2O_3/\alpha\text{-}Al_2O_3$: a) Reactant, b) TS and c) Product structures.

Table 7.11 DFT-calculated activation barriers and reaction energies for the activation of the 2nd (terminal) C-H activation of propane on different Cr-O pairs on $2Cr_2O_3/\alpha\text{-}Al_2O_3$.

Path	**Cr3a-O1 Path**	**Cr3a-O2a Path**
E_{act} **(kJ/mol)**	139.9	147.8
E_{rxn} **(kJ/mol)**	109.6	84.3

Table 7.12 Evolution of bond distances during the 2nd (terminal) C-H activation of propane on different Cr-O pairs on amorphous $2Cr_2O_3/\alpha\text{-}Al_2O_3$

Path	**Bond Distance**	**Reactant**	**TS**	**Product**
Cr3a-O1 Path	**2nd H-Cr (Å)**	3.1	1.7	1.6
	C-Cr (Å)	2.1	3.7	4.4
Cr3a-O2a Path	**2nd H-Cr (Å)**	3.1	1.8	1.6
	C-Cr (Å)	2.1	3.8	5.0

A detailed Bader charge analysis of this 2nd C-H activation over the Cr3a-O2a site pair is shown in Figure 7.6. The results indicate that terminal C-H bond of the propyl is activated by the Cr site to form propylene which desorbs and a Cr-hydride intermediate ($H^{\delta-}$-$Cr^{\delta+}$). Overall the Cr_2O_3 complex loses 0.16 eletrons during the activation of propane. The monomeric Cr/α-Al_2O_3 system, on the other hand, gained a very small amount of negative charge (-0.02 e) overall in the activation of propane. The Cr_2O_3 complex examined here has a slightly weaker electron affinity than that for the monomeric Cr complex.

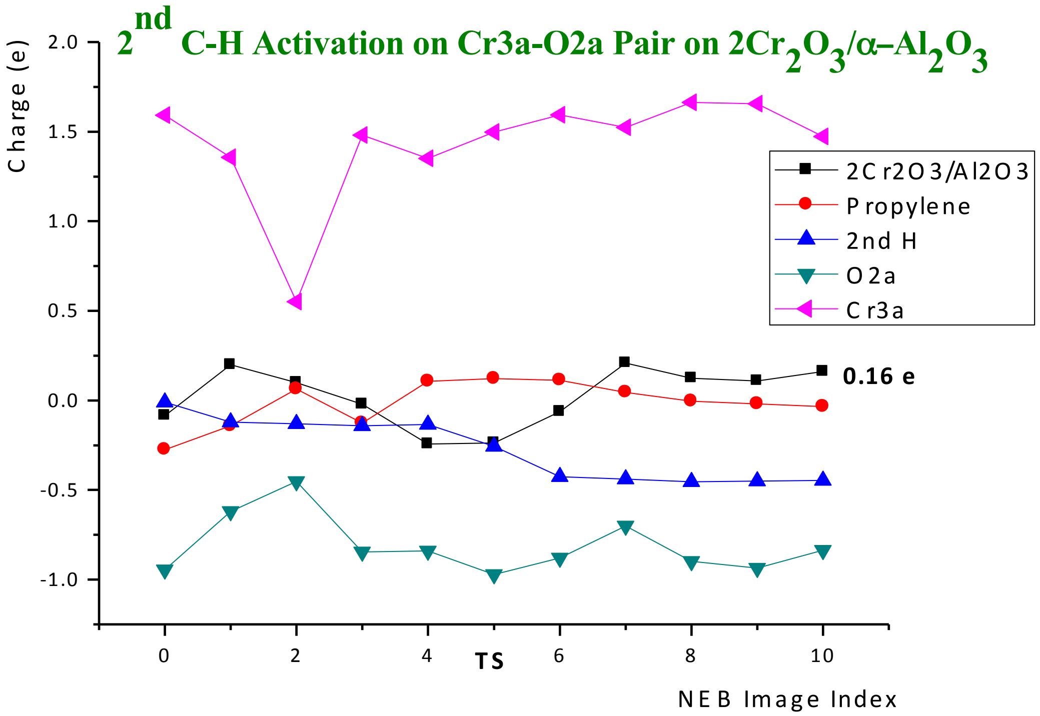

Figure 7.6 Bader charge analysis of the changes in charge on the Cr3a, O2a, H and propylene during the activation of the 2nd (terminal) C-H bond of propane to form propylene over the Cr3a-O2a site pair on amorphous $2Cr_2O_3$/α-Al_2O_3.

Since Cr sites on this cluster bind propyl more weakly than those on α-Cr_2O_3 and monomer Cr/α-Al_2O_3, the barriers for this 2nd C-H activation step (139.9 kJ/mol for Cr3a-O1 and 147.8 kJ/mol on Cr3a-O2) are lower than on those on the α-Cr_2O_3 and monomer Cr/α-Al_2O_3 surfaces (202.6 kJ/mol and 217.1 kJ/mol respectively). The reaction energies do not differ very much over these three cases though, as the reaction energy is directly related to the difference in the binding strengths for the propyl and the H at these Cr sites which are similar on these three species (see the "Difference" term in Table 7.13). The activation barriers for the 2nd C-H are much more sensitive in moving from α-Cr_2O_3 and the monomer Cr/α-Al_2O_3 to the 2Cr2O3/α-Al_2O_3 since the H is not completely bound to the Cr site yet in the transition state, and as such the barriers are much more dependent on the binding strength of propyl on Cr sites.

Table 7.13 DFT-calculated binding energies for the propyl and H on Cr site and differences in the propyl and H binding energies on Cr sites of different surfaces

	2Cr_2O_3/α-Al_2O_3	**α-Cr_2O_3**	**Monomer Cr/α-Al_2O_3**
Propyl-Cr (kJ/mol)	-170.9	-246.0	-232.5
H-Cr (kJ/mol)	-1.9	-78.2	-56.0
Difference (kJ/mol)	-169.0	-167.8	-176.5

7.3.1.3 Product Desorption and Reaction Energy Profiles of Propane Dehydrogenation on Amorphous 2Cr_2O_3/α-Al_2O_3

In the last step of the recombination of H_2, the activation barrier is higher in the Cr3a-O1 pathway compared with the Cr3a-O2a pathway (65.2 vs 42.1 kJ/mol respectively). This is due to the stronger binding of H on the O1 site than on the O2a site (see Table 7.8).

In summary, the apparent activation barrier for the overall reaction is calculated to be a little lower on the Cr3a-O2a pair than on the Cr3a-O1 pair (212.2 vs 233.1 kJ/mol). The reaction energy profiles which follow the energies for all of the individual steps in the overall PDH cycle for these two paths are shown in Figure 7.7.1 and 7.7.2. The results show that the energy well in the overall diagram is very shallow for both paths as it involves the physical adsorption of the propane molecule (-10.3 and -11.8 kJ/mol respectively). The highest point in energy profile for the path over the Cr3a-O1 site involves the recombination of the $H^{\delta+}$ with $H^{\delta-}$ to form H_2 whereas that on the Cr3-O2 path involves the 2nd C-H activation, This suggest that the C-H activation is easier than H-H recombination at the Cr3a-O1 site pair which is consistent with the stronger binding of H on O1 site than on O2a site.

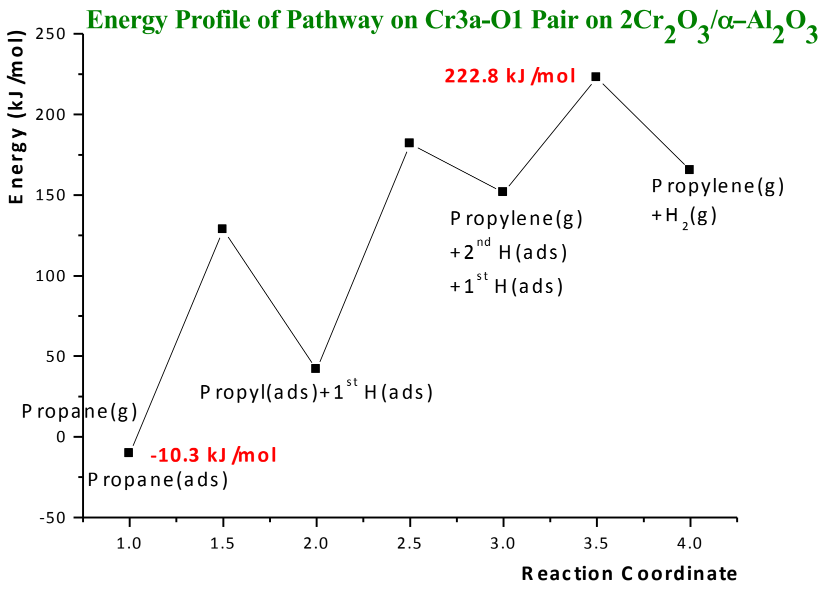

Figure 7.7.1 DFT-calculated reaction energy profile for propane dehydrogenation at the Cr3a-O1 site pair on amorphous $2Cr_2O_3/\alpha\text{-}Al_2O_3$

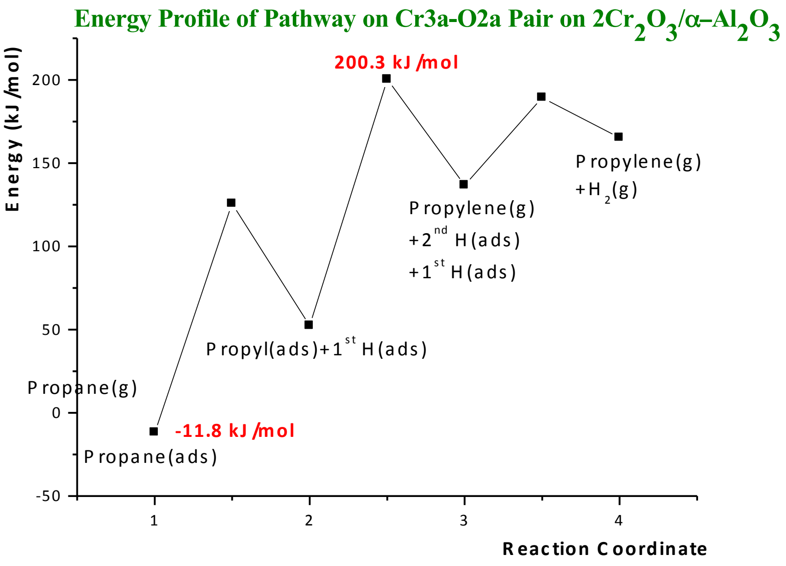

Figure 7.7.2 DFT-calculated reaction energy profile for propane dehydrogenation at the Cr3a-O2a pair on amorphous $2Cr_2O_3/\alpha\text{-}Al_2O_3$.

7.3.1.4 Comparison of Amorphous $2Cr_2O_3/\alpha\text{-}Al_2O_3$ with $Cr/\alpha\text{-}Al_2O_3$ Complexes and $\alpha\text{-}Cr_2O_3$ for Propane Dehydrogenation

In order to understand the differences in propane dehydrogenation activity over the $2Cr_2O_3/\alpha\text{-}Al_2O_3$ and the monomer $Cr/\alpha\text{-}Al_2O_3$ surfaces we compare the overall reaction energy profiles of the two shown in Figures 7.7.2 and Figure 6.9.1 in Chapter 6. The H binding energies at the O sites on these two surfaces are similar to each another, so the higher reaction energy found in activating the 1st C-H bond on $2Cr_2O_3/\alpha\text{-}Al_2O_3$ verses $Cr/\alpha\text{-}Al_2O_3$ is due to the weaker binding of propyl on the Cr site on $2Cr_2O_3/\alpha\text{-}Al_2O_3$. The weaker propyl binding energy at the Cr site, however, subsequently lowers the barrier for the 2nd C-H activation where propylene desorbs from the Cr site. The overall energy of the TS in the 2nd C-H activation is therefore only slightly higher on the $2Cr_2O_3/\alpha\text{-}Al_2O_3$ than that on $Cr/\alpha\text{-}Al_2O_3$ (200.3 vs 180.9 kJ/mol). This second C-H activation step appears to be the peak in overall profile for both the $2Cr_2O_3/\alpha\text{-}Al_2O_3$ and the $Cr/\alpha\text{-}Al_2O_3$ systems.

The weaker Cr-propyl binding for the $2Cr_2O_3/\alpha\text{-}Al_2O_3$ system also increases the energy well for this system closer to zero (-11.8 vs -36.3 kJ/mol), which reduces the overall barrier with respect to the lowest energy state which is the adsorbed propane. The lowest energy reference state for propane dehydrogenation over the $Cr/\alpha\text{-}Al_2O_3$ system, on the other hand, occurs after the 1st C-H activation as the formed propyl is strongly bound to the surface. The overall barrier for the activation of propane over amorphous $2Cr_2O_3/\alpha\text{-}Al_2O_3$ (212.1 kJ/mol) is then very similar to that on the monomer $Cr/\alpha\text{-}Al_2O_3$ (217.1 kJ/mol).

In the crystalline α-Cr_2O_3 case, the energy well is also at the physical adsorption of propane molecule and close to the zero-line (-9.6 kJ/mol), and the 1st C-H activation also has a positive reaction energy as a compromise between the weaker binding of H on the O site and the stronger binding of propyl on the Cr site. On the other hand, the stronger binding of propyl leads to a higher barrier for the 2nd C-H activation, and thus the energy of the 2nd C-H activation TS is significantly higher (248.4 kJ/mol). Since it is also the peak of the energy profile of the whole reaction, the overall barrier for the turnover cycle (258.0 kJ/mol) is higher than those in the other two cases.

The results here are consistent with previous speculation that the moderate binding properties of reaction sites on amorphous $2Cr_2O_3$/α-Al_2O_3 complex provide the active sites in catalytic propane dehydrogenation as they avoid the deep energy wells as well as the high energy peaks in the overall reaction energy profile.

7.3.2 C-H Activation of Propane on Amorphous $3Cr_2O_3$/α-Al_2O_3

7.3.2.1 The 1st and 2nd C-H Activation of Propane on Amorphous $3Cr_2O_3$/α-Al_2O_3

The $3Cr_2O_3$/α-Al_2O_3 system examined in this work was also comprised of a symmetric structure. The three Cr sites all sit in 3-fold positions. Similar to the $2Cr_2O_3$/α-Al_2O_3 system, the Cr-O pairs located in the upper layer (Cr3a) were found to be more favored than those in the lower layers where repulsive interactions between substrate hydroxyl groups and reaction species are significant.

The Cr3a sites bind to O sites (O2a, O2b and O2c) that bridge two Cr3a centers. The O2a site which resides at the top of the cluster has the weakest H binding energy. As a result, the barrier to activate the 1st (secondary) C-H bond of propane over the Cr3a-O2a site pair was found to have the highest activation energy and reaction energy (see Table 7.14). The other two O sites interact with H more strongly than O2a site and result in lower activation and reaction energies, and the Cr3a-O2b pair leads to the lowest energies since the O2b site binds H the most strongly among these three O2 sites (see Table 7.4.1).

The activation of the 2nd (terminal) C-H activation for all three paths proceed over the same Cr3a site and such have activation barriers and reaction energies that are very similar. The low barrier for this second C-H activation step is the result of the relatively weak binding of propyl intermediate to Cr site. While the relative interaction of H to the O2b and O2c sites is stronger than that to the O2a site, they are still non-bonding interactions as both are higher than positive 20 kJ/mol. The recombination of H_2 therefore readily occurs for all three pathways and does not contribute to the overall barrier.

Table 7.14 DFT-calculated activation barriers and reaction energies for the activation of C-H bonds of propane at different Cr-O site pairs on the $3Cr_2O_3/\alpha$-Al_2O_3 surface

Path	**Energy**	**1st C-H Activation**	**2nd C-H Activation**
Cr3a-O2a Path	**E_{act} (kJ/mol)**	170.5	137.0
	E_{rxn} (kJ/mol)	125.0	102.4
Cr3a-O2b Path	**E_{act} (kJ/mol)**	134.7	128.9
	E_{rxn} (kJ/mol)	83.5	104.2
Cr3a-O2c Path	**E_{act} (kJ/mol)**	157.9	135.1
	E_{rxn} (kJ/mol)	112.3	104.4

Due to the lowest reaction energies on the Cr3a-O2b pair, this path is discussed here as an example to explore the reaction mechanism in more detail. The first 1st C-H activation of propane involves a heterolytic splitting as shown in Figure 7.8.1 and Table 7.15. The second C-H activation occurs at the Cr3a site where the propyl is activated by the Cr site to form propylene which desorbs and a Cr-hydride intermediate ($H^{\delta-}$-$Cr^{\delta+}$). (see Figure 7.8.2 and Table 7.15). A detailed analysis of the changes in the charges as 1st and 2nd C-H bond activation steps proceed is shown in Figure 7.9.1 and 7.9.2, respectively. The small degree of electron transfer (-0.09 e) that occurs into the $3Cr_2O_3/\alpha$-Al_2O_3 after the first and 2nd C-H activation suggests that the $3Cr_2O_3/\alpha$-Al_2O_3 system has a greater electron affinity than $2Cr_2O_3/\alpha$-Al_2O_3, but similar to that for Cr/α-Al_2O_3.

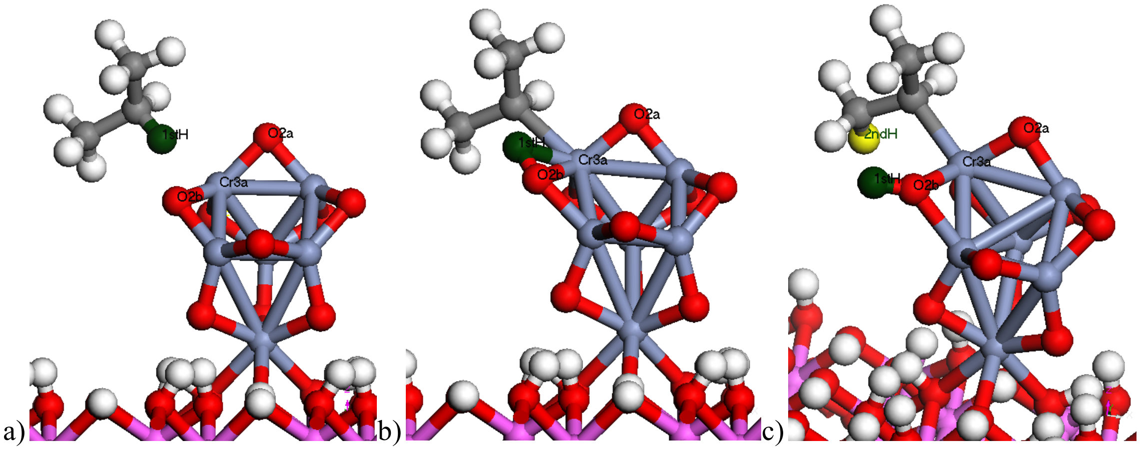

Figure 7.8.1 The activation of the 1st (secondary) C-H bond of propane on Cr3a-O2b site pair on amorphous $3Cr_2O_3/\alpha\text{-}Al_2O_3$: a) Reactant, b) TS and c) Product structures.

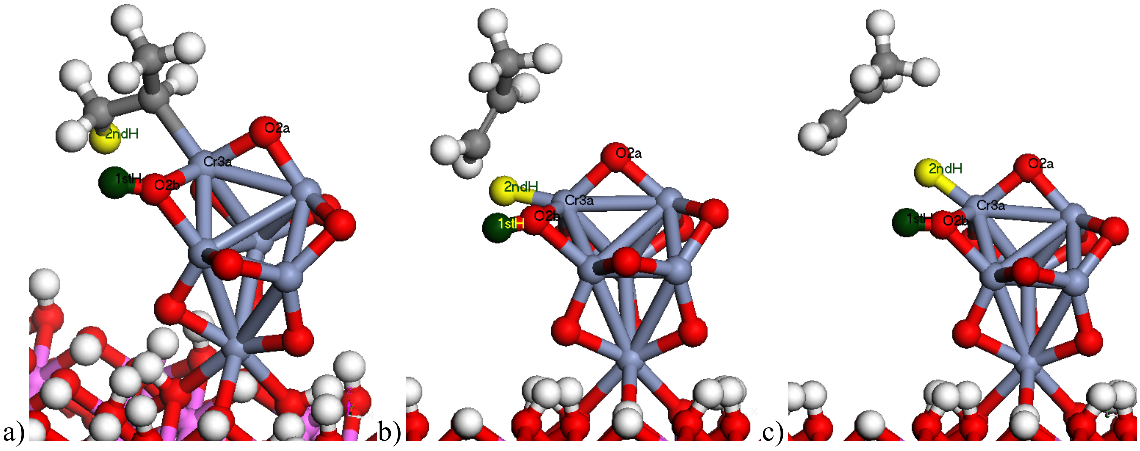

Figure 7.8.2 2nd The activation of the 2nd (terminal) C-H bond of the bound propyl intermediate on the Cr3a-O2b site pair on amorphous $3Cr_2O_3/\alpha\text{-}Al_2O_3$: a) Reactant, b) TS, and c) Product structures.

Table 7.15 Evolution of bond distances during the two C-H bond activation of propane over the Cr3a-O2b pair on the $3Cr_2O_3/\alpha\text{-}Al_2O_3$ surface

Step	**Bond Distance**	**Reactant**	**TS**	**Product**
1st C-H Activation	**1st H-O (Å)**	2.4	1.1	1.0
	C-Cr (Å)	3.1	2.2	2.1
2nd C-H Activation	**2nd H-Cr (Å)**	3.1	1.7	1.6
	C-Cr (Å)	2.1	3.3	4.6

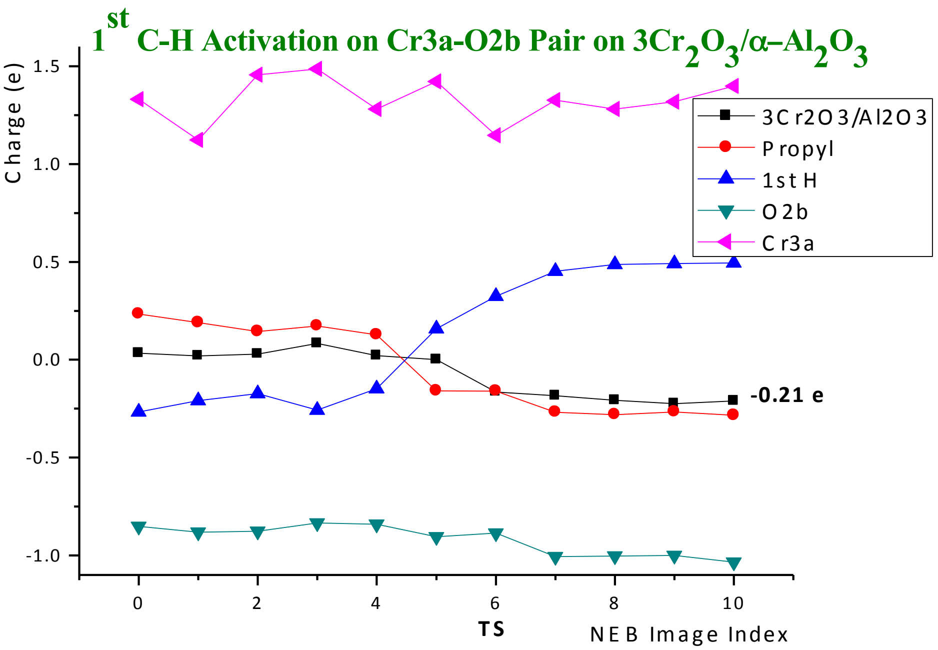

Figure 7.9.1 Bader charge analysis of the changes in charge on the Cr3a, O2b, H and propane during the activation of the 1st (secondary) C-H bond of propane to form the propyl and H intermediates at the Cr3a-O2b site pair on amorphous $3Cr_2O_3/\alpha\text{-}Al_2O_3$.

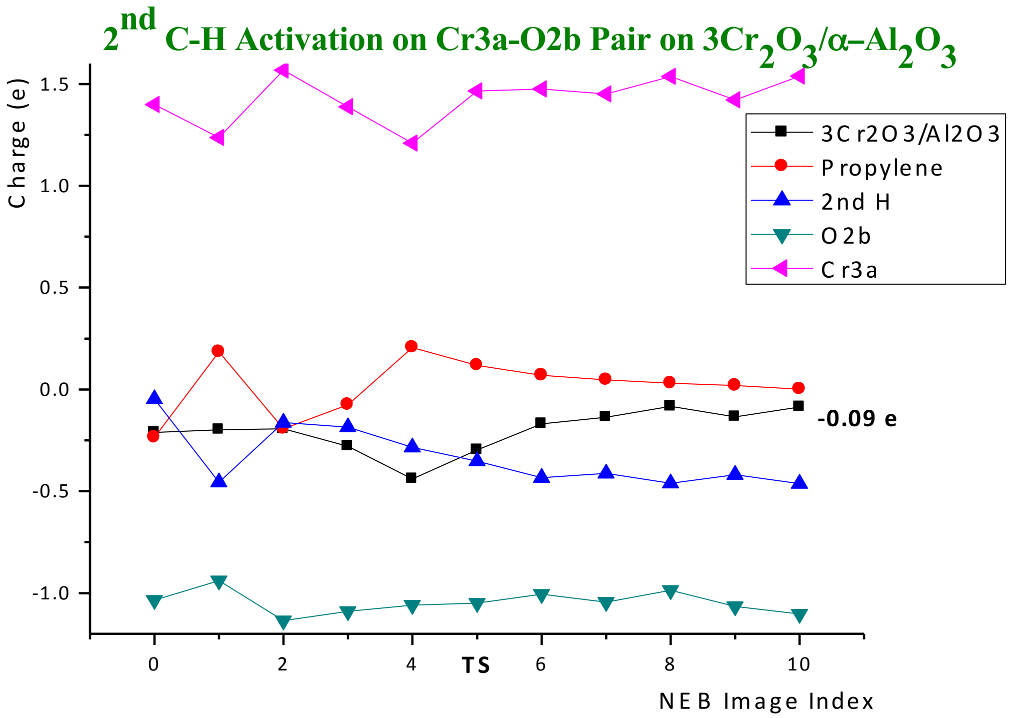

Figure 7.9.2 Bader charge analysis of the changes in charge on the Cr3a, O2b, H and propylene during the activation of the 2nd (terminal) C-H bond of propane to form the propylene and H intermediates at the Cr3a-O2b site pair on amorphous $3Cr_2O_3/\alpha\text{-}Al_2O_3$.

The bindings for the different reaction sites on the $3Cr_2O_3/\alpha\text{-}Al_2O_3$ system (reported in Table 7.8) were weaker than those for the $2Cr_2O_3/\alpha\text{-}Al_2O_3$ system. As a result, the calculated reaction energy is higher for the 1st C-H activation on Cr3a-O2b sites for the $3Cr_2O_3/\alpha\text{-}Al_2O_3$ system (83.5 kJ/mol) verses the Cr3a-O1 (41.8 kJ/mol) or Cr3a-O2a (52.5 kJ/mol) sites for the $2Cr_2O_3/\alpha\text{-}Al_2O_3$ system. The activation barriers for the 2nd (terminal) C-H bond, however, were slightly lower on Cr3a-O2b of $3Cr_2O_3/\alpha\text{-}Al_2O_3$ (128.9 kJ/mol) than the Cr3a-O2a sites of $2Cr_2O_3/\alpha\text{-}Al_2O_3$ (147.8 kJ/mol) due to the weaker propyl binding on the Cr site, for the $2Cr_2O_3/\alpha\text{-}Al_2O_3$ system. The overall energy for the 2nd C-H activation transition state was calculated to be a little higher (218.1 kJ/mol) at the Cr3a site on the $3Cr_2O_3/\alpha\text{-}Al_2O_3$ than on the Cr3a site on the $2Cr_2O_3/\alpha\text{-}Al_2O_3$ system (200.3 kJ/mol).

7.3.2.2 Reaction Energy Profile of Propane Dehydrogenation on Amorphous $2Cr_2O_3/\alpha\text{-}Al_2O_3$ and Comparison with Amorphous $2Cr_2O_3/\alpha\text{-}Al_2O_3$ and $Cr/\alpha\text{-}Al_2O_3$ Complexes

The weak interactions of H to the O and the Cr sites on $3Cr_2O_3/\alpha\text{-}Al_2O_3$ would lead to facile H-H recombination with a barrier of only 21.8 kJ/mol. This only slightly increases the energy level for the 2nd C-H activation by 3.1 kJ/moml. So although the TS of the H_2 recombination is the highest point of the energy profile for the $3Cr_2O_3/\alpha\text{-}Al_2O_3$ system, it is very close to the TS of the 2nd C-H activation, as is shown in Figure 7.10. The energy well for the $3Cr_2O_3/\alpha\text{-}Al_2O_3$ system involves the physical adsorption of propane which is only -7.1 kJ/mol. The overall activation barrier for propane dehydrogenation at the Cr3a sites on the $3Cr_2O_3/\alpha\text{-}Al_2O_3$ complex is 222.5 kJ/mol, which is slightly higher than that (212.1 kJ/mol) on $2Cr_2O_3/\alpha\text{-}Al_2O_3$.

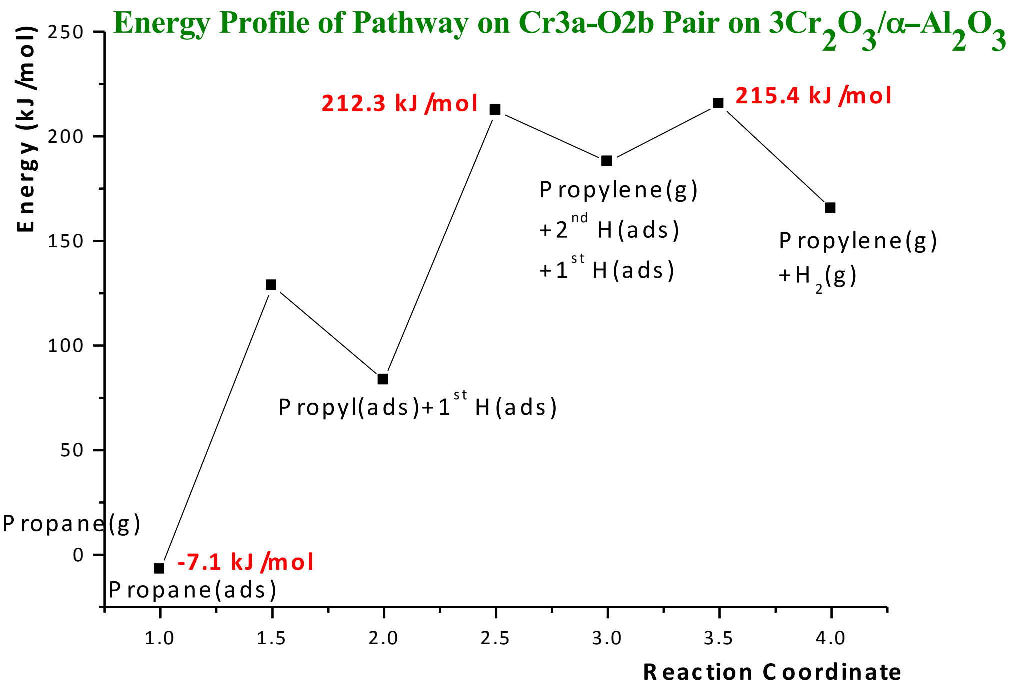

Figure 7.10 DFT-calculated reaction energy profile for propane dehydrogenation at the Cr3a-O2b site pair on amorphous $3Cr_2O_3/\alpha-Al_2O_3$.

The reaction energy to activate the 1st C-H bond of propane on the $3Cr_2O_3/\alpha-Al_2O_3$ complex was calculated to be higher than that on the monomer $Cr/\alpha-Al_2O_3$ complex due to the weaker hydrogen binding to the O and Cr sites on $3Cr_2O_3/\alpha-Al_2O_3$ complex. The weaker binding of propyl on the Cr site, however, also acts to lower the barrier in the 2nd C-H activation. The recombination of $H^{\delta+}$ with $H^{\delta-}$ occurs quite easily on both the $3Cr_2O_3/\alpha-Al_2O_3$ and monomeric $Cr/\alpha-Al_2O_3$ complexes and therefore does not contribute or contributes very little to the overall apparent activation barrier. By combining all of the elementary steps in the dehydrogenation of propane over the Cr3a-O2b sites on the $3Cr_2O_3/\alpha-Al_2O_3$, the highest energy in the energy profile is 215.4 kJ/mol which is somewhat higher than the highest energy of 180.9 kJ/mol on the monomer Cr/α-Al_2O_3complex and the 200.3 kJ/mol on the $2Cr_2O_3$/α-Al_2O_3 complex. However, since the lowest point in the energy profile is shallower than that in Cr/α-Al_2O_3 and $2Cr_2O_3$/α-Al_2O_3 (-7.1 vs -36.3 vs -11.8 kJ/mol), the amorphous $3Cr_2O_3$/α-Al_2O_3 complex has an overall barrier (222.5 kJ/mol) only slightly higher than that in the monomer Cr/α-Al_2O_3 case (217.1 kJ/mol) and that (212.1 kJ/mol) on $2Cr_2O_3$/α-Al_2O_3.

7.3.3 C-H Activation of Propane on Amorphous $4Cr_2O_3$/α-Al_2O_3, $5Cr_2O_3$/α-Al_2O_3 and $6Cr_2O_3$/α-Al_2O_3

The complexity of the Cr_2O_3/α-Al_2O_3 system increases as the size of the amorphous Cr_2O_3 cluster increases due to the increase in the distribution of different types of O and Cr sites. This results in a much broader distribution of H and propyl binding energies at the different O and Cr sites and thus a broader range of reaction energies and activation barriers with increasing Cr_2O_3 cluster size. The results derived from different sites on the cluster (similar to those discussed above) and presented in Table 7.16 indicate that most active sites for the overall dehydrogenation of propane are those with moderate H and propyl binding energies.The $2Cr_2O_3$/α-Al_2O_3 and $3Cr_2O_3$/α-Al_2O_3 are included in Table 7.16 for comparison purposes. The overall reaction energy profiles for the catalytic dehydrogenation of propane over the 4, 5, and 6 Cr_2O_3/α-Al_2O_3 are shown in Figure 7.11 for comparison. The reaction steps and the reaction mechanism for the 4, 5, and 6 Cr_2O_3/α-Al_2O_3 systems are identical to those presented above for the Cr/α-Al_2O_3 and the 2 and 3 Cr_2O_3/α-Al_2O_3 complexes.

Table 7.16 DFT-calculated H and propyl binding energies at the most reactive Cr-O pairs ("Reactive O/Cr" in table) along with the overall DFT-calculated apparent activation barriers for propane dehydrogenation on each of the amorphous 2, 3, 4, 5 and 6 Cr_2O_3/α-Al_2O_3 complexes.

E_{ads} **(kJ/mol)**	**2Cr_2O_3/ α-Al_2O_3**	**3Cr_2O_3/ α-Al_2O_3**	**4Cr_2O_3/ α-Al_2O_3**	**5Cr_2O_3/ α-Al_2O_3**	**6Cr_2O_3/ α-Al_2O_3**
H-O	-38.6 – 69.5	20.1 – 56.0	-56.0 – 28.8	-59.0 – 46.3	-66.9 – 46.3
Reactive O	**0.9**	**20.1**	**22.2**	**-14.2**	**-38.9**
H-Cr	-1.9	23.2 – 39.6	-8.7 – 97.5	-4.5 – 18.2	-11.2 – 135.7
H-Reactive Cr	**-1.9**	**39.6**	**36.0**	**-4.5**	**-11.2**
Propyl-Cr	-170.9 – -168.8	-120.6 – -118.7	-177.5 – -71.4	-176.8 – -101.3	-195.9 – -23.1
Propyl-Reactive Cr	**-170.9**	**-120.6**	**-110.2**	**-168.3**	**-195.9**
$E_{ovr\text{-}act}$ **(kJ/mol)**	212.1	219.5	233.1	238.6	216.3

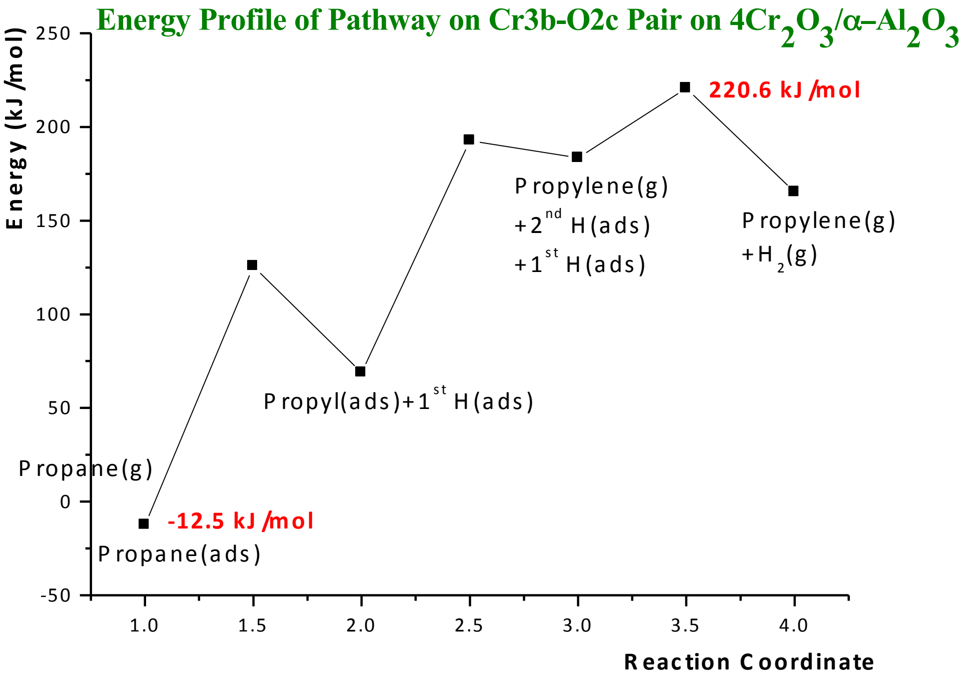
Energy Profile of Pathway on Cr3b-O2c Pair on 4Cr2O3/α–Al2O3
Energy (kJ/mol)
250
200
150
100
50
0
-50
1.0
1.5
2.0
2.5
3.0
3.5
4.0
Reaction Coordinate
220.6 kJ/mol
-12.5 kJ/mol
Propane(g)
Propane(ads)
Propyl(ads)+1st H(ads)
Propylene(g) +2nd H(ads) +1st H(ads)
Propylene(g) +H2(g)

a)

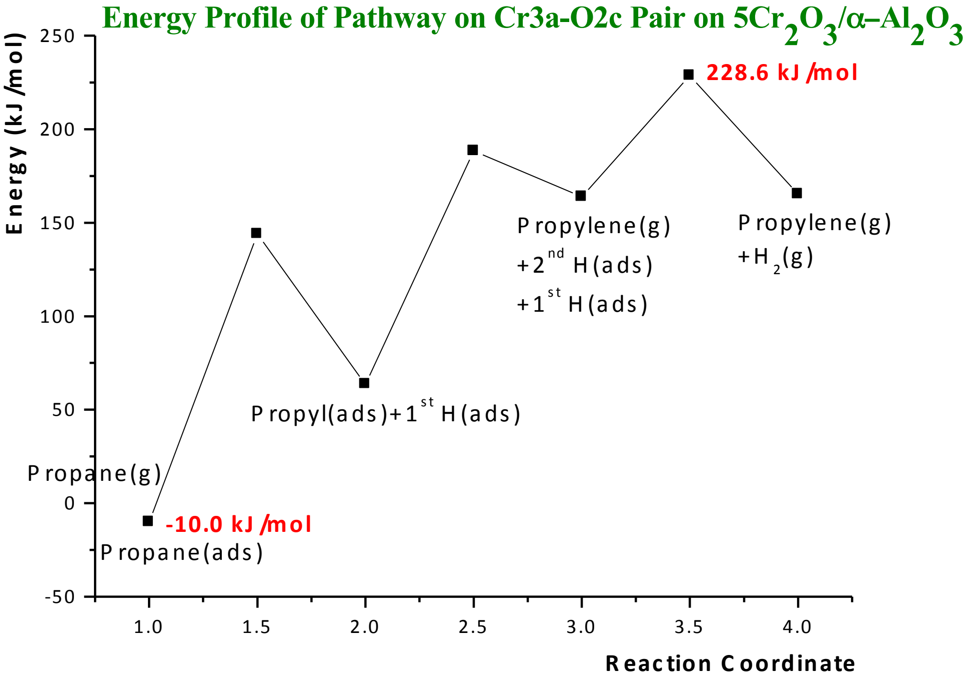
Energy Profile of Pathway on Cr3a-O2c Pair on 5Cr2O3/α–Al2O3
Energy (kJ/mol)
250
200
150
100
50
0
-50
1.0
1.5
2.0
2.5
3.0
3.5
4.0
Reaction Coordinate
228.6 kJ/mol
-10.0 kJ/mol
Propane(g)
Propane(ads)
Propyl(ads)+1st H(ads)
Propylene(g) +2nd H(ads) +1st H(ads)
Propylene(g) +H2(g)

b)

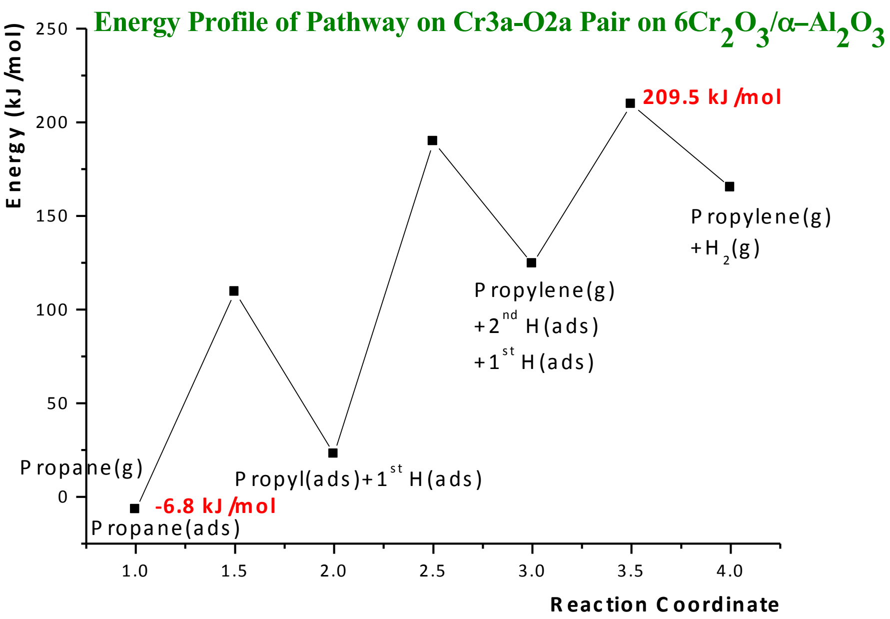

c)

Figure 7.11 DFT-calculated reaction energy profiles for propane dehydrogenation at Cr-O site pairs on the amorphous: a) $4Cr_2O_3/\alpha-Al_2O_3$, b) $5Cr_2O_3/\alpha-Al_2O_3$ and c) 6 $Cr_2O_3/\alpha-Al_2O_3$ complexes.

7.3.3.1 Comparison of Binding Properties and Catalytic Activities between Different Amorphous $Cr_2O_3/\alpha-Al_2O_3$ Complexes

A closer analysis of the Table 7.16 indicates that strongest H and propyl binding energies at the reactive O and Cr sites, respectively, are associated with the $6Cr_2O_3/\alpha-Al_2O_3$. The strong H and propyl binding interactions at these Cr and O sites make them the most favorable for the activation of the initial C-H activation of propane with a barrier of only 22.7 kJ/mol, but the least favorable for the subsequent activation of the propyl to form propane resulting in a barrier of 166.9 kJ/mol as this step requires the dissociation of the strong Cr-C bond as shown in Figure 7.11. The low calculated barrier of 216.3 kJ/mol is close to the overall barriers of 212.1 kJ/mol and 219.5 kJ/mol for the $2Cr_2O_3/\alpha\text{-}Al_2O_3$ and $3Cr_2O_3/\alpha\text{-}Al_2O_3$ complexes, respectively.

While the overall barriers on these complexes are similar, the barriers for the individual C-H activation steps are different. The reactive Cr and O sites on $3Cr_2O_3/\alpha\text{-}Al_2O_3$ and $4Cr_2O_3/\alpha\text{-}Al_2O_3$ complexes both have weaker H and propyl binding energies than those for the $6Cr_2O_3/\alpha\text{-}Al_2O_3$ system. The weaker H and propyl interactions result in higher activation barriers and reaction energies for the 1st C-H activation ($E_{a(3Cr2O3/\alpha\text{-}Al2O3)}$ = 83.5 kJ/mol and $E_{a(4Cr2O3/\alpha\text{-}Al2O3)}$ = 68.8 kJ/mol vs. $E_{a(6Cr2O3/\alpha\text{-}Al2O3)}$ = 22.7 kJ/mol), but lower activation barriers and reaction energies ($E_{a(3Cr2O3/\alpha\text{-}Al2O3)}$ = 128.9 kJ/mol and $E_{a(4Cr2O3/\alpha\text{-}Al2O3)}$ = 123.9 kJ/mol vs. $E_{a(6Cr2O3/\alpha\text{-}Al2O3)}$ = 166.9 kJ/mol) for the 2nd C-H activation.

The energetics for the first and second C-H bond activation steps subsequently balance one another out and as a result the overall apparent activation barriers for propane dehydrogenation over the 3, 4 and 6 $Cr_2O_3/\alpha\text{-}Al_2O_3$ complexes are similar as shown in Table 7.16 and Figure 7.11. The first step requires Cr-O site pairs that will strongly bind the propyl and H fragments and stabilize the transition state. The subsequent activation of the C-H bond of the bound propyl and the recombinative desorption of H_2 however are enhanced by weaker Cr-C, Cr-H and O-H bonds. This suggests that the “moderate” binding properties of the Cr and O sites necessary for propane dehydrogenation could cover quite a broad range of values. As seen in Table

7.16, the bindings of H on O and Cr sites are distributed between -40 kJ/mol and 40 kJ/mol. In comparison, the H binding on O sites (82.0 kJ/mol) turned out to be too weak for propane dehydrogenation on α-Cr_2O_3, and the H binding on O sites (-114.8 kJ/mol) turned out to be too strong on α-Al_2O_3.

The binding energy for propyl on reactive Cr sites takes on a range of values from-110 kJ/mol to -196 kJ/mol in Table 7.16. The propyl binding energy on the monomer Cr/α-Al_2O_3, however, was calculated to be significantly stronger at -232.5 kJ/mol. While the propyl binding energy is much stronger in the monomeric Cr/α-Al_2O_3 system, the overall reaction barrier 0f 217.1 kJ/mol is very similar to the barriers on the 2, 3 and 6 Cr_2O_3/α-Al_2O_3 complexes.

This again is due to the fact that the stronger propyl binding stabilizes the transition state and lowers the barrier for the 1st C-H activation, but acts to inhibit the desorption of propylene and increases the barrier for the 2nd C-H activation. The sensitivity of the overall propane dehydrogenation barrier to the propyl binding energy does not appear to be as important as the sensitivity to the H binding energy.

7.3.3.2 Comparison of Electronic Properties between Different Amorphous Cr_2O_3/α-Al_2O_3 Complexes

A detailed Bader charge analysis of the changes in the charges on the Cr, O, H and propyl intermediates as well as the Cr_2O_3/α-Al_2O_3 complexes were carried out for the propane activation on the 4, 5 and 6Cr_2O_3/α-Al_2O_3 complexes. They all turned out to gain or lose very small amounts of charge (-0.03 e to 0.05 e) from or to propane after two steps of C-H activation as shown from Figure 7.12.1 to Figure 7.12.3. Combining with previous results on 2 and 3 $Cr_2O_3/\alpha\text{-}Al_2O_3$ complexes (see Figure 7.6 and Figure 7.9.2), it could be concluded that the $Cr_2O_3/\alpha\text{-}Al_2O_3$ complexes are very weak electron acceptors.

The reaction mechanism on 4, 5, and $6Cr_2O_3/\alpha\text{-}Al_2O_3$ complexes are also similar as other smaller complexes as in Figure 7.12.1-7.12.3. Both the 1st and 2nd C-H activation steps appear to occur via a heterolytic mechanism. The propyl and H intermediates that form in the first step are negatively and positively charged, respectively, and interact with the Cr^{3+} and O^{2-} sites on the surface. The subsequent C-H activation of the resulting propyl species involves the formation of the surface hydride and the desorption of propylene.

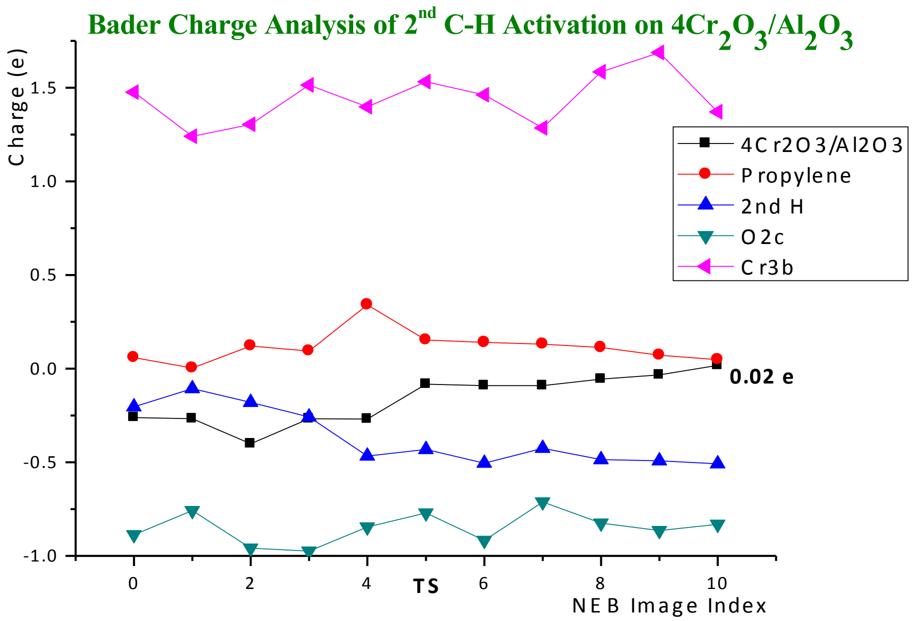

Figure 7.12.1 Bader charge analysis for the Cr3b, O2c, H and propylene for the 2nd C-H bond activation over the Cr3b-O2c pair on amorphous $4Cr_2O_3/\alpha\text{-}Al_2O_3$

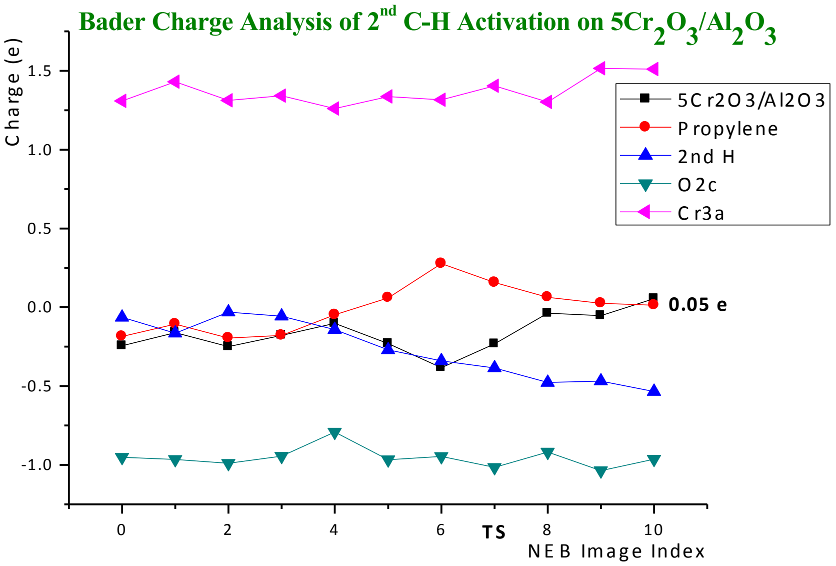

Figure 7.12.2 Bader charge analysis for the Cr3a, O2c, H and propylene for the 2nd C-H bond activation over the Cr3a-O2c pair on amorphous $5Cr_2O_3/\alpha\text{-}Al_2O_3$

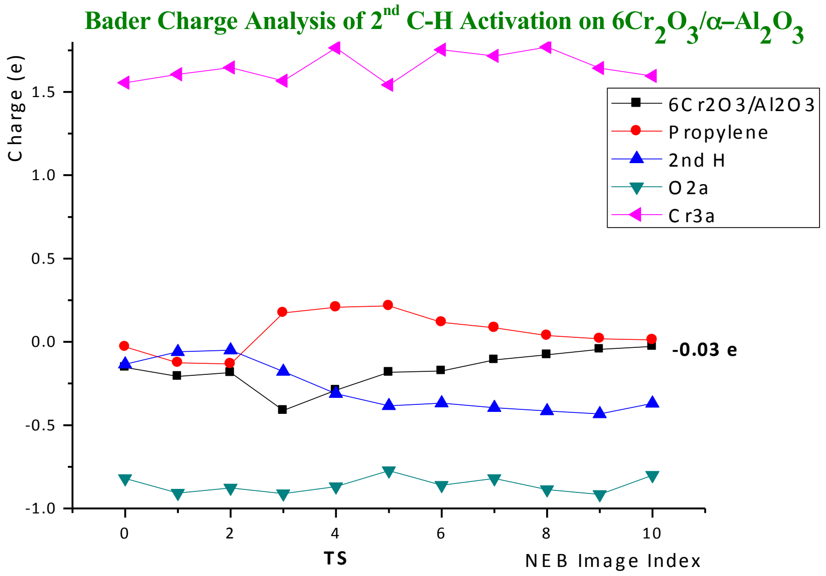

Figure 7.12.3 Bader charge analysis for the Cr3a, O2a, H and propylene for the 2nd C-H bond activation over the Cr3a-O2a pair on amorphous $6Cr_2O_3/\alpha\text{-}Al_2O_3$.

7.4 Conclusions

A series of different of amorphous Cr_2O_3 clusters were supported on α-Al_2O_3 and analyzed for propane dehydrogenation. While the properties of the individual Cr and O sites on these clusters were quite different than those on the Cr/α-Al_2O_3 systems examined in Chapter 6, the total barriers for propane dehydrogenation turnover which reflect their overall catalytic activity were quite similar to those on the Cr/α-Al_2O_3 complexes.

7.4.1 Reaction Mechanism, Reaction Energetics and Binding Properties of Active Sites on Cr_2O_3/α-Al_2O_3 Complexes

The reaction appears to proceed via the heterolytic activation of the secondary C-H bond of propane over a Cr-O sites pair to form a Cr-propyl$^{\delta-}$ and O-H$^{\delta+}$ surface intermediates. A terminal C-H bond of the propyl intermediate is subsequently activated by the Cr site to form propylene that desorbs into the gas phase and a Cr-H$^{\delta-}$intermediate. The H$^{\delta+}$ and H$^{\delta+}$ that reside on the neighboring Cr and O pair subsequently recombine and desorb as H_2 to complete the overall catalytic cycle. The reaction energies and activation barriers for the both C-H activation steps are controlled by the strength of the Cr-propyl$^{\delta-}$, O-H$^{\delta+}$ and Cr-H$^{\delta-}$ interactions. These interactions were found to be controlled by the properties of the Cr and O sites as well as the properties of the specific Cr_2O_3/α-Al_2O_3 clusters examined.

The activation of the 1st C-H bond of propane was found to be enhanced by Cr-O sites with strong Cr-propyl and O-H binding energies as they stabilize the transition state for this reaction. The Cr-propyl and O-H binding energies on different $Cr_2O_3/\alpha\text{-}Al_2O_3$ demonstrate a distribution of different strengths. While the binding energies of propyl to the Cr sites were calculated to be rather strong ranging from -110 to -200 kJ/mol, they are significantly weaker than the Cr-propyl binding energies on the $\alpha\text{-}Cr_2O_3$ and $Cr/\alpha\text{-}Al_2O_3$. The O-H binding energies on the $Cr_2O_3/\alpha\text{-}Al_2O_3$ complexes were calculated to be much more moderate ranging from -40 to +40 kJ/mol and closer to those found on the and $Cr/\alpha\text{-}Al_2O_3$ surfaces.

The activation of the terminal C-H bond of the bound propyl intermediate occurs at the same Cr site. This reaction, however, is favored by a weaker Cr-propyl bond as it involves the direct desorption of propylene. The intrinsic barriers calculated for this step on the $Cr_2O_3/\alpha\text{-}Al_2O_3$ complexes (~100-140 kJ/mol) were found to be considerably lower than the corresponding barrier of 217.1 kJ/mol on the $Cr/\alpha\text{-}Al_2O_3$ surface. The barrier for this step is the highest energy state in the potential energy profile for $Cr/\alpha\text{-}Al_2O_3$ and hence is the total barrier for catalytic turnover.

In analyzing different Cr-O sites on the different $Cr_2O_3/\alpha\text{-}Al_2O_3$ complexes, we find that the Cr-O site pairs that reside in the outer layers are favored over those in the layers closer to the Al_2O_3support due to repulsive interactions between the reaction intermediates and substrate hydroxyl groups. The most active O sites are those which reside at 2-fold bridge sites between two Cr centers. The binding energies for H at these sites are rather moderate as they are weaker than those at the 1-fold O sites but stronger than those at the 3-fold O sites. The reactive Cr centers are those bound to three oxygens

(3-fold). The 4-fold Cr sites are either unavailable due to steric effects or reconstruct to 3-fold sites when binding reaction species.

7.4.1 Electronic Properties of Cr_2O_3/α-Al_2O_3 Complexes

The Bader charge analyses indicate that the most active Cr-Al oxide complexes are those which demonstrate very weak electron affinity. Those systems with strong electron affinity aid in the activation of the initial C-H bond but are then inhibited by the less active propyl and hydrogen species that result, such as the α-Al_2O_3 surfaces. The lowest overall activation energies require moderate propyl and hydrogen binding energies which allow for both the activation of propane and the subsequent removal of the propyl and hydrogen products.

Some of the amorphous Cr_2O_3/α-Al_2O_3 complexes (3 and 6Cr_2O_3/α-Al_2O_3) gain a small amount of negative charge from propane during reaction, while other complexes (2, 4 and 5Cr_2O_3/α-Al_2O_3) lose a small degree of negative charge to the propane, which is similar to α-Cr_2O_3. Since the catalytic activities of these complexes are quite higher than α-Cr_2O_3, the overall electron acceptability should not be the only factor that correlates to the electronic properties and thus the catalytic activity of the catalyst surface.

The similar charge transfer properties for these Cr_2O_3/α-Al_2O_3 complexes and α-Cr_2O_3 should be due to the fact that the O-sites on the Cr_2O_3 complexes hold the negative charge more strongly than those on α-Cr_2O_3, and that the Cr sites hold the negative charge more weakly than α-Cr_2O_3. Therefore, the balanced electron affinities of reaction sites and the balanced binding energies are also important to the catalytic activity for propane dehydrogenation turnover cycle. For the $Cr_2O_3/\alpha\text{-}Al_2O_3$ complexes with similar overall electron affinities to those for $\alpha\text{-}Cr_2O_3$, the reaction energies are similar in the 1st and the 2nd C-H activations. However, they have lower activation energies for the 2nd C-H activation than $\alpha\text{-}Cr_2O_3$ due to the weaker electron acceptability of Cr sites and weaker binding at the Cr site, and thus lower barriers for the turnover cycle propane dehydrogenation.

In summary, the electron affinity/acceptability of each single reaction site together with the overall electron affinity/acceptability of the oxide are both important to the overall activation of propane to propylene and hydrogen. With similar total electron acceptabilities, the moderately distributed electron affinities of the O and Cr sites are more helpful to the overall activity than the polarized electron acceptability between O and Cr sites. This moderately distributed electronic property is consistent with the moderate coordination states of reaction sites, as the O sites are more unsaturated and the Cr sites are more saturated regarding the coordination number on the $Cr_2O_3/\alpha\text{-}Al_2O_3$ complexes compared with the crystalline $\alpha\text{-}Cr_2O_3$. And essentially, the moderate binding abilities of reactions sites that are critical to the catalytic activity in propane dehydrogenation are results of the moderate electronic properties of the oxides.

Chapter 8 Summary and Recommendations for Future Work

First principle density functional theoretical studies were carried out in this thesis to examine the mechanisms that control the catalytic conversion of propane into propylene and hydrogen over low-cost refractory metal oxides, compare a series of different series of different oxides including α-Al_2O_3, α-Cr_2O_3 and mixed Cr-Al oxide complexes, namely, grafted Cr/α-Al_2O_3 and amorphous Cr_2O_3/α-Al_2O_3, and explore the influence of oxide structure and properties on catalytic reactivity. More specifically we examined different catalyst structures, surface compositions, and active metal and oxygen sites on the overall reaction pathways and energetics and the elementary steps and mechanisms that control propane dehydrogenation over refractory metal oxides.

8.1 Reaction Pathways and Possible Reaction Mechanisms

In all the oxides examined with the exception of the fully hydroxylated Al_2O_3, the reaction appears to proceed by the heterolytic activation of the 1st (secondary) C-H bond of propane over a vicinal metal-O site pairs to form metal-propyl and O-H intermediates. The barriers for this reaction are moderate over the different Al_2O_3 and Cr_2O_3 surfaces. The initial activation of propane over the fully hydroxylated Al_2O_3 surface cannot proceed via the activation over M-O site pairs as there are no metal sites that are exposed on the surface. As such the 1st C-H activation instead the C-H activation of propane proceeds homolytically over two vicinal OH groups on the hydroxylated surface. The barrier for this reaction is very high.

The terminal C-H of the bound propyl intermediate that forms on these different oxide surfaces can subsequently react either by a hydrogen abstraction from an adjacent O site on the surface or via a hydride transfer to the initial metal center to form propylene that desorbs into the gas phase thus resulting in O-H or an M-H surface intermediates. The O-sites on the Al_2O_3 surfaces were calculated to be much more basic than those on the Cr_2O_3 surfaces and thus carried out the hydrogen abstraction resulting in the formation of a surface $O^{\delta-}$-$H^{\delta+}$ intermediate and propylene that desorbs into the gas phase. The 2nd C-H activation proceeds on the Cr-containing oxides instead via a metal catalyzed C-H activation over the same Cr site or neighboring a neighboring Cr cation sites that act as Lewis acid centers thus resulting in the formation of $Cr^{\delta+}$-$H^{\delta-}$ and propylene that desorbs.

The hydrogen intermediates that form on the Al_2O_3 and Cr_2O_3 surfaces ultimately recombine and desorb as H_2 to free up sites and enable catalytic turnover. This step is rather difficult on the α-Al_2O_3 surface as the hydrogens that form are very strongly held to the basic oxygen sites. In addition both of the hydrogens that form on Al_2O_3 are protonic in nature. As a result, the barrier for the recombinative desorption of H_2 over the α-Al_2O_3 was found to be very high and ultimately the highest energy state in over the overall catalytic cycle.

The catalytic removal of hydrogen was also found to lead to the high activation barriers on the α-Al_2O_3 surface with O vacancies. While the intrinsic barrier for the recombination of hydrogen from the defect Al_2O_3 surface was calculated to be lower at vacancy cites on the Al_2O_3 surface due to the weaker O-H bonds, the overall activation barrier for propane dehydrogenation was found to be considerably higher on the Al_2O_3

surface with defects than that on the pristine Al_2O_3 surface due to the very strong propyl-Al bonds that form in the initial activation of propane at Al sites with O vacancies which result in the formation of a very deep well in the overall potential energy surface for the Al_2O_3 surface with defects.

In the fully hydroxylated α-Al_2O_3 system, there is no deep energy state in the activation of the C-H bonds, since the binding energies for the propyl and H intermediates that form are significantly weaker than those on the other two Al_2O_3 facets. The barrier for H_2 recombination, however, is still extremely high, because the two H that form are both protons which reside at separate OH sites. This results in an unstable and unfeasible transition state.

Therefore, while the α-Al_2O_3 surfaces can readily activate C-H bonds, they cannot maintain catalytic activity as the reaction intermediates that result cannot be readily removed.

The recombinative desorption of H_2 on the Cr-containing surfaces was found to be significantly easier as the hydrogens were more weakly held to the Cr and O sites and can readily undergo heterolytic recombination of $H^{\delta+}$ and $H^{\delta-}$ from vicinal $O^{\delta-}$-$H^{\delta+}$ and $Cr^{\delta+}$-$H^{\delta-}$ sites.

The O-H and Cr-H binding energies on the α-Cr_2O_3 surfaces were calculated to be significantly weaker than those on the Al_2O_3 surfaces and as such the intrinsic barriers for the recombination of H_2 were much lower on the Cr_2O_3 surfaces. The highest barrier along the overall potential energy surface involves the 2nd C-H activation step as there is a significant barrier required to break the strong propyl-Cr bond. Thus for most of the Cr surfaces, the highest point along the overall potential energy surface involves the TS for the 2nd C-H activation. The apparent barrier therefore tends to involve the energy of this state relative to the gas phase alkane which involves the sum of the reaction energy of the 1st C-H activation and the energy barrier of the 2nd C-H activation.

In general, the reaction energy for the activation of the first 1st C-H bond of propane decreases with increased binding of H to the O site and propyl to the Cr site. The barrier to activate the 2nd C-H bond, however, increases with increased binding of propyl to the Cr site. The decrease in the overall reaction endothermicity for the first C-H activation step and the increase in the activation barrier for the second C-H step with the increase in the propyl-Cr binding energy tend to cancel one another out. This holds provided that the binding of propyl does not become so strong that the barrier of the 2nd C-H activation becomes insurmountable to prevent the reaction or the binding of propyl is so weak that the 1st C-H activation is so endothermic that it results prevents the overall turnover. Neither of these exceptions occurred in the systems that were examined. .

Therefore, the critical factor controlling the overall activation barrier for propane dehydrogenation is the binding energy of H to the oxygen in the refractory oxide. If the O-H binding energy is too strong, there is a deep energy well due to the initial C-H bond activation, such as in the case of propane dehydrogenation over α-Al_2O_3; if the H-binding energy is too weak, the reaction energy of the 1st C-H activation increases which will affect the energy of the TS of the 2nd C-H activation such as the case on the α-Cr_2O_3 surface. The increase in the overall energy for the first step together with the high barrier for the 2nd C-H bond activation step makes this surface relatively inactive from propane activation especially in comparison with the three types of Cr-containing oxides. The results are consistent with the experimental observations reported in the previous literature.

In comparison, the Cr sites on Cr/α-Al_2O_3 complex have similarly strong binding with propyl, while the O sites bind H with a moderate strength. As such the overall reaction energy for the 1st C-H activation step is exothermic but not as bad over the low energy over the Al_2O_3 systems. The recombination of hydrogen to form H_2 occurs quite easily. As such the highest point of the energy path is associated with the TS of the 2nd C-H activation. The overall barrier for PDH is solely determined by the 2nd C-H activation barrier but can be overcome at high temperature in PDH reaction.

The binding energies for propyl at the Cr sites on amorphous Cr_2O_3/α-Al_2O_3 are weaker than the previous Cr/Al_2O_3 surfaces whereas the binding energies for H to the O sites are distributed in a moderate range similar to those found for other Cr/α-Al_2O_3 systems due to the more moderate coordination states of both O sites and Cr sites. As a result, the reaction energies for the 1st C-H activation are more endothermic and the barriers for the 2nd C-H activation are lower on the amorphous Cr_2O_3/α-Al_2O_3 surface than those on Cr/α-Al_2O_3. Combining these two energies together, the barrier for the overall PDH reaction is similar to those found on Cr/α-Al_2O_3 complexes. This is consistent with the overall activity being strongly influenced by the O-H binding energies.

As for the binding of H on Cr sites, it influences both the reaction energy of the 2nd C-H activation and the recombination of H_2. But since on these pure or mixed Cr oxides, the difference between the binding strength of propyl and that of H on Cr sites is roughly the same in all the cases, the reaction energy of the 2nd C-H activation is also close to each other. The binding of H on Cr sites mainly affects the H_2 recombination in that if the H binds on Cr sites too strongly, the recovery of reaction sites would be difficult. In our study, the difficult regeneration of reaction sites was not observed on Cr containing oxides. When the Cr sites bind H more strongly like on α-Cr_2O_3 and Cr/α-Al_2O_3 complexes, the bindings of H on O sites are quite weak or moderate, so the activation barrier and reaction energy of H_2 desorption are not high.

Therefore, the moderate bindings, especially the moderate bindings of H on O sites, are the key factors for a decent activity, which help the propane activation turnover cycle persistently run by avoiding both low energy wells and high energy peaks in the energy profile.

8.2 Influence of Electronic Properties of Catalyst Surfaces

The Bader charge analysis showed that Al_2O_3 surfaces have too strong electron acceptabilities, while the mixed Al-Cr oxide complexes have weaker electron acceptabilities, so they hold the external electron from reaction intermediates moderately in C-H activations, and release them with low barriers in H_2 recombination. The electron acceptability is related to the saturation extent of electron density of the oxides. Among the oxides examined, the Al_2O_3 surfaces are most unsaturated in the electron density, while the Al-Cr oxide complexes, influenced by the saturated α-$Cr_2O_{3,}$ are more saturated. Therefore, the oxides with the more saturated electron density and thus the weaker electron acceptability are helpful for the activity in propane dehydrogenation in our study.

Moreover, α-Cr_2O_3 and Cr_2O_3/α-Al_2O_3 have similarly weak electron acceptability but different catalytic activities for propane dehydrogenation. So, in addition to the overall electron acceptability of the oxide, the respective electron acceptability of O sites and Cr sites are also important. The reaction energies are more correlated to the total electron acceptability, while the activation energies are influenced by the respective electron acceptability of single sites. So when the electron acceptability on some site is strong, the activation barrier might get high in the single step that is greatly affected by this site, such as the 2nd C-H activation on the Cr site on α-Cr_2O_3. So although α-Cr_2O_3 and Cr_2O_3/α-Al_2O_3 have similar overall electron affinities and thus similar reaction energies in all steps, there is quite a difference in the single barrier of the 2nd C-H activation. Since the TS of the 2nd C-H activation is the peak of the energy profile, there is accordingly a difference in the overall barrier for the turnover cycle.

Therefore, compared with crystalline α-Cr_2O_3, the higher activity on Cr/α-Al_2O_3 is due to more moderate binding properties and more moderate electron properties in total, since the bindings on Cr sites are similar to α-Cr_2O_3while the bindings on O sites are more moderate under the influence of the α-Al_2O_3 substrate. On the other hand, the increase in activity from Cr/α-Al_2O_3 is due to more moderate coordination states and thus more moderate distribution between the properties of O and Cr sites, with similar total binding abilities and total electron acceptabilities.

8.3 Recommendations for Future Work

As for the future work, the effort on the refractory oxides should be focused on looking for the oxides with moderately saturated electronic density that could lead to moderately weak electron acceptabilities and moderate binding properties. Such oxides may be obtained though the mixing of different oxides with different electronic properties, as in the case of Cr/α-Al_2O_3 complexes. For example, the complexes based on Al oxides could be tuned by other oxides with weaker binding abilities and weaker electron acceptability, and the complexes based on Cr oxides could be tuned by other oxides with stronger binding properties and stronger electron acceptability. Moreover, the complexes composed by other metal oxides with different properties might also be candidates for potential new catalysts. Currently, one example under consideration is the spinel structure of Al species like $MgAl_2O_4$ and $NiAl_2O_4$.

In addition, the moderate properties brought by the moderate coordination states as in the Cr_2O_3/α-Al_2O_3 case might be obtained in different forms other than the crystalline oxides. Here we could study the amorphous γ-Al_2O_3 as it was reported to be active for the activation of H_2 and methane. Although it is probably inactive for the turnover cycle of propane dehydrogenation as the support of commercial CrO_x/γ-Al_2O_3 catalysts, it still might lead to further insights into this catalytic system to study the γ-Al_2O_3 and also the interaction between γ-Al_2O_3 and CrO_x.

References

[1] S.D. Rossi, G. Ferraris, S. Fremiotti, A. Cimino, V. Indovina, *App. Catal. A* **81** (1992), 113.

[2] M. P. Lobera, C. Téllez, J. Herguido, M. Menéndez, *App. Catal. A* **349** (2008), 156.

[3] D. Sanfilippo, F. Buonomo, G. Fusco, M. Lupieri, I. Miracca, *Chem. Eng. Sci* **47** (1992), 2313.

[4] P. Sun, G. Siddiqi, W. Vining, M. Chi, A. T. Bell, *J. Catal*. **282** (2011), 165.

[5] M. Heinritz-Adrian, S. Wenzel, F. Youssef, *Digiditalrefining*, 2008, Article 1000632**.**

[6] D. Sanfilipo, I. Miracca, *Catal. Today* **111** (2006), 133.

[7] C. Boswell, *ICIS*, 2012, Article 9549968.

[8] M. M. Bhasin, J. H. McCain, B. V. Vora, T. Imai, P. R. Pujado, *App. Catal. A* **221** (2001), 397.

[9] I. M. Dahl, K. Grande, K.-J. Jens, E. Rytter, A. Slagtern, *App. Catal*. **77** (1991), 163.

[10] G. Fu, X. Xu, X. Lu, H. Wan, *J. Phys. Chem. B* **109** (2005), 6416.

[11] K. Chen, A. T. Bell, E. Iglesia, *J. Phys. Chem. B* **104** (2000), 1292.

[12] M. M. Bettahar, G. Costentin, L. Savary**,** J. C. Lavalley, *Appl.Catal. A* **145** (1996), 1.

[13] L. Lin, T. Zhang, J. Zang, Z. Xu, *App. Catal*. **67** (1990), 11.

[14] D. I. Kondarides, K. Tomishige, Y. Nagasawa, U. Lee, Y. Iwasawa, *J. Mol. Catal. A* **111** (1996), 145.

[15] B. M. Weckhuysen, R. A. Schoonheydt, *Catal. Today* **51** (1999), 223.

[16] P. L. D. Cola, R. Glaser, J. Weitkamp, *App. Catal. A* **306** (2006), 85.

[17] Wilhelm, C. Frederick, US Patent 3909451, 1975.

[18] J. H. Brophy, A. L. Tonkovich, G. Roberts, M. B. Schmidt, G. B. Chadwell, US Patent 007405338B2, 2008.

[19] W. Pan, S. M. Casey, B. K. Glover, F. Xu, US Patent 0090321318, 2009.

[20] UOP, Private Meeting, 2010.

[21] K. Tanabe, T. Yamaguchi, *Catal. Today* **20** (1994), 185.

[22] C. Copéret, *Chem. Rev*. **110** (2010), 656.

[23] B. M. Weckhuysen, I. E. Wachs, R. A. Schoonheydt, *Chem. Rev.* **96** (1996), 3327.

[24] J. Joubert, A. Salameh, V. Krakoviack, F. Delbecq, P. Sautet, C. Copéret, J. M. Basset, *J. Phys. Chem. B* **110** (2006), 23944.

[25] D. Farcasiu, P. Lukinskas*, Chem. Commun*. (2001), 77.

[26] W. Pan, S. M. Casey, B. K. Glover, F. Xu, US Patent 0090325784, 2009.

[27] W. Pan, S. M. Casey, B. K. Glover, F. Xu, US Patent 0090325791, 2009.

[28] S. M. K. Airaksinen, M. E. Harlin, A. O. I. Krause, *Ind. Eng. Chem. Res.* **41** (2002), 5619.

[29] J. Gascón, C. Téllez, J. Herguido, M. Menéndez, *App. Catal. A*. **248** (2003), 105.

[30] L. Xu*, X. Feng, M. Neurock, *Density Functional Theory Study of Non-Oxidative Dehydrogenation of Propane into Propene on ZrO_2*, to be Submitted.

[31] G. Kresse, J. Furthmuller, *Phys. Rev. B* **54** (1996), 11169.

[32] G. Kresse, J. Furthmuller, *Comp. Mater. Sci.* **6** (1996), 15.

[33] G. Vignale, M. Rasolt, *Phys. Rev. Lett.* **59** (1987), 2360.

[34] J. P. Perdew, J. A. Chevary, S. H. Vosko, K. A. Jackson, M. R.Pederson, D. J. Singh, C. Fiolhais, *Phys. Rev. B* **46** (1992), 6671.

[35] J. P. Perdew, W. Yue, *Phys. Rev. B* **33** (1986), 8800.

[36] G. Kresse, D. Joubert, *Phys. Rev. B* **59** (1999), 1758.

[37] H. J. Monkhorst, J. D. Pack*, Phys. Rev. B* **13** (1976), 5188.

[38] H. Jónsson, *Annu*. *Rev. Phys. Chem.* **51** (2000), 623.

[39] G. Mills, H. Johnsson, G. K. Schenter, *Surf. Sci.* **324** (1995), 305.

[40] G. Henkelman, B. P. Uberuaga, H. Jónsson, *J. Chem. Phys.* **113** (2000), 9901.

[41] G. Henkelman, H. Jónsson, *J. Chem. Phys.* **113** (2000), 9978.

[42] G. Henkelman, H.Jonsson, *J. Chem. Phys.* **111** (1999), 7010.

[43] R. A. Olsen, G. J. Kroes, G. Henkelman, A. Arnaldsson, H. Jónsson, *J. Chem. Phys.* **121** (2004), 9776.

[44] A. Heyden, A. T. Bell, F. J. Keil, *J. Chem. Phys*. **123** (2005), 224101.

[45] W. Tang, E. Sanville, G. Henkelman, *J. Phys.: Condens. Matter* **21** (2009), 084204.

[46] L. Xu, G. Henkelman, *Phys. Rev. B* **77** (2008), 205404.

[47] J. Ahn, J. W. Rabalais, *Surf. Sci.* **388** (1997), 121.

[48] E. A. Soares, M. A. Van Hove, C. F. Walters, K. F. McCarty, *Phys. Rev. B* **645** (2002), 195405.

[49] V. A. Ranea, I. Carmichael, W. F. Schneider, *J. Phys. Chem. C* **113** (2009), 2149.

[50] P. Liu, T. Kendelewicz, G. E. Brown Jr., E. J. Nelson, S. A. Chambers, *Surf. Sci.* **417** (1998), 53.

[51] K. C. Hass, W. F. Schneider, A. Curioni, W. Andreoni, *Science* **282** (1998), 265.

[52] K. C. Hass, W. F. Schneider, A. Curioni, W. Andreoni, *J. Phys. Chem. B* **104** (2000), 5527.

[53] P. J. Eng, T. P. Trainor, G. E. Brown Jr., G. A. Waychunas, M. Newville, S. R. Sutton, M. L. Rivers, *Science* **288** (2000), 1029.

[54] L. Zhang, C. Tian, G. A. Waychunas, Y. R. Shen, *J. Am. Chem. Soc.* **130** (2008), 7686.

[55] D. Damidot, *Cem. Concr. Res.* **36** (2006), 783.

[56] G. Job, F. Herrmann, *Eur. J. Phys.* **27** (2006), 353.

[57] S. Lillehaug, K. J. Børve, M. Sierka, J. Sauer*, J. Phys. Org. Chem.* **17** (2004), 990.

[58] Q. Li, Z. Sui, X. Zhou, D. Chen, *App. Catal. A* **398** (2011), 18.

[59] C. J. A. Mota, D. L. Bhering, A. Ramírez-solís, *Int. J. Quant. Chem*. **105** (2005), 174.

[60] F. Cavani, M. Koutyrev, F. Trifiro, A. Bartolini, D. Ghisletti, R. Iezzi, A. Santucci, G. Del Piero, *J. Catal.* **158** (1996), 236.

[61] S. DeRossi, M. P. Casaletto, G. Ferraris, A. Cimino, G. Minelli, *App. Catal. A* **167** (1998), 257

[62] A. Hakuli, A. Kytökivi, A. O. I. Krause, *App. Catal. A*. **190** (2000), 219

[63] M. J. Capitán, J. A. Odriozola, A. Márquez, J. F. Sanz, *J. Catal*. **156** (1995), 273.

[64] L. Xu*, X. Feng*, A. Bhattacharyya, W. Pan, M. Neurock, *Density Functional Theory Study of Non-Oxidative Dehydrogenation of Propane into Propene on* ZrO_2 *and* Al_2O_3, to be Submitted.

[65] R. L. Puurunen, B. M.Weckhuysen, *J. Catal*. **210** (2002), 418.

[66] S. Derossi, G. Ferraris, S. Fremiotti, E. Garrone, G. Ghiotti, M. C. Campa, V. Indovina, *J. Catal.* **148** (1994), 36.

[67] F. D. Hardcastle, I. E. Wachs, *J. Mol. Catal*. **46** (1988), 173.

[68] M. A. Vuurman, D. J. Stufkens, A. Oskam, J. A. Moulijn, F. Kapteijn*, J. Mol. Catal*. **60** (1990), 83.

[69] B. M. Weckhuysen, L. M. D. Ridder, R. A. Schoonheydt, *J. Phys. Chem.* **97** (1993), 4756.

[70] B. M. Weckhuysen, A. A. Verberckmoes, A. L. Buttiens, R. A. Schoonheydt, *J. Phys. Chem*. **98** (1994), 579.

[71] B. M. Weckhuysen, L. M. D. Ridder, P. J. Grobet, R. A. Schoonheydt, *J. Phys. Chem.* **99** (1995), 320.

[72] K. Ding, H. C. Anderson, *Phys. Rev. B* **34** (1986), 6987.

[73] R. Biswas, G. S. Grest, C. M. Soukoulis, *Phys. Rev. B* **36** (1987), 7437.

[74] W. D. Luedtke, U. Landman, *Phys. Rev. B* **37** (1988), 4656.

[75] M. Ishimaru, I.-T. Bae, Y. Hirotsu, S. Matsumura, K. E. Sickafus, *Phys. Rev. Lett*. **89** (2002), 055502.